INAUGURAL – DISSERTATION

Zur

Erlangung der Doktorwürde

der

Naturwissenschaftlich-Mathematischen Gesamtfakultät

der

Ruprecht – Karls - Universität

Heidelberg

Deutschland

STRUCTURAL EVOLUTION IN THE PALAEOPROTEROZOIC BASEMENT (BANDED IRON FORMATION AND RELATED ROCKS) OF SW EGYPT

Vorgelegt von

Mostafa Fahmy Mostafa Elkady

Aus Ägypten

2003

Gutachter : Prof. Dr. Reinhard O. Greiling

Prof. Dr. Wolfgang Dachroth

To the Memory of my Mother

My Father

And

My Family

Abstract

Structural evolution in the Palaeoproterozoic Banded Iron Formation of SW Egypt

M.F.Elkady
Geol.Pal.Inst.INF 234, D-69120 Heidelberg, Germany.Ruprecht-Karls-Universitaet Heidelberg.
On leave from: Egyptian Geological Survey, 3 Slah Salem st., Abbassia Cairo Egypt.

The exposed basement of the Western Desert of Egypt is part of the pre-Pan-African East Sahara Craton. The Gabel Uweinat-Bir Safsaf Aswan Uplift is situated at the eastern fringe of this craton, and its high-grade metamorphic and granitoid rock associations are markedly distinct from the metavolcanic-metasedimentary-ophiolitic sequences of the Eastern Desert of Egypt (Nubian Shield). Crystalline basement rocks cover an area of some 40,000 km^2 in SW Egypt.

The fieldwork and mapping of the basement rocks in the present area were carried out during the winters 1998, 1999 and at last in 2001 for altogether about 10 months of fieldwork. A detailed field geologic-structural map to the scale of 1:60,000 and two cross sections, perpendicular to the regional structural trend for the whole area, are prepared using vertical aerial photographs and Landsat images. Detailed petrographic studies of the different rock units were carried out to determine their compositional character and the effect of deformation on each rock unit. Some 125 rock specimens representing the different rock units were collected and more than 130 thin sections were examined petrographically using the polarizing microscope. Microstructure studies and (analyses) attempted to determine the structural evolution and possible transport direction from about 40 oriented thin sections parallel and perpendicular to the foliation. Further structural data, from the anisotropy of the magnetic susceptibility (AMS) was determined from 31 oriented samples, which were cored and cut (200 cylinders). The magnetic susceptibility measurements were analyzed with the Kappa bridge.

The BIF is exposed as an upper unit, while anatexite forms a middle one, underlain by ultramafic-mafic units.

The BIF shows large quartz crystals with wavy extinction and undeformed recrystallized quartz.

The Anatexite sequences were affected by granulite facies metamorphism, followed by a retrograde metamorphism. The petrographic study shows some orthopyroxene crystals altered to hornblende, biotite and chlorite.

The structural analysis of the area indicated that it was subjected to major tectonic deformation including folding, overthrusting, shearing and faulting. The area is built

up of thrust slices of the BIF and Anatexite, which extend for more than 25 km in N15°E direction, dipping to the west with angles between 30° to 70°. The thickness of slices horses is up to 4 km. The thrust sequence in this area has about 20 km width.

Thrust Faults have been derived from overturned folds, the shear surface replacing one of the limbs of the fold. The structure is dominated by a series of nearly parallel, minor thrust faults, or high angle reverse faults, which dissect the rock into slices, sheets, plates, blocks or wedges that are approximately equidistant and have the same displacement and are all steeply inclined to the WNW (285°).

Restoration of this thrust sequence shows that the anatexite forms a basement to the overlying BIF. Both metamorphic banding in the anatexite and the layering in the BIF restore to a horizontal primary orientation.

The Deformational Evolution

Three major deformation phases can be discerned in the study area (D1, D2 and D3), the three phases D1, D2 and D3 affected only the basement rocks and are followed by Phanerozoic brittle deformation affecting both the basement and the overlying sedimentary rocks in the investigated area.

The D1 structures indicate a crustal thickening followed by crustal thinning and developed the melano- and leucosome in the Anatexite sequences. A foliation (S1) observed in the thin section of the BIF as simple shear mylonitization zones. Generally in (D1) the Anatexite bands are parallel with the mylonitic shear zones in the BIF.

The D2 structures dominate in the BIF as a micro and macro folding (F2) associated with low angle thrust or shear zones (S2). In the Anatexite and the Ultramafic-mafic sequences minor folds with the same characters as in the BIF are observed. Generally in (D2) the BIF and Anatexite bands had E-W strike and dipped shallowly to the south (S2), and contain minor folds (F2) with E-W axial surfaces.

The D1 and D2 deformations are both of them overprinted by the D3 structures, which refolded the F2 at a perpendicular direction of the fold axes by F3. The D3 affected refolding and thrusting at the BIF, Anatexite sequences and Ultramfic-mafic bands as F3 and S3. The F3 has NNE trend and plunge with an angle of 15°. The foliation S3, is parallel to the fold axial surfaces and thrust surfaces. The dip angle ranges between 30° and 70° to the WWN (285°).

ACKNOWLEDGEMENT

This dissertation is contribution to a project between the Egyptian Geological Survey, Cairo (Mr. Aboul Hassan Abdolraouf) and the Geolgisches-Palaeontologisches Institute, Heidelberg University, Germany (Prof R.O.Greiling). Funding by BMFT/KFA Jülich and logistic support and field facilities by the Egyptian Geological Survey are gratefully acknowledged.

I wish to express my deep sense of gratitude to the scientists who supervised this work namely Prof. R.O.Greiling, Professor of Structural Geology and Director of the Geolgisches-Palaeontologisches Institute, Heidelberg University for guidance in the field, valuable suggestions and discussions, continuous help during the progress of the work and critical reading of the manuscript. Prof. A.A. Dardir, Chairman of the Egyptian Company for Salt “Amesal”, and former Chairman of the Egyptian Geological Survey for his continuous advice and encouragement. Prof. H. Flick, in the Geolgisches-Palaeontologisches Institute, Heidelberg University for his kindness, invaluable and continuous advice and discussions as well as reading the manuscript, Dr. A. Kontny Assistance Professor in the Geolgisches-Palaeontologisches Institute, Heidelberg University for her kindness, invaluable and continuous advice and discussions, Prof. W. Dachroth, the Professor of Applied and Engineering Geology in the Geolgisches-Palaeontologisches Institute, Heidelberg University for his kindness, invaluable and continuous advice and discussions, Dr Z. El Alfy the Director of the Egyptian Geological Survey for his continuous advice, discussions, encouragement and reading of the manuscript.

The conclusion and results of the work have improved much due to critical and constructive discussions both in the field and during the office work. Field and office discussions were carried out with Drs. A. Khaled, M.F. Sadek, W. Ghebr.eab, M.M. Abdeen and Geologests M. Khattab, A. Salem, G. Shaban, colleagues in EGSMA.

The author is greatly indebted to Dr. W. Janiesch the Chairman of SAS Institute Germany, Mrs A. Dörrhofer the Director of the SAS-Germany, Mr. K. Hessenauer, the former Manager in SAS-Germany, for bestow him a part time Job to finance my study and live during my stay in Heidelberg, and my kind-heartedly thanks for all the staff of SAS Germany for their kindly relationship, tolerance, sympathies, encouragement and advices during my work with them.

The author is thankful to Mr Abol Hassan Abel Raouf, the Chairman of Egyptian Geological Survey for his advices tolerance and support to finish this work, Mr. G.

Naim and Mr .M. El Hinnawy the former Chairman's of Egyptian Geological Survey for their agree to continue this work in Geological Institute of Heidelberg University.
I greatfully acknowledge the Mr. R. Koch the PC graphic in geological Institute, librarians Mr. M. Bühler, Mrs K. Seehaus, and technical assistance of the geological Institute in Heidelberg Mr. Will (Photo-Lab.) and Mrs O. Wallerath for preparing the thin sections, the help of the colleagues Dipl. Geol. F Cueto, and L. Nano for their kind help in the Computer soft and hardware in the Geolgisches-Palaeontologisches Institute, Heidelberg University.
Thanks are also rendered to the Secretary Staff in the Geolgisches-Palaeontologisches Institute, Heidelberg University Mrs G. Froelich, J. Kontny and A. Hoffman for their kindness helps.

STRUCTURAL EVOLUTION IN THE PALAEOPROTEROZOIC BASEMENT (BANDED IRON FORMATION AND RELATED ROCKS) OF SW EGYPT

LIST OF CONTENTS

LIST OF ILLUSTRATIONS

LIST OF TABLES

CHAPTER 1
INTRODUCTION

1-1 General Statements

The exposed basement rocks of the Western Desert of Egypt form part of the pre Pan-African East Saharan Craton (Fig 1). High-grade metamorphism and granitoid rock associations in this craton are markedly distinct from the metavolcanic-metasedimentary-ophiolitic sequences of the Eastern Desert of Egypt (Nubian Shield). Crystalline basement rocks cover an area of some 40.000 km^2 in the Gabal Uweinat area at the junction of the borders of Egypt, Sudan and Libya.

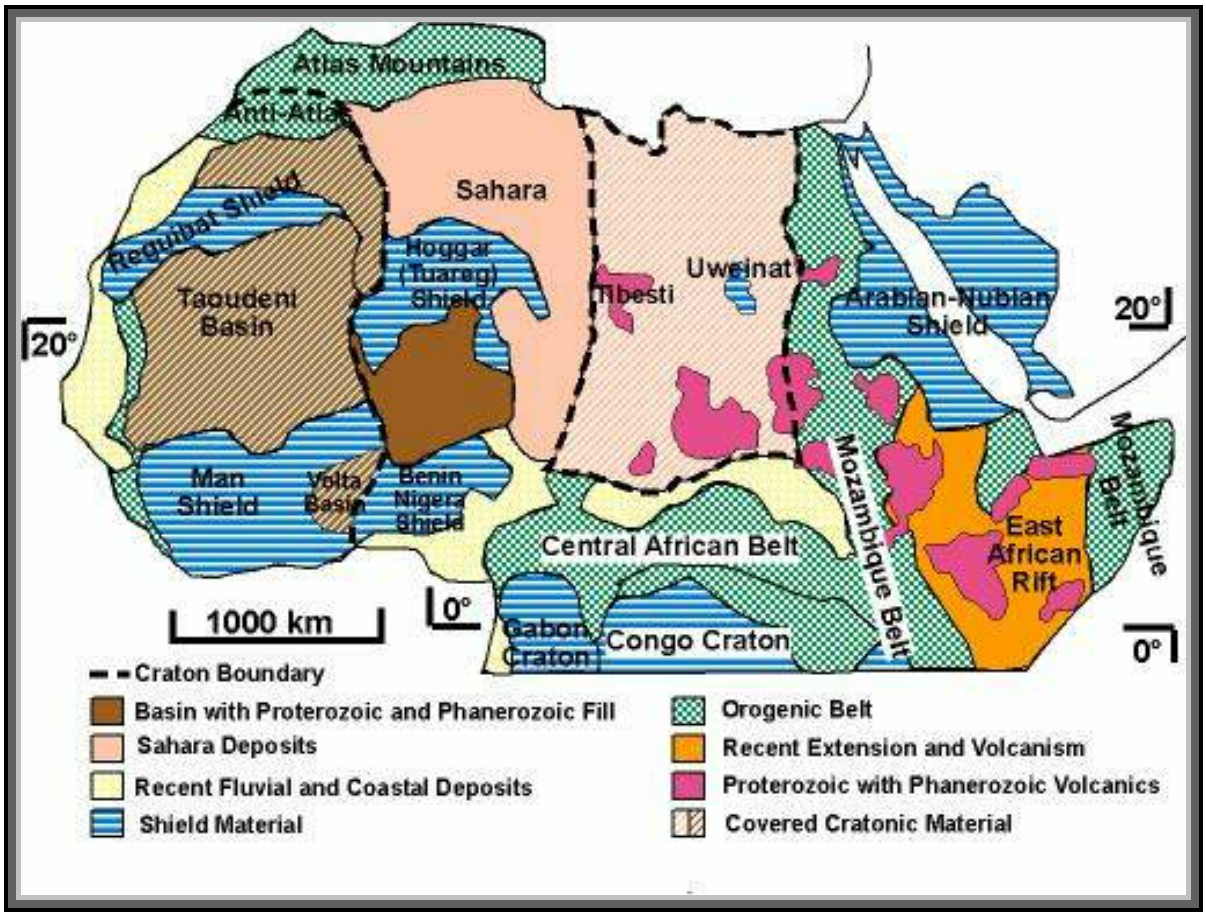

Fig-1 Generalized geologic division of Northern Africa. Major division include shield material, covered cratonic material, basins filled with Proterozoic and Phanerozoic sediments, Sahara eposits, recent fluvial and coastal deposits, orogenic belts, regions of recent extension, and Proterozoic regions with Phanerozoic volcanics. After Goodwin (1996)

The area around Gabal Uweinat received little attention from geological research, because it is poorly accessible and very arid. Previous work on the basement rocks in this area, especially regarding structure and economic minerals is very limited.

The basement around Gabal Uweinat, SW Egypt, is considered as the oldest basement in NE Africa. Sm/Nd model ages show a crustal differentiation between 3200 and 3000 Ma ago (Harris et al, 1984).

In the present work regional structures, microstructures, tectonic evolution and potentially important mineral deposits are examined. A geological mapping was prepared with the help of aerial photographs of scale 1 : 60,000 as well as satellite images of a scale of 1 : 100,000. The major geological units in the region on which the present work has given emphasis are the Banded Iron Formation (BIF) and the Anatexite Sequences.

The study area covers about 500 km^2 and is located within the Gabal Uweinat region. It is bounded by geographical co-ordinates of 26°00` to 26° 25` E and 22°00` to 22°25` N (Fig.2). The southern boundary coincides with the Egyptian-Sudanese boundary.

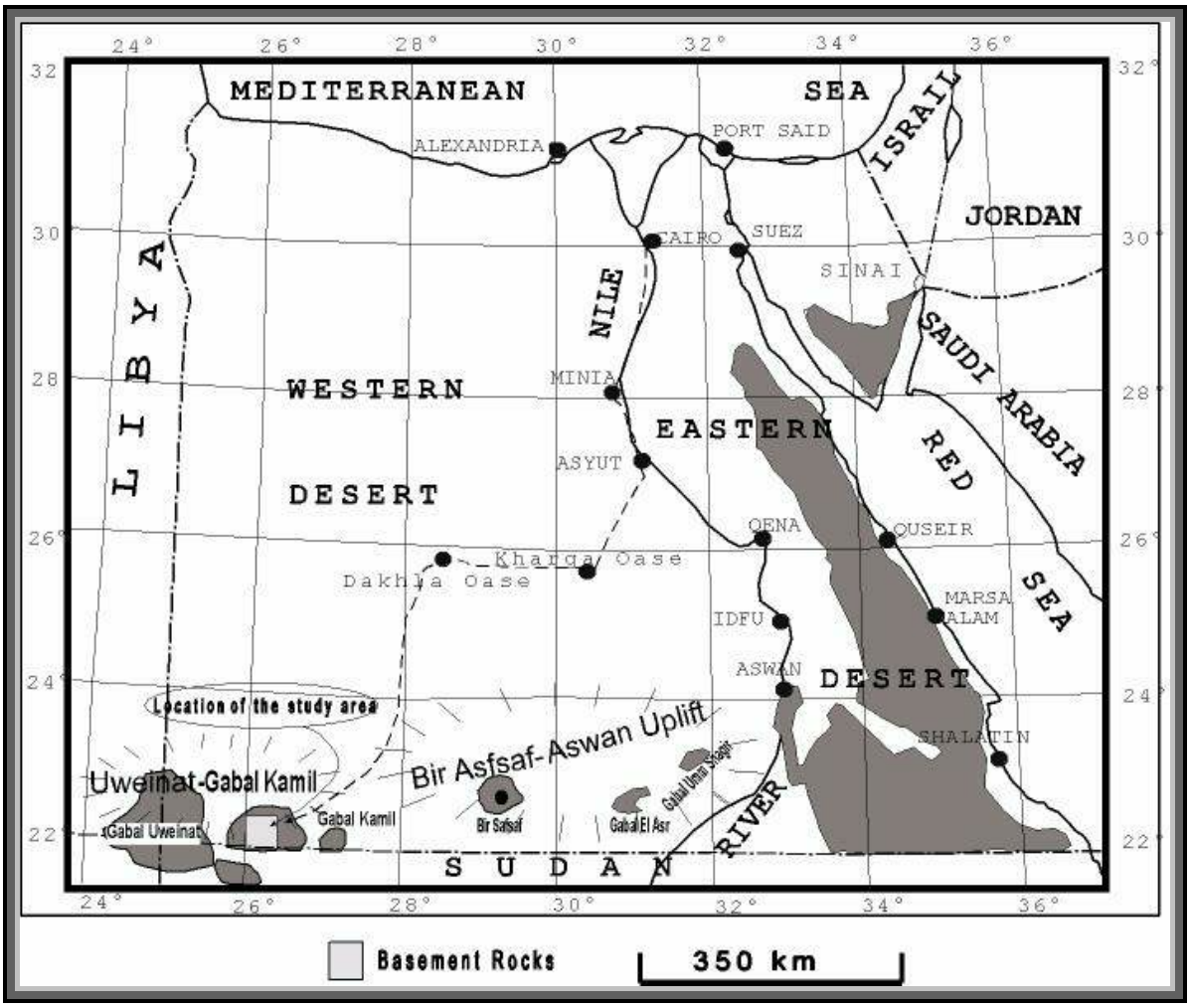

Fig 2 Location map showing the Uweinat area in the SW corner of Egypt in North East Africa

I-2 Accessibility

The area of investigation is approximately 1500 km to the SW of Cairo. It can be reached by asphaltic roads from Cairo to Kharga Oasis (600 km), then 200 km toward the west Dakhla Oasis. From Dakhla Oasis there is a north south asphaltic road, to the village known as East Uweinat (ca. 270 km). It is recommended to stay overnight in East Uweinat before driving approximately 400 km actually on desert roads to the area of investigation, starting early in the morning (at the first morning light). The desert routes are very difficult to drive where thick sand sheet coverage prevails in addition to groups of huge sand dunes. The way hardly shows any landmark. However, with new navigation devices (GPS) and 4 wheel drive cars can reach the area in the evening.

I-3 Climate and Population

The area is arid, no rainfall occurred during field seasons and probably for many years before. The weather during winter is pleasant, with temperatures between 15° and 30° C during the day and 5° and 10° C at night. In the summer, however, it is hot with temperatures between 40° to 50° C during the day and 20° to 30° C at night. Clouds of dust and sand frequently accompany the wind, which blows as sandstorms from the north, often in the spring. Little vegetation is observed. The nearest settlement is East Uweinat village which is 400 km to the east of the study area

1-4 Geological Setting: East Saharan Craton / East African Orogeny

The East Gabal Uweinat area occupies a place close to the boundary between the East Saharan Craton (Nile Craton) and the East African Orogen. The study area lies about 100 kilometres east of Gabal Uweinat, 100 kilometres west of Gabal Kamil, and about 750 kilometres southwest of Aswan (fig 2). The pre-Pan-African basement is surrounded and unconformably overlain by sandstone strata of Devonian and Cretaceous ages, called the Nubian Sandstone formation. Some minor intrusions were emplaced into the basement and occasionally the cover sedimentary rocks. These intrusions are syenite, granite complexes and numerous plugs and dykes of alkaline and basic nature. Despite its remoteness the area has been described by a number of workers including Menchikoff (1927) and Sandford (1935) who reported on the petrology of the rocks. More recently structure, metamorphism, younger intrusions, and geochronology of the rocks have been described by: Mahrholz (1968), Klerkx (1971), Hunting Geology and Geophysics Limited (1974), Klerkx and

Deutsch (1977), Klerkx (1980), Schandelmeier et al. (1983), Schanelmeier & Darbyshire (1984) and Richter et al. (1986), Conoco Corporation (1987), Said et al. (1998), Naim et al. (1998), Greiling et al. (2000) and Khalid et al. (2000).

It is currently accepted that the Arabian-Nubian Shield of NE Africa developed through a process of horizontal crustal accretion during the Pan-African period (Gass 1981, Vail 1983, Kröner 1985) from about 950 to 550 Ma ago. The western edge of this Shield with its extensive volcano-sedimentary-ophiolitic and granitoid assemblage was accreted onto the old Nile Craton to the west of the Nile into a series of high grade migmatitic gneisses, migmatites and partly granulites with intercalated high grade supracrustal rocks like marbles, calcsilicates and amphibolites. Although not enough discrete pre-Pan-African ages from these rocks in southern Egypt and northern Sudan are yet available, there is considerable evidence that these rocks belong to an older sialic continental plate (Abdel-Monem and Hurley 1979, Harris et al. 1984, Bernau et al. 1987) which was named Nile Craton (Rocci 1965, referring to the Uweinat inlier), East Saharan Craton (Kröner 1979) referring to the area between Hoggar and Arabian-Nubian Shield. The extent of the East African Craton is not well defined as the bulk of the assumed cratonic body lies beneath a thick layer of Phanerozoic sediments, the Sahara desert. The existence of a cratonic body beneath the Sahara is proposed on the basis of scattered Precambrian outcrops in the region (Condie, 1982). The oldest of these outcrops is the Archean Uweinat Inlier. Other outcrops such as Tibesti, Kordofan, and Darfour display Proterozoic basement material mingled with Phanerozoic volcanics (Goodwin 1996, Cahen and Snelling 1984, Vincent 1970) (Fig 1).

The North African or the Nile Craton, according to some authors, is the north continuation of the Mozambique belt. It is exposed west of the Nile (Fig 1). It represents the old continental crust to which some intra-oceanic island arcs from east were accreted, collided and obducted during the Neo-Proterozoic time to form the Arabian-Nubian Shield. This process of converging plates included magmatic activity that is referred as Pan-African orogeny (Kennedy 1964). The Nile Craton in Egypt is completely covered by Phanerozoic sedimentary rocks except at Gabal Uweinat, where the Archean to Early Proterozoic rocks are exposed. Although, the exact boundary between the East African Craton and the former island arcs is not known, it is believed that the early Proterozoic continental crust extends eastward into the Eastern Desert underneath the Pan-African ophiolite and volcano-sedimentary cover

(El-Gaby et al., 1988). It crops out in the cover of large swells or gneiss domes in Central Eastern Desert, North Eastern Desert and Sinai. On the other hand these gneiss domes were referred to as Pan-African tier 1, which underlies an ophiolite and volcano-sedimentary sequence forming tier 2 (Bennet et al. 1983)

Extensive areas are covered by generally flat lying, undisturbed sedimentary strata of the Nubian Group (Klitzsch, 1983). Basement rocks occur as structural highs of varying size. The distance between some of them is several hundreds of kilometres and this, no doubt, restricts correlation of rock units. Fig 2 shows these areas as:

The Uweinat-Gabal Kamil basement inlier and the Bir Safsaf-Aswan uplift. Many smaller outcrops of basement rocks in both areas show the same rock associations as in the above mentioned basement inliers.

1-4-1 Gabal Uweinat – Gabal Kamil Basement Inlier

The major rock assemblages of the Gabal Uweinat-Gabal Kamil basement inlier were subdivided by Klerkx (1980) and Richter (1986) on the basis of their rock types and metamorphic grade into three units (Table 1) namely, the Granoblastite Formation, the Anatexite Formation and the Metasedimentary Formation. The Granoblastite Formation (Karkur Murr series) consists mainly of a group of pyroxene ganulites containing charnockitic, noritic, and diopsidic gneisses and metaquartzites. The Anatexite Formation (Ain Dua series) is dominated by migmatites interpreted as anatectic granulites and contains abundant supracrustal intercalations. The Granoblastite Formation (Karkur Murr series) underwent granulite facies metamorphism, high pressure–high temperature, while low pressure–high temperature for the Anatexite Formation (Ayn Dua series). The Metasedimentary Formation is a low to medium grade supracrustal sequences with intercalations of bimodal basaltic-rhyolitic rocks believed to be the source of the layered iron quartzite. The tectonic environment of these rocks is interpreted as an intarcontinental rift (Richter 1986).

Klerkx´s 1980	**Richter 1986**
------	Metasedimentary Formation
Ayn Dua Series (1840 Ma)	Anatexite Formation (1840 Ma)
Karkur Murr Series (2670 Ma)	Granoblastite Formation (2670 Ma)

Table 1 Compilation of the age and major rock units in the basement of the Uweinat region.

The intrusive rocks are among the most prominent features of the Gabal Uweinat region. They intruded most of the basement in the study area. Based on the general geologic setting, microscopic appearance and bulk composition, at least four principal suites were recognized by Richter (1986), these are:

1- Grey-green, calc-alkaline granitoids.

2- Red, alkaline granites (sensu strictu)

3- Prophyritic, calc-alkaline granitoids.

4- Alkaline syenitic to alkali-granitic ring complex

The major style of the folding of the basement is tight to tight-isoclinal folds. NNE to NE fold axis trends dominate, but locally they change to E-W. Axial surfaces are frequently overturned to the east. The deformation of the area occurred in the Early to Middle-Proterozoic, accompanied with and succeeded by a regional anatectic event (-1800 Ma) (Klerkx 1980, Cahen et al 1984).

1-4-2 Bir Safsaf-Aswan Uplift

The Bir Safsaf-Aswan uplift forms a major basement high in southern Egypt. Basement is exposed in three areas: Bir Safsaf, Gabal El Asr and Gabal Umm Shaghir. The Precambrian rock units are similar in all three areas (Bernau et al. 1987)

The oldest unit consists of high-grade gneisses of granitic composition, frequently with migmatitic structures. Intercalated into this series are amphibolites, marbles and calc-silicate rocks. Metagranodiorites and metatrondhjemites also occur within the granitic gneisses. This series could be the equivalent to Richter´s (1986) Anatexite Formation, except that granulites and granoblastites, like in the western part of the Gabal Kamil area are absent. However, detailed investigation of Schandelmeier et al. (1987) on the metamorphic development of calcsilicate rocks from the Bir Safsaf-Aswan uplift revealed P-T relationships which are very similar to those of the granulites and granoblastites from the Gabal Uweinat-Gabal Kamil area.

The migmatitic gneisses are intruded by small bodies of syntectonic S-type granites and disrupted by intrusions of late tectonic (Large ion lithophyle elements) LILE-enriched diorites, granodiorites and biotite-granites. Dykes and volcanic plugs of various ages are common (Schandelmeier et al. 1987).

The pre-Pan African deformational history is much more unclear than in the Gabal Uweinat-Gabal Kamil area. Migmatization, intensive fracturing and intrusion of granitoids have dislocated the original gneissic foliation in many places. Mylonitic

shear zones in the Gabal El Asr and Gabal Umm Shaghir areas (Fig 2), which generally strike E-W, post-date the migmatization, this can be clearly seen from quartz-c-axes fabrics (Bernau et al. 1987). The mylonitic shear surfaces seem to be related to thrust fault movements in the Late Proterozoic, contemporaneous with generally SW to W directed thrusting which occurred when the Nubian Shield was accreted onto continental Africa.

1-4-3 The Pan-African Basement in the Eastern Desert (East African Orogeny)

The term Pan-African was first introduced by Kennedy (1964) to describe the wide tectono-thermal events which affected much of Africa including the Arabian and Nubian Shields from 650 to 450 Ma ago. The time span of the Pan-African was expanded by Gass (1981) to 1.200-450 Ma and restricted to 950-450 Ma (Kröner 1984). The Pan-African belt in East Africa is composed mainly of two contrasting units (Pohl 1984): the Arabian-Nubian Shield in the north and the Mozambique belt in the south. El Gaby (1988) summarized the previous works and classified the Pan-African belt into three categories (Fig 3):

1-Ensimatic terranes of volcanic arcs and associated ophiolitic melanges which are the main characteristic belts of the Arabian-Nubian Shield.

2- Orogenically deformed upper Proterozoic sediments and igneous rocks deposited in “geosynclines” (e.g. Damara belt in Namibia),

3- Deformed and rejuvenated older basement rocks (e.g. Mozambique belt)

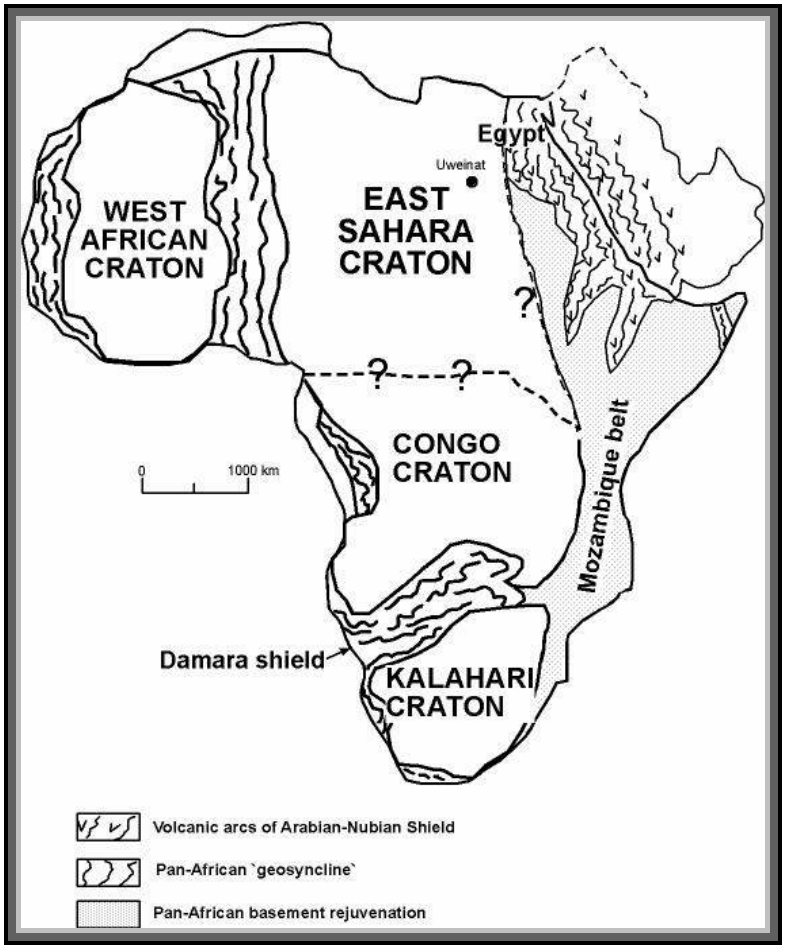

Fig 3 Generalized map showing the division of the African continent into cratons and orogenic belts (after Pohl 1984)

1-4-4 Pan-African Orogeny.

The Pan-African orogenic cycle has long been recognized as a period of major crustal accretion, where continental, island arc, and oceanic terranes were brought together to form the crystalline basement of the Gondwana supercontinent. Some parts of the Pan-African orogen are also characterized by continental collisional tectonics.

Areas of late Proterozoic tectono-thermal activity form a large part of the surface area of Gondwanaland particularly in Africa. The Pan-African system of mobile crustal zones comprises areas of tectonic, magmatic and metamorphic activity. These mobile zones separate Cartons that were tectonically stable during this period, such as the West African, East Shara Craton, Congo and Kalahari Cratons of Africa, Guyana-Brazil in South America, and Peninsula India.

The occurrence of the Nile Craton (pre-Pan-African rocks) beneath the Arabian-Nubian Shield is highly disputed. Many authors (e.g., Dixon and Golombek 1988; Abdelsalam and Dawoud 1991; Schandelmeier et al. 1983, 1987, 1993, 1994; Sultan et al. 1993; Greiling et al. 1994) concur that the boundary between the juvenile crust of the Arabian-Nubian Shield and the Eastern Sahara Craton (termed locally the Nile Craton by some of these authors) in Egypt and northern Sudan occurs as a north-south-trending line and Wadi Allaqi lies to the east of this line. Sultan et al. (1993) produced evidence from radiometric age dates (U-Pb and Pb/Pb on single and multi-grain zircons in gneisses) to support this position of the boundary.

El Gaby et al. (1984, 1988) from a synthesis of available geological, geochemical and radiometric age data initially for the central Eastern Desert and later for the entire Egyptian Pan-African rocks, supported an hypothesis that the continental cratonic crust extend eastward into the Eastern Desert underneath the Pan-African cover and is now exposed in several tectonic windows. On the other hand, and based on the field observations and structural analyses (e.g., Shackleton et al. 1980, Ries et al. 1983, Bennet and Mosley, 1987, Greiling et al. 1988,1994), it is argued that these windows represent metamorphosed island arc rocks pertaining to the Pan-African Orogeny.

1-5 Previous Work

The earliest scientific geologic report on the Uweinat area, that already mentioned the leptitic character of the basement along the slopes of the Gabal Uweinat massif is that by Menchikoff (1927). His early study included major-element analyses of 12 metamorphic and magmatic rocks. Menchikoff opt.cit accompanied the prince Kemal-El-Din-Hussein during the 1925 to 1926 expedition which was the first scientific survey of Gabal Uweinat. For about 40 years, geological research in this area was fixed on the sedimentary rocks, disregarding the basement, until Mahrholz (1968) published some radiometric age data from samples collected in the Uweinat region. In the early seventies, more information was supplied by Hunting Geology & Geophysics Ltd. (1974) who conducted exploration work on behalf of the Libyan Government. Klerkx and co-workers carried out fieldwork on the basement southeast of Gabal Uweinat during the mid and late seventies. Their results (Klerkx & Deutsch 1977, Klerkx 1980, Klerkx & Rundle 1976) improved the knowledge on this remote area considerably, providing fundamental information on its crustal composition.

Based on petrography and Rb/Sr whole rock age data, Klerkx (1980) recognized two major basement series

a) The granulitic Karkur Murr series at the eastern and southeastern slopes of Gabal Uweinat.
b) The migmatic Ayn Dua series, which crops out along the northern, western and southern margin of the massif.

Both series are separated by a clastic horizon, the II Passo mylonite as referred by Klerkx and Deutsch (1977).

In addition to geochronologic work on basement rocks, Klerkx & Rundle (1976) dated a number of magmatic rocks by the K/Ar method. Schandelmeier et al. (1983) and Schandelmeier & Darbyshire (1984) investigated the eastern extension of the area. Mapping of the area was performed by combined Landsat-MSS image interpretation and field checks, including intensive sampling. Based on the ideas of Klerkx (1980), Richter (1986) distinguished three basement formations by their lithofacies and metamorphic history. These three formations that can be partly correlated with Klerkx´s (1980) series, are: a) the high grade granulitic Granoblastite Formation as lower unit, overlain by b) the clearly remobilized Anatexite Formation, and c) the probably youngest, clearly bedded Metasedimentary Formation. The latter has no equivalent on the Libyan side whereas the other two correspond to Klerkx´s (1980) series in the following manner

Ayn Dua Series	=	Anatexite Formation
Karkur Murr Series	=	Granoblastite Formation

The contacts between the three formations are not clear because they are covered by extensive sand sheets (Richter 1986). Richter (1986) noted an “itabiritic sequence” of iron quartzite that crops out for several kilometres in the area. It consists mainly of quartz bands alternating with bands of hematite and goethite with relics of titanomagnetite. Bands of marble and amphibolites are present and represent a minor proportion of the Metasedimentary Formation.

In spite of the previous description of the Metasedimentary Formation including an itabiritic sequence, Richter & Schandelmeier (1986) mapped the area around latitude 22º 00' N and longitude 26º 00' E as Granoblastite Formation. Actually this is occupied by Banded Iron Formation and Anatexite Succession, while the itabiritic sequence according to their map is located at a ring structure in the Sudan to the east of the Gabal Kissu ring complex.

Conoco-Corporation (1987) compiled the geological maps of Egypt at scale of 1: 500,000 and used the classification made by Richter & Schandelmeier (1986).

In 1992 the Geological Survey of Egypt (EGSMA) and the Industrial Research Center of Libya (IRC), planned to map the border sheets through scientific cooperation. The work started at Arkenu in Libya and Gabal Nazar in Egypt. In later stages of the work, field mapping extended to cover the Gabal Kamil sheet in Egypt and Gabal Uweinat in Libya.

Said et al. (1998) concluded that the structure of the Banded Iron Formation is well defined showing folds, thrusts and wrench faults and late E-W normal faults.

Naim et al. (1998) stated that the Banded Iron Formation to the west of Gabal Kamil area represents a huge deposit of Banded Iron Formation. Mineralogical studies showed that the iron ore minerals are goethite, hematite and magnetite which alternate with silica bands. Sulphides occur in trace amounts and are represented by pyrite, chalcopyrite, pyrrhotite and galena. Gold was detected by Scanning Electron Microscope (SEM).

Greiling et al. (2000) stated that numerous layers of Banded Iron Formation and associated gneisses and amphibolites characterize the basement in southwestern Egypt. They strike broadly NNE-SSW and dip mostly toward WNW. Numerous repetitions of the Banded Iron Formation and shearing at their margins point to structural imbrications.

Khalid et al. (2000) reported the distribution of Banded Iron Formation in both SW Egypt and the Libyan territory, and stated that the Banded Iron Formation in this region was deposited chemically in three small separate basins: Uweinat, Arkenu, and Gabal Kamil.

Schenk et al.(2002) applied U/Pb dating of 1974 $^{+}/_{-}$ 4 Ma for the time of granulite-facies metamorphism and orogenic reworking in Uweinat area.

1.6 Objective of the Present Investigation

For the Uweinat area in NE Africa, no tectonic development models in Archaean – Early Proterozoic times are as yet available. Therefore, this work tries to answer some questions about the tectonic development of this area, namely:

What is the origin of the ultramafic-mafic rocks and their associated calc-silicates, which crop out only at a few locations?

What is the origin of the anatexite sequences with felsic and mafic bands?

How many deformation phases affected this area?

1.7 Methods

To answer the above questions, fieldwork and detailed mapping of the basement rocks were carried out in the study area during the winters 1998, 1999 and 2001 for about 8 months altogether.

The petrological characteristics and contact relationships between the different rock units were examined along traverses crossing the whole area in an East-West direction. These traverses were generally perpendicular to the strike of the rock units, and major structures.

A detailed field geologic-structural map and two cross sections A-A` and B-B´ for the whole area were prepared using field data, aerial photographs and Landsat images.

In addition, detailed structural geological maps were prepared for four sub-areas (A, B ,C and D), to show the different minor structures which were recorded and documented during fieldwork.

Detailed petrographic studies of the different rock units were carried out to determine their compositional character and the effect of deformation on each rock unit. About 125 rock specimens, representing the different rock units, were collected. From these samples more than 100 thin sections were examined. Microstructural studies attempted to determine the transport direction from about 40 oriented thin sections parallel or perpendicular to the foliation and the lineation.

For the geochemical characterization of the different rock units encountered in the study area, 25 selected samples were analyzed for major and trace element contents using XRF and spectral analysis techniques. These analyses were carried out in the laboratories of the Geological Survey of Egypt.

Anisotropy of magnetic susceptibility (AMS) was determined for 31 oriented samples, from which 200 cylinders were cored. The magnetic susceptibility measurements were carried out with the susceptibility bridge KLY-2 (GEOFYZIKA BRNO, CSFR, JELINEK 1980).

CHAPTER 2

ROCK TYPES AND LITHOSTRATIGRAPHY

2- Rock Types and Lithostratigraphy

The rock types outcropping in the study area are shown in the geological map (Fig 2.1), while (Fig 2.1a) shows samples location map of the oriented samples. The succession of the rock units in the area (Fig 2.2), starting with the oldest is as follows:

A- Sedimentary rocks:

7 - Sand Dunes

6 - Phanerozoic cover

B- Basement:

5 - Dykes

4 - Young Granites

3 - Banded Iron Formation (BIF).

The BIF consists of four units, with gradational contact between them. The stratigraphy of the units is shown below

iv- Meta-chert and jaspilite bands

iii- Well-banded iron-silica succession

ii- Fuchsite-bearing quartz bands

i- Metapelite volcanosedimentary bands alternating with iron-silica bands (Algoma-type).

The upper three units represent the upper BIF (iv, iii, ii), they have a Superior-type BIF character, while the lower unit (i), the base of the BIF, has Algoma-type character

2 - Anatexite Sequence

The Anatexite sequence consists mainly of migmatitic rocks with leucosomes and melanosomes. Leucosomes comprise the leucocratic, quartzofeldspathic or feldspathic fraction of the rock. The melanosome is the melanocratic, mafic-rich fraction of the migmatitic rock, complementary to the leucosome.

1 – Ultramafic-mafic and calc-silicate rocks (UM).

These rock units are treated in ascending sequence, with the stratigraphic lowest and probably oldest rocks first.

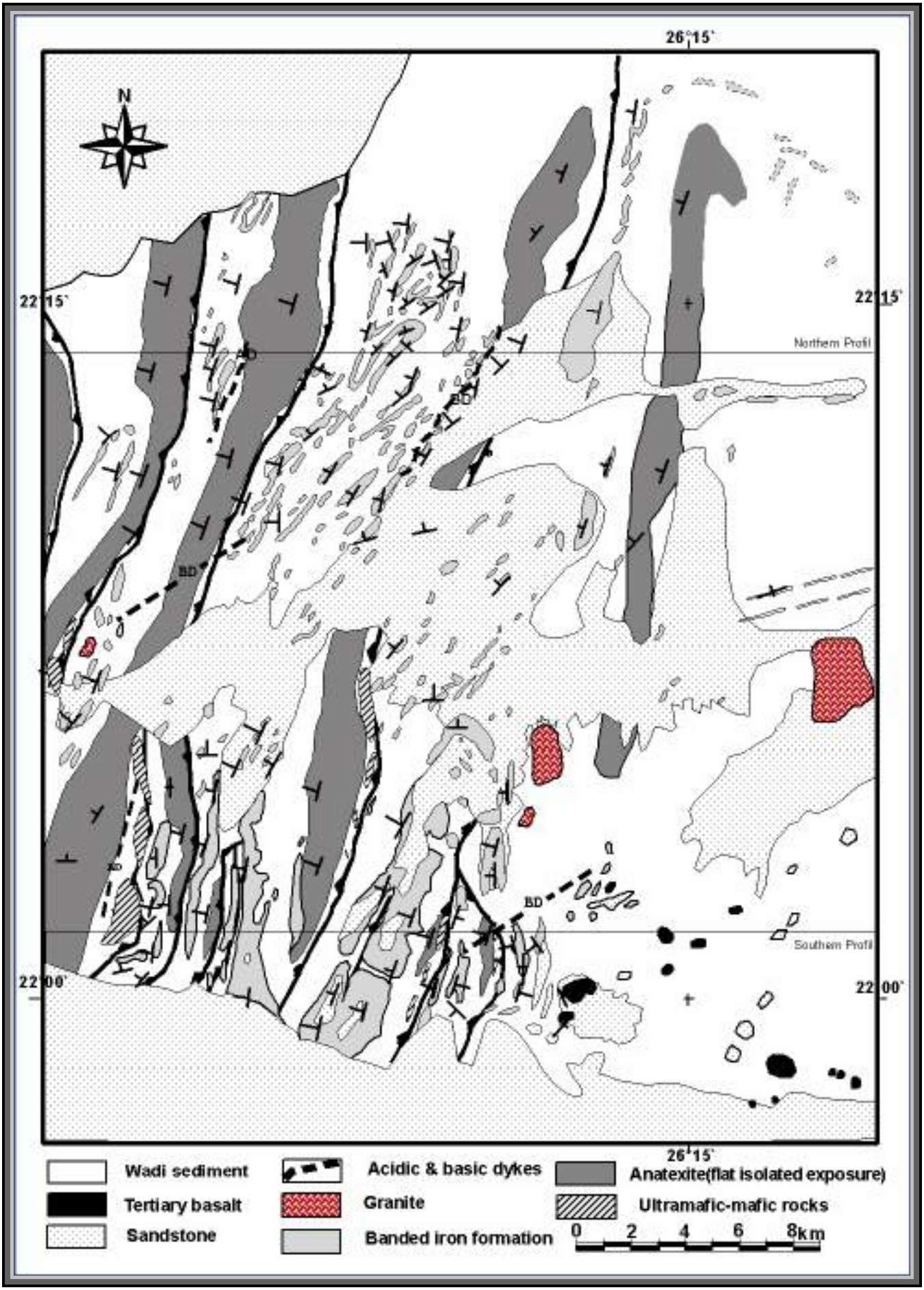

Fig 2.1 Geological map of the study area

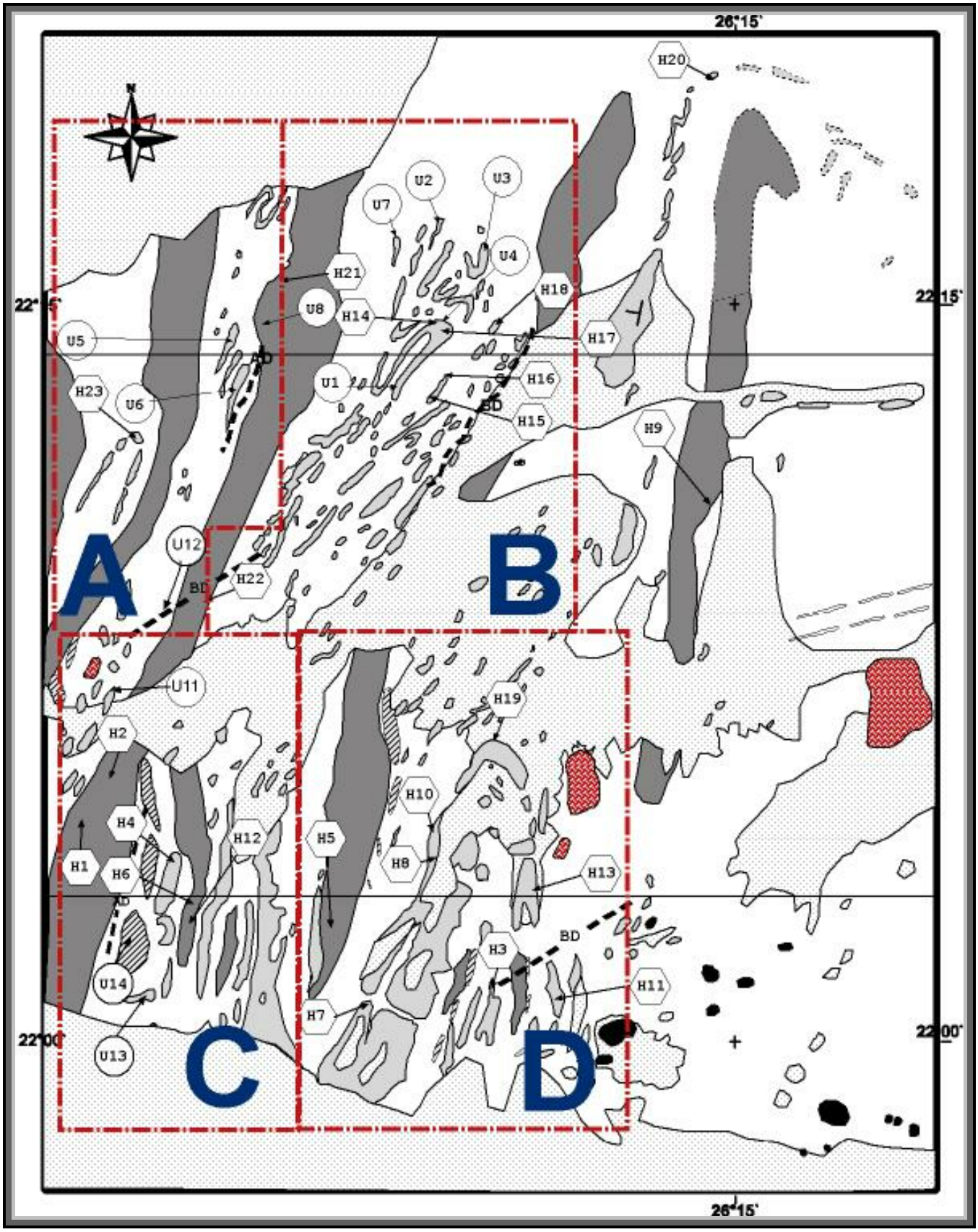

Fig 2.1a Sample and Sub-areas location map in the study area (oriented samples)

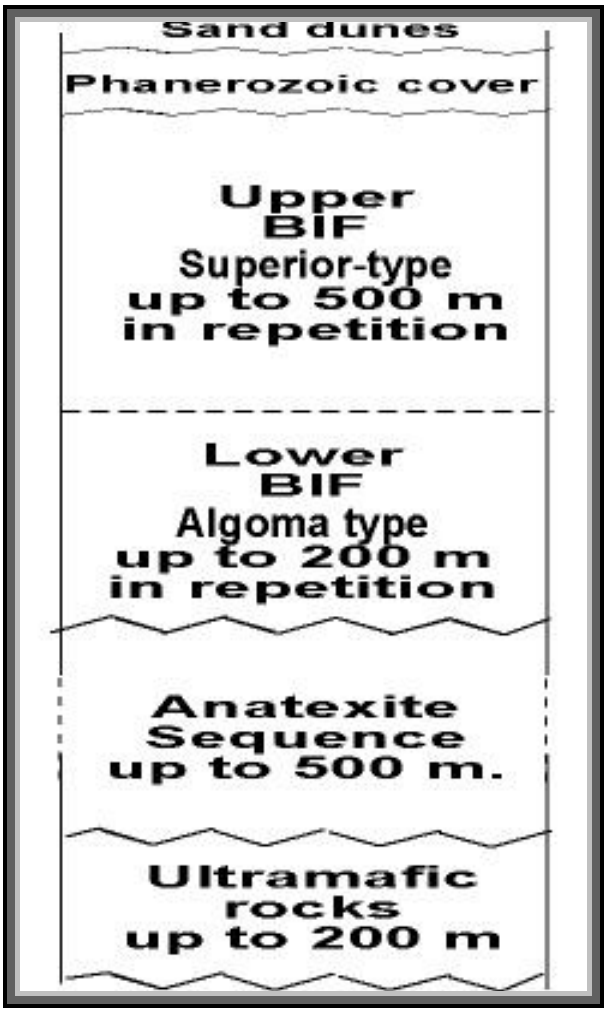

Fig 2.2 Shows the main succession in the present area.

2.1 Ultramafic-Mafic and Calc Silicate Rocks

The ultramafic-mafic and calc-silicate rocks (UM) are exposed as spots or bands beneath the Anatexite Sequence in some localities of the area, especially in the southern part. These rocks represent less than 5% of the rock units here. They are highly deformed as shown in Figures 2.3, 2.4 and 2.5. The rocks are grey to green, fine to medium-grained, and their outcrops are often obscured by a sandy veneer. In the southern part of the area some bands trend NNW-SSE with 45°dip angle to the SW and extend for more than 4 km at the wadi level with widths of more than 50 metres. These bands consist mainly of forsterite and/or spinel marble, minor serpentinite and highly deformed, fine-grained gabbro-norite. To the southwest of the present area, the exposures of the UM are represented by bands and spots of highly deformed gabbroic rocks, serpentinite and talc-carbonate, grading upward, and alternating with the melansome in the Anatexite Sequence.

These rocks show rusty brown, brownish green and greyish weathered surfaces with brownish, white veinlets giving a characteristic mesh structure. In places, these rocks contain black nodules of forsterite or spinel minerals. The contact between the UM and the underlying BIF is tectonic. The tectonic contact is a thrust, parallel with the main thrusts elsewhere in the investigated area.

Generally these rocks consist essentially of interlayered wherlite (olivine + clinopyroxene ± chromite cumulates) and clinopyroxenite (cpx cumulates) and gabbro (cpx + plagioclase cumulates). Olivine compositions are quite forsteritic. The rocks are variably transformed into foliated metamorphic equivalents (talc-tremolite serpentinite, talc-serpentine tremolitite, hornblendite, amphibolite) characterized by pervasive metamorphic recrystallization under amphibolite facies metamorphism.

The presence of olivine and spinel in these ultramafic-mafic rocks indicate that their parent rock was formed at a relatively high temperature and high pressure, and originated in the upper mantle.

2.1.1 Spinel (Forsterite) Marble

The microscopic study of the spinel (forsterite) marble shows mainly interlobate calcite and dolomite crystals with polysynthetic twinning, with anhedral to subhedral crystals of olivine, serpentine +/- spinel, +/- orthopyroxene, minor amounts of iron oxide and inclusions of recrystallized quartz (Figs 2.6, 2.7). The olivine occurs as anhedral to subhedral crystals, highly cracked and altered to serpentine along their cracks.

Fig 2.3 Ultamafic (UM) rocks alternating with gabbroid (gab) rocks in the wadi between sub-areas (C & D) (looking east).

Fig 2.4

Fig 2.5

Fig 2.4 Bands of spinel marble (grey), show alternation between spinel rich and carbonate rich marble bands in sub-area (C).

Fig 2.5 Ultramafic rocks composed of alternating bands of serpentine (greenish grey), spinel marble rich in olivine (olive to dark grey), aggregates of forsterite (greenish black) in sub-area (D).

The alteration is clear in the crystal cores and along curved fractures and rims. These crystals exhibit greyish colour due to serpentinization. They contain inclusions of carbonate and iron oxides. The curved fractures are filled with secondary magnetite, antigorite and carbonate giving the characteristic mesh texture.

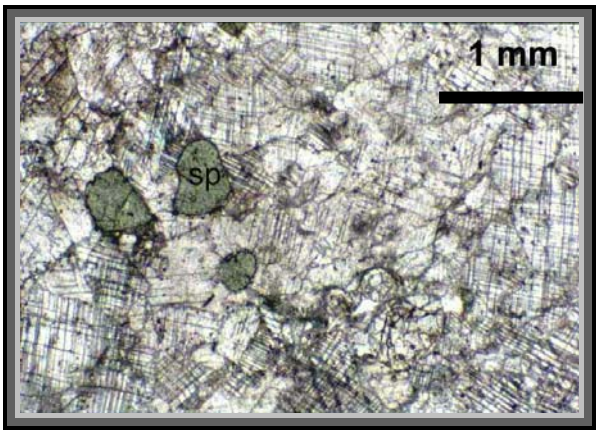

Fig 2.6

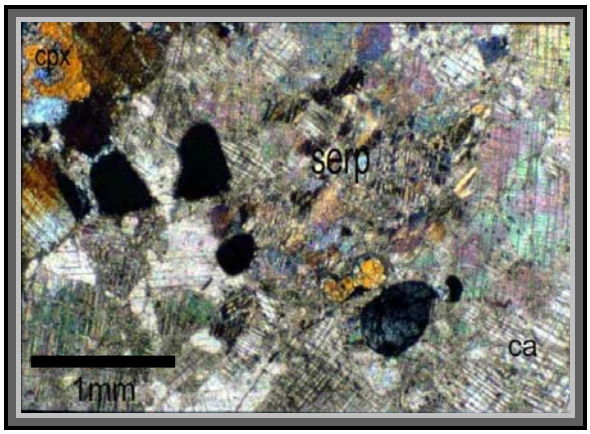

Fig 2.7

Fig 2.6 Calcite-dolomite with interlobate texture, spinel (sp) with green colour, subhedral crystals and high relief. Sample No U-14 PPL. (Plane Polarized Light).

Fig 2.7 The same photomicrograph under C.N (Crossed Nicols) highlights some serpentine (serp), olivine and clinopyroxene (cpx). Sample Nr U-14 from sub-area (C).

The serpentine is fine to medium grained and exhibits pseudomorphs after olivine (Fig 2.8) and it often breaks down to talc and carbonate. Irregular antigorite inclusions are also present within the olivine crystals and along their fractures. Orthopyroxene (enstatite) shows also anhedral to subhedral crystals with rounded edges, perfect cleavage, with grey to yellow interference colours, and high relief. Spinel crystals have a light green colour and are isotropic under crossed nicols. Spinel crystals are also anhedral to subhedral with rounded edges and high relief. Orthopyroxene shows alterations to serpentine and talc carbonate. The rocks do not show any clear minor structures because they are highly altered and recrystallized.

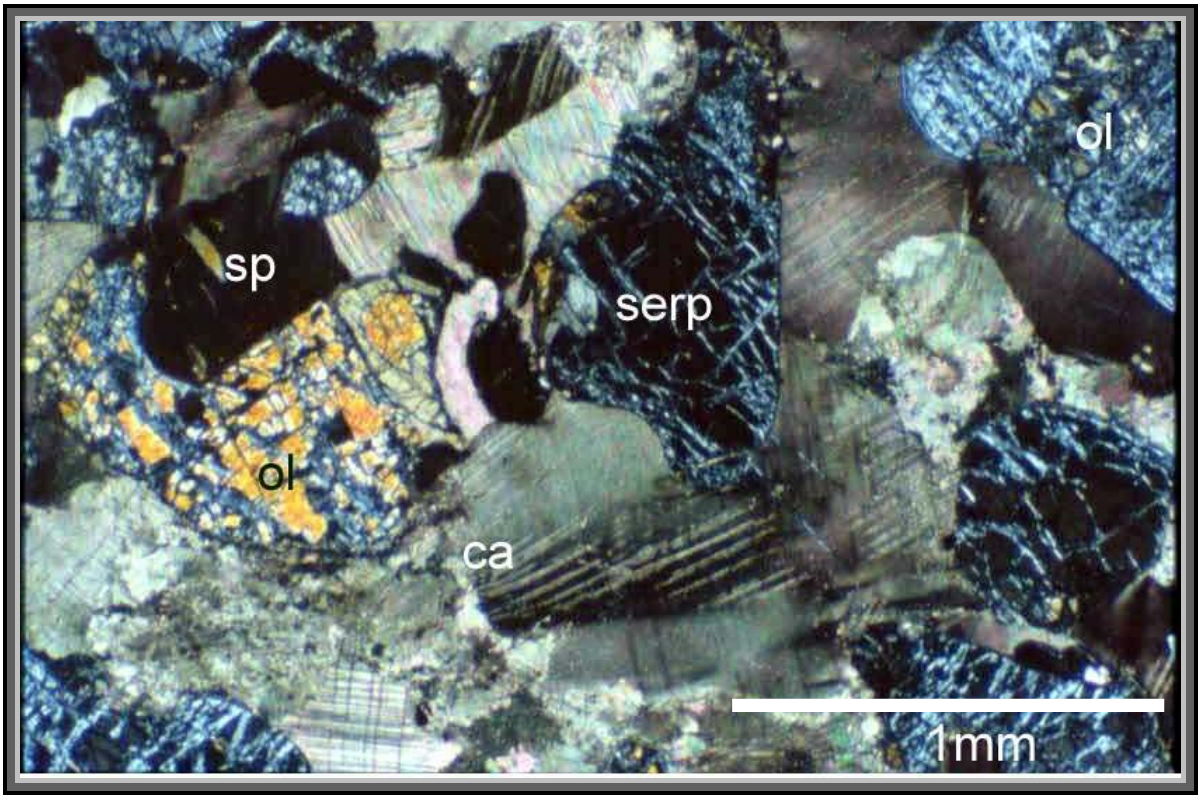

Fig 2.8 Calcite (ca) with polysynthetic twinning, serpentine and talc (serp) pseudomorphs after olivine (ol). The isotropic crystals (black) represent spinel (sp) with some remnants of olivine. Sample No. U-14, sub-area C. (C.N).

2.1.2 Serpentinite and Talc Carbonate

Serpentinite and talc carbonate show grey and brown colours with coarse grained texture. The serpentine shows strongly corroded remnants of olivine and pyroxene in networks of serpentine with mesh structure. The rock shows serpentinization from olivine and pyroxene. Calcite and talc are often common at the border of the

serpentine grains forming mesh texture (Fig 2.8). The carbonate shows rhombohedral cleavage of polysynthetic twinning. Some hematite and magnetite occur as secondary minerals. Magnetite is the predominant opaque mineral. It occurs as black irregularly scattered grains and as secondary mineral after olivine.

2.1.3 Gabbro-Norite Rocks

Under the microscope the gabbro-norite rocks are fine to medium-grained and consist mainly of plagioclase, orthopyroxene and clinopyroxene. The plagioclase is of calcic-type, represented by labradorite (An50). It is highly saussuritized and displays cloudy appearance. Orthopyroxene is represented by hypersthene. It forms rimmed-crystals with distinctive mesh-texture and partially altered to chlorite and talc. The clinopyroxene is represented by augite, partially altered to hornblende or/and chlorite. The thin sections in figures 2.9 & 2.10 show plagioclase and chlorite pseudomorph after pyroxene.

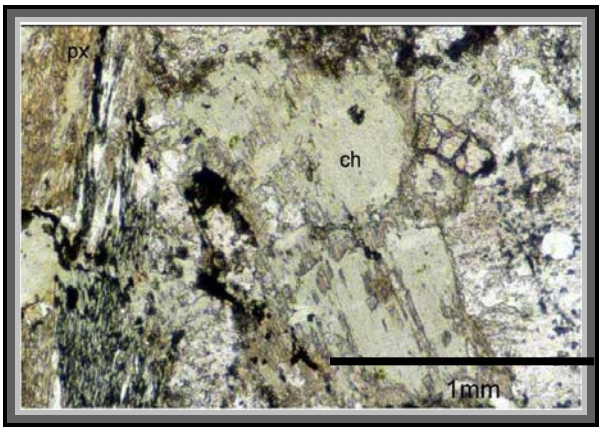

Fig 2.9

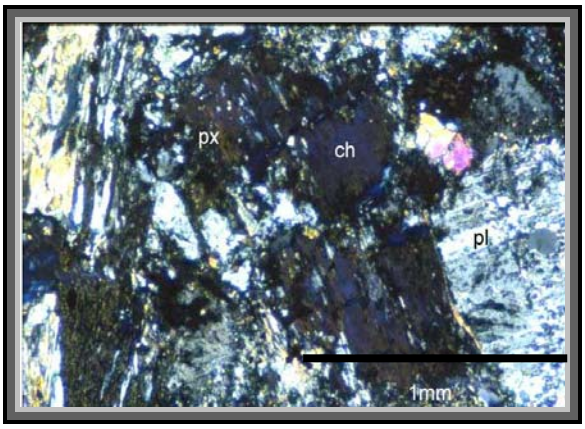

Fig 2.10

Fig 2.9 Gabbro-norite showing chlorite (ch, greenish brown) pesudomorph after (px) orthopyroxene Sample No. H-6 (PPL.)

Fig 2.10 The gabbro-norite showing plagioclase with weak albite twinning (pl) and chlorite (ch) pesudomorh after opx (px, blueish brown). Sample No. H-6, sub-area C (C.N).

2.2 Anatexite Sequence

In the investigated area the Anatexite Sequence is usually found in the valleys as isolated exposures of low relief, consisting of leucosome and melanosome bands.

The leucosome bands with felsic components are buff grey to white, medium to coarse grained, and composed mainly of quartz and alkali-feldspar.

The melanosome bands of mafic components are greyish green to dark green, fine to medium-grained, and are composed mainly of amphibole and plagioclase. Both bands are arranged in layers or schlieren and as patches (Figs 2.11 & 2.12).

A unique feature of the Anatexite Sequences is the replacement of a primary prograde mineralogy by later retrograde mineral assemblages, or even more than one.

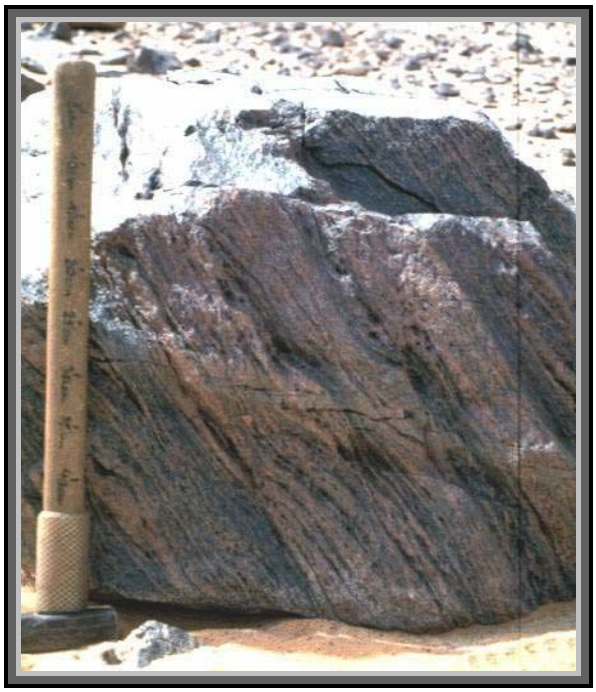

Fig 2.11

Fig 2.12

Fig 2.11 Light and dark bands in the Anatexite Sequence (view to the south in the sub-area (A)

Fig 2.12 A polished surface of the Anatexite Sequence showing the dark and light bands at centimetre scale.

The Anatexite Sequence covers about 30% of the outcrop surface in the investigated area. The banding trends NNE-SSW and dips about 65° toward NW. The Anatexite Sequence has a thickness ranging from 500 metres to more than 2 kilometres, the extension along strike may exceed 20 kilometres. The thickness of the leucosome and melanosome bands varies between a few centimetres to a few metres. Generally the leucosome bands show medium to coarse-grained or pegmatitic textures, while the melanosome exhibits finer-grained texture. Individual anatexite bands can generally be followed for short distances because the exposures are interrupted by Phanerozoic cover rocks or sand dunes.

The contact with the underlying ultramafic-mafic rocks is mostly a secondary, transitional contact with an increase in the mafic minerals toward the gabbroic, serpentinite and related rocks. The direct contact between the Anatexite Sequence and the overlying BIF is very rarely observed. Tectonic contact between the Anatexite Sequence and the lower part of the BIF indicate detachment thrust fault, due to the early south-north maximum stress. The Anatexite Sequences is overlain by metapelitic bands alternating with iron-rich and silica-rich bands. This alternation contains a high amount of garnet and subordinate orthopyroxene minerals (enstatite and hypersthene), and calcite.

2.2.1 a- Petrographic Study of the Anatexite Sequences

The characteristic feature of the Anatexite Sequence is the predominance of migmatic gneiss, i.e. diatexites, metatexites and metablastites. Whereas the highly mobilized, medium-grained diatexites are of a homogeneous to nebulitic texture, rarely showing foliation, metatexites and metablastites are well-foliated and a two-phase nature - melanosome and leucosome – becomes obvious, arranged in the form of layers or schlieren and patches.

These rocks exhibit seriate granoblastic or porphyroblastic and in places equigranular textures, and are composed mainly of intermediate plagioclase, orthopyroxene, hornblende, biotite, and chlorite with subordinate amounts of quartz in the melanosome, and alkali-feldspar, quartz, orthopyroxene, biotite, and chlorite in the leucosome. In general, plagioclase is idioblastic and strongly saussuritisized. Later albite or albite-rich plagioclase is unaltered. Antiperthite was occasionally formed. Alkali-feldspar is variably shaped and appears as microcline, perthite or mesoperthitic-chessboard-albite. The perthites tend to form megablasts. Two types of quartz dominate in the leucosome, the older one is deformed and shows large grains with wavy extinction, while the later phase one is fine grained and recrystallized. Quartz occurs as anhedral grains, which are stretched and display ribbon structure and predominantly is rich in inclusions. Brownish-green biotite is the dominant mafic component and shows replacement by intergrown, subparallel chlorite. The chlorite, sphene and/or epidote are dominant in most samples. A similar alteration may be seen in the subordinate green hornblende. Orthopyroxene is represented by hypersthene which occurs as skeletal-shaped anhedral grains, partially altered to talc and chlorite. Cordierite, if present, occurs as anhedral grains or irregular porphyroblastic grains with numerous inclusions of quartz.

Rarely, pale green clinopyroxene is present in relics, enclosed by chlorite, biotite or hornblende. Talc, actinolite, sericite, and chlorite appear as further retrograde alteration products (Richter et al. 1986).

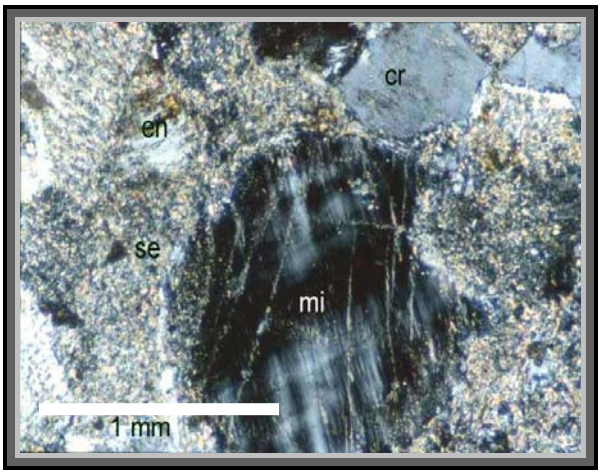

Fig 2.13

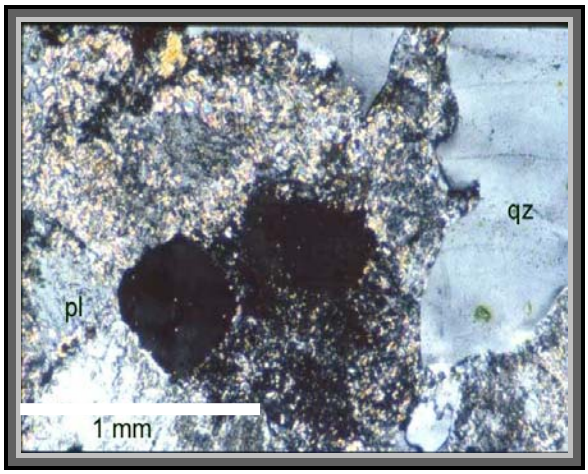

Fig 2.14

Fig 2.13 Dark anatexite band showing a large microcline crystal surrounded by sericite, cordierite (cr) and altered enstatite (en). Sample No. U-8, sub-area (C), (C.N.).

Fig 2.14 Light anatexite band showing alteration in plagioclase (pl) to sericite with granoblastic texture with the wavy extinction quartz, iron oxides are also present. Sample No. U-8, sub-area (C), (C.N.).

2.2.1.b Microscopic Study:

Microscopically the Anatexite Sequence is composed of plagioclase, alkali-feldspar (microcline), quartz (Figs 2.13 and 2.14), biotite, amphibole, cordierite and altered pyroxenes (Fig 2.15). Locally, subordinate orthopyroxene, cordierite, and iron oxides occur additionally. In general, plagioclase is idioblastic and strongly saussuritisized. Younger albite or albite-rich plagioclase is unaltered. Antiperthite has occasionally developed (Fig 2.16). Alkali-feldspar is variably shaped, being microcline or perthite. The perthites tend to form megablasts. Quartz has predominantly grown interstitially, is rich in inclusions and often shows ribbon structures. The orthopyroxene (enstatite and hypersthene) coexists with cordierite. Cordierite often shows a mesh texture, and was breakdown to hornblende or biotite and / or chlorite (Fig 2.15 & 2.16). This shows the retrograde metamorphism from granulite facies to amphibolite facies or even upper green-schist facies.

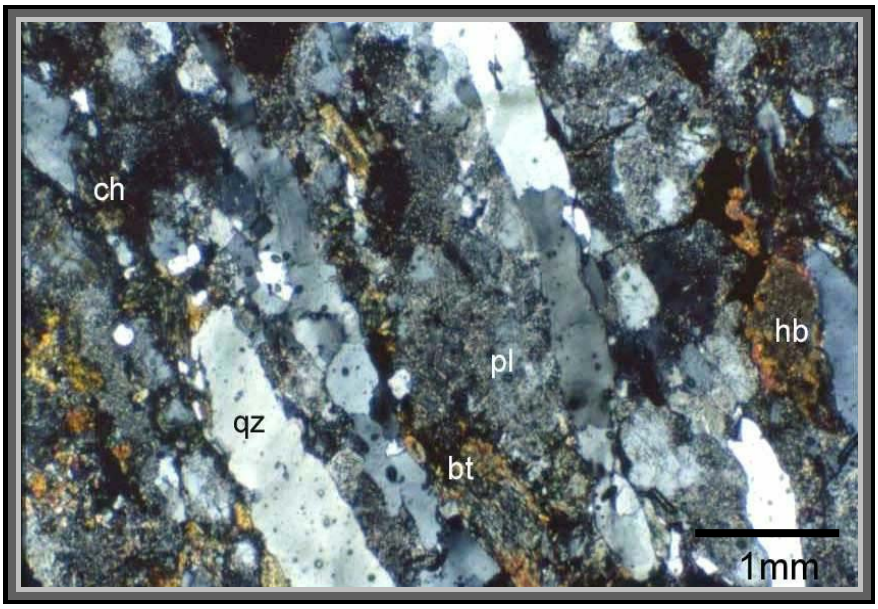

Fig 2.15 Anatexite band showing bands alternation and exhibit a large elongated quartz (qz) with wavy extinction, altered plagioclase (pl), hornblende (hb), biotite (bt) and chlorite (ch), a gneissic texture is clear. Sample No. H-5, sub-area (D),(C.N.).

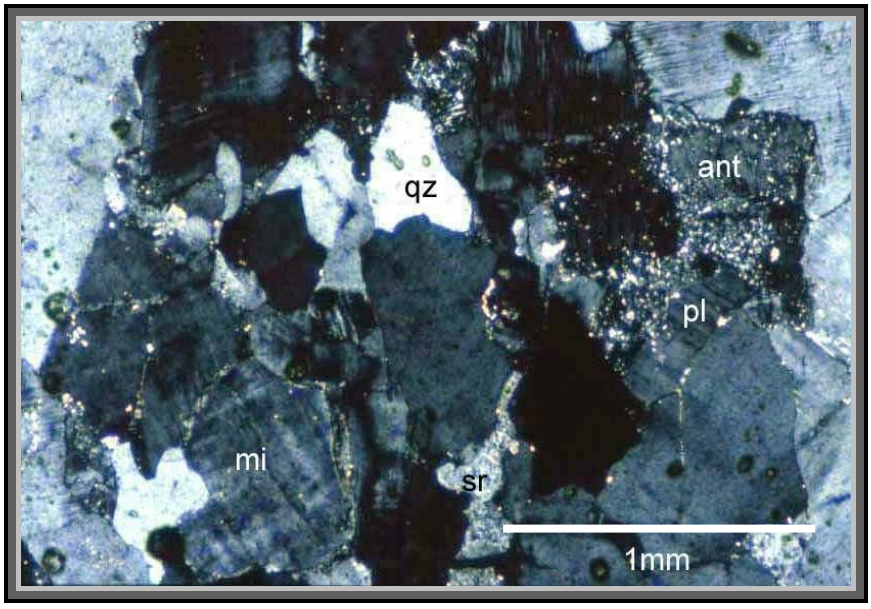

Fig 2.16 Light anatexite band showing microcline (mi), antiperthite (ant), quartz (qz), sericte, chlorite and some iron oxide. Sample No. H-21, sub-area (B), (C.N.).

2.3 The Banded Iron Formation (BIF)

The BIF represents about 30 % of the rock units cropping out in the investigated area. It crops out in a repetition of elongate low to moderate hills with an average elevation of 50 to 70 metres above the ground level, and trending NNE (Fig 2.17).

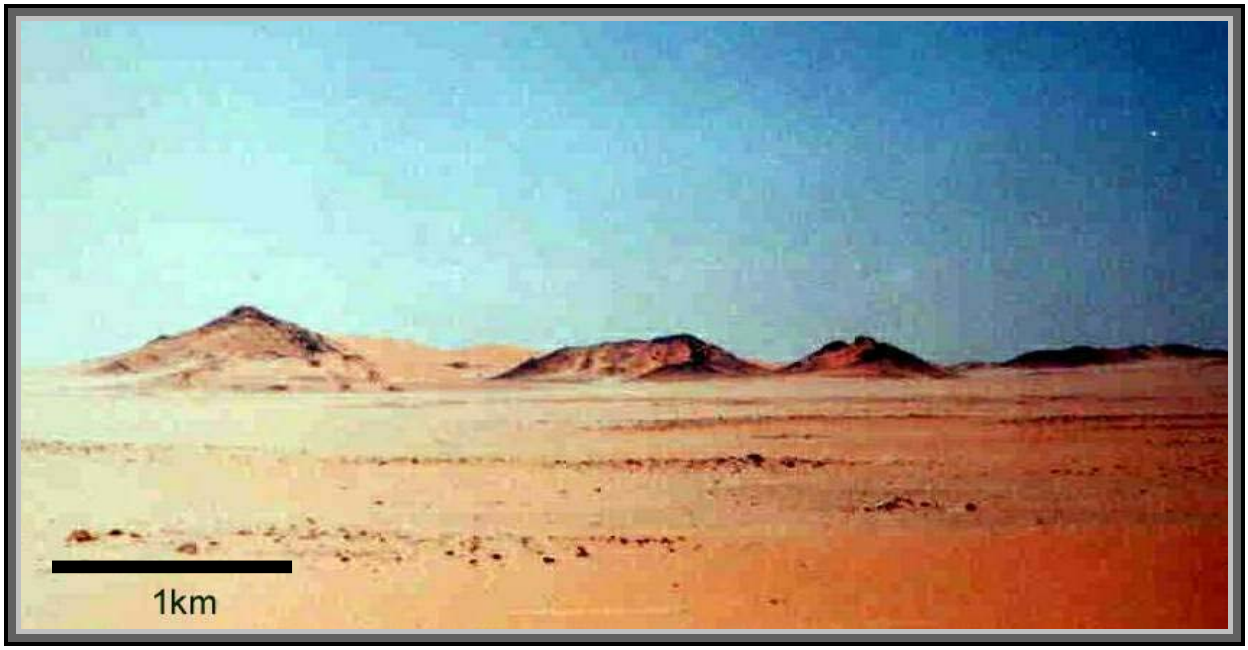

Fig 2.17 General view of the BIF hills in the north of the sub-area A (view to the south)

The BIF is built up of accumulated clastics of psammitic and subordinate pelitic character. The BIF bands are well-foliated and generally fine-grained. The lower part of the BIF exhibits a frequently cataclastic metamorphism, but some parts still show weak graded bedding. The BIF succession consists of variegated bands with colours of yellow, red, brown, black and grey. The iron-rich bands are composed of black magnetite and dark greyish brown and red hematite alternating with quartz bands, whereas the silica-rich bands consist mainly of quartz or chert and jaspilite. Generally, the chert bands dominate in the upper parts of the BIF while the quartz bands (metamorphosed chert bands) increase toward the base. Chert and jaspilite bands occupy the top of the formation. The chert contains more hematite and shows remnants of thin layering in contrast to the quartz rich bands in the middle and lower part of the BIF succession. On the basis of their structural position the BIF beds seem to be younging toward west. The iron oxides and magnetic minerals in the BIF bands are distributed in different proportions as is described in Chapter 6 (AMS).

The BIF differs from base to top as follows:

- Metapelitic and volcanosedimentary bands, consist mainly of altered feldspars, quartz, biotite, carbonate and garnet. These bands are highly deformed and show cataclastic texture, due to the early dynamic deformation. They range in thickness from a few metres to more than twenty metres. These bands alternate upward with iron-rich and silica-rich bands ranging in thickness between few centimetres and more than half metre (Fig 2.18). The metapelitic and volcanosedimentary bands are overlain by fuchsite bearing quartz bands.
- Fuchsite bearing quartz bands have a thickness of up to 100 metres. They alternate with deformed quartz bands. The fuchsite bearing quartz bands are a light green and consist mainly of quartz, fuchsite and iron oxide. The deformed quartz bands are a white to grey and consist mainly of quartz with subordinate amounts of iron oxides. Generally, the bands exhibit penetrative foliation parallel to the primary banding. The thicknesses of the alternation between the fuchsite bearing quartz and the deformed quartz bands range between 3 and 1 metres respectively. The quartz bands are overlain by well banded iron-silica bands.
- The well banded iron-silica bands show a gradational boundary with the underlying fuchsite bearing quartz bands over a few meters contact. In the lower part of these bands the silica-rich bands dominate as a few metres thick, while the iron rich bands are a few cm thick. In the upper part, however the thickness of the iron-rich bands increases to few metres of magnetite-hematite rich bands, while the silica rich bands are only a few cm thick.
- Lower part of the iron-silica-rich bands often contains highly altered mylonite zones due to an earlier shear zone. The upper parts of these bands alternate by with overlying chert bands. The magnetite-hematite rich bands are interlayered with brown to yellow chert bands. The thickness of the chert bands ranges between a few centimeters, at the border with the magnetite-hematite rich bands, to more than five metres toward the top of the BIF and exhibit a red to yellow colour due to the increase in iron oxides (Fig 2.19).

All of BIF bands strike NNE parallel to the regional strike direction and have dips ranging between 10° and 70° to the WNW. Most of the BIF bands are separated by shear zones and mylonite bands, developed during the south-north maximum stress.

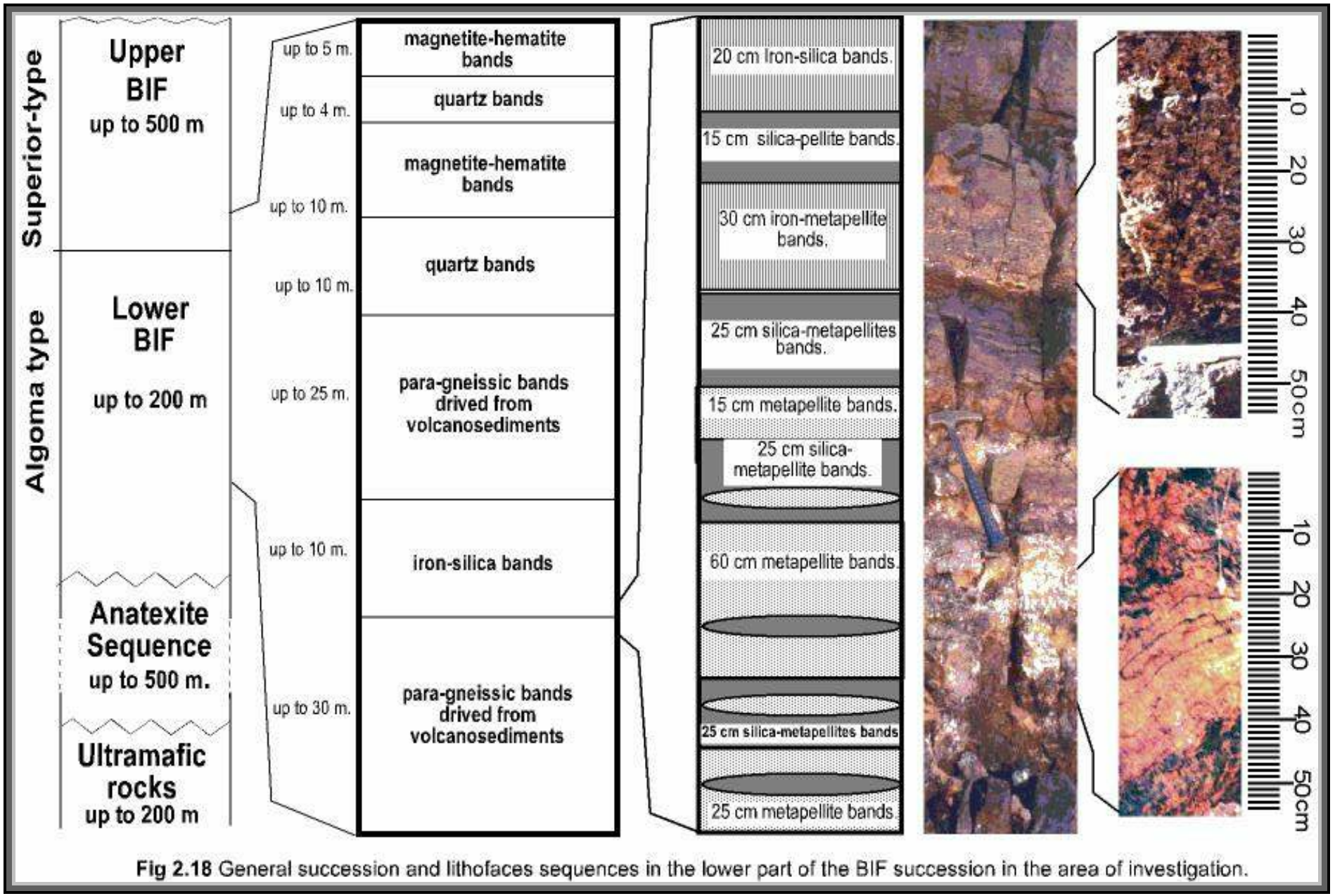

Fig 2.18 General succession and lithofaces sequences in the lower part of the BIF succession in the area of investigation.

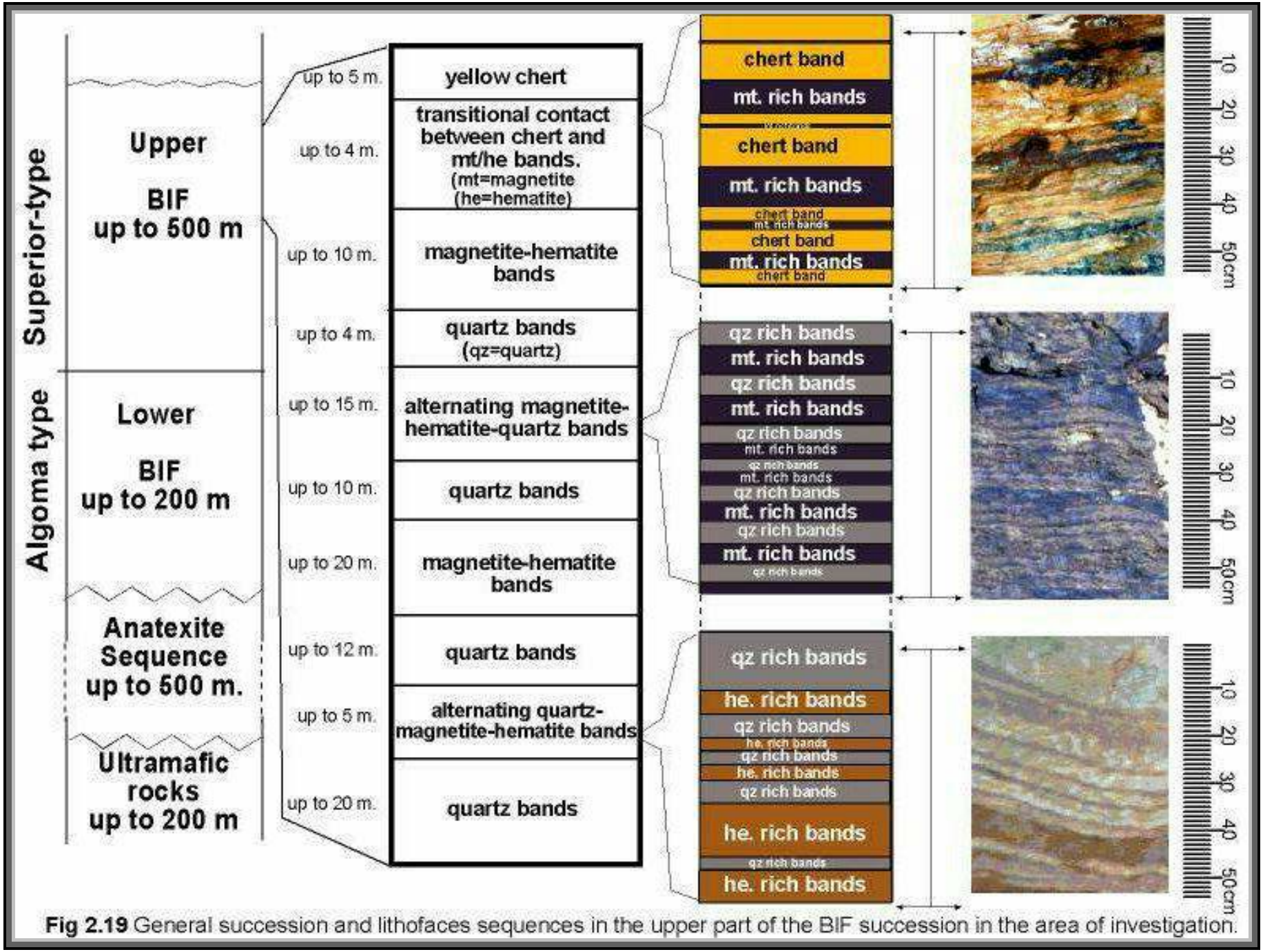

Fig 2.19 General succession and lithofaces sequences in the upper part of the BIF succession in the area of investigation.

2.3.1 Meta-chert,

The meta-chert is hard, extremely dense or fine-grained crystalline rocks and shows alternations of microcrystalline quartz and relics of primary deposition. The meta-chert is composed mainly of quartz, hematite and subordinate amounts of opal and chalcedony. The crystalline silica bands are a few millimetres in thickness, while the dense silica bands exhibit thicknesses ranging between a few centimetres and more than one metre. These bands show colour variations from the top to the base depending on the iron oxide content, which increases from top to base. Consequently colours range from light yellow at the top to yellow, red or brown at the base. In the field, the chert is exposed as high ridges composed of well banded chert (Fig 2.20) or large chert fragments with more than 20 centimetres of diameter. Highly sheared and brecciated bands occur mostly adjacent to shear zones are parallel with the banding and major thrusts and show minor cleavage parallel to the major thrust surfaces (Fig.2.21). The thickness of the chert bands ranges between 5 and 10 metres, extends for a few km in NNE-SSW direction. In some places of the study area the chert bands alternate with jaspilite bands. The quartz grains are sometimes stained with reddish brown colour as an indicator for hematite minerals, giving rise to jasper, a variety of chert associated with iron oxide ores and containing iron-oxide impurities that give it various colours (here red or yellow to brown). The chert bands show well developed bands in some exposures or highly brecciated bands in others. The fragments have diameters from a few millimetres to more than 70 centimetres. These fragments are welded with hematite and iron oxides. This breccia represents a fault breccia. The chert bands have mostly low magnetic susceptibility in comparison with the other BIF bands (see AMS, chapter 5).

2.3.1.1 Microscopic Study of the Chert Bands

Microscopically, the chert bands exhibit microcrystalline texture in the well-banded chert, which indicate a primary deposition. The bands, which close to the thrust surfaces showing cataclastic structure in the brecciated bands. They consist mainly of quartz and hematite (Fig 2.22). In places, zones or halos exhibit different concentrations of secondary hematite and recrystallized quartz (Fig 2.23).

Fig 2.20

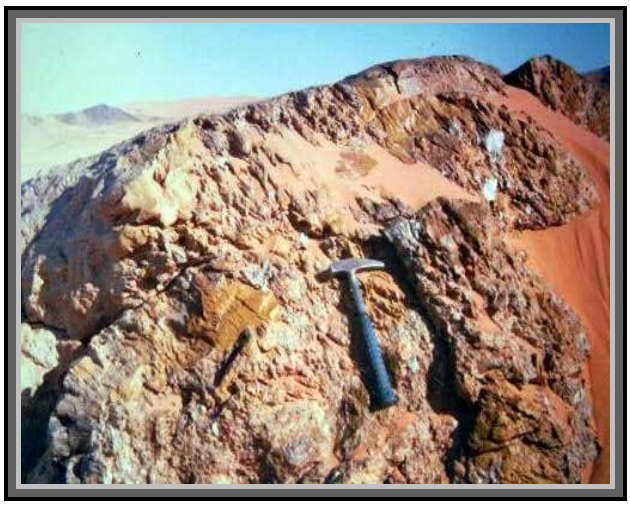

Fig 2.21

Fig 2.20 Well banded light coloured chert alternating with brown chert. Foliation is parallel to bedding planes of the bands (view to the west in sub-area A)

Fig 2.21 Highly sheared and brecciated chert, cleavage parallel with the thrust surface (view to the east in sub-area B)

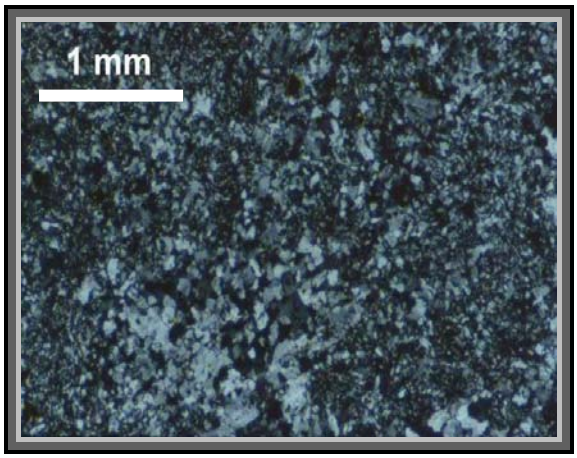

Fig 2.22

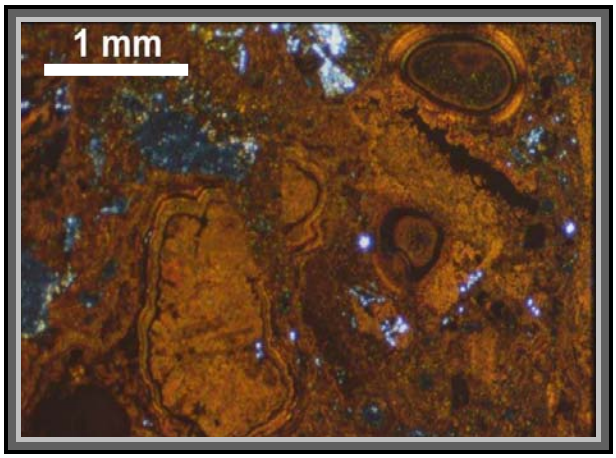

Fig 2.23

Fig 2.22 Very fine-grained meta-chert composed mainly of fine-grained quartz and iron oxides. Sample No. U-7, sub-area B, (C.N).

Fig 2.23 The brecciated meta-chert showing zoning of secondary hematite and recrystallized quartz grains. Sample No. H-3, sub-area D, (PPL).

The meta-chert also contains some chalcedony in the shape of concretionary masses with radial fibers and concentric texture and also amorphous silica as opal. It sometimes contains impurities such as calcite and iron oxides. In addition, recrystallized quartz is present as inclusions. Hematite is concentrated in spots showing zoning, often adjacent to quartz, which developed around the hematite aggregates during deformational processes.

Jasper bands are composed mainly of fine-grained quartz and hematite (Figs. 2.24 & 2.25).

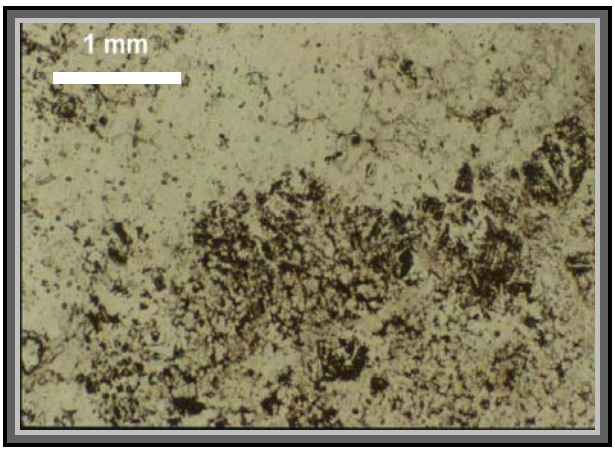

Fig 2.24

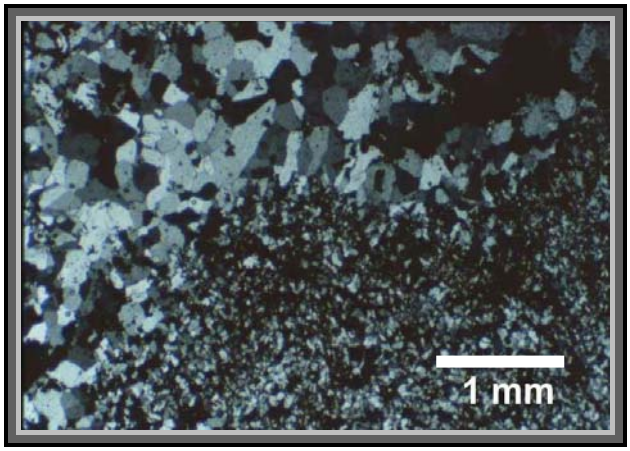

Fig 2.25

Fig 2.24 Jasper band showing mainly hematite and fine-grained graded-bedded quartz. Sample No. H-7, sub-area D, (PPL)

Fig 2.25 The same as Fig 2.24 with cross nichols showing hematite (dark brown), fine-grained quartz and recrystallized quartz in the jasper.

2.3.2 Well-Banded Iron-Silica Bands

Well-banded iron-silica bands often underlie the chert-jaspilite bands and are composed primarily of magnetite-hematite-rich bands alternating with quartz-rich bands. The magnetite-hematite-rich bands show alternation with quartz bands. The thickness of quartz bands increases to the east and the thickness of the iron rich bands decreases in that direction. This alternation of magnetite-hematite-quartz bands is more than 50 metres thick. It is parallel to the overlying chert bands, and the trend is 010°/70°.

The magnetite–hematite bands constitute hard rocks of very fine-grained iron-rich greyish black bands. The mineral assemblage is mainly deformed quartz bands alternating with iron-rich bands mainly composed of hematite, goethite and magnetite. The magnetite is clearly observed to be the original iron mineral together with hematite. Hematite, in general, is the predominant mineral. Goethite occurs as secondary mineral after magnetite and hematite. Graphite occurs in most of the BIF samples.

Fig 2.26 BIF with graphite components. The cavity was the primary location of now removed graphite, view to the west in sub-area A

The graphite occurs as spots of varying sizes, aligned in the bands and might have had a biogenic source. In places, it is found as cavity filling. At the surface this appears as weathered cavities with high concentration of graphite (Fig 2.26). These bands have a very high magnetic susceptibility due to the high amount of magnetite, while in the quartz rich bands the magnetic susceptibility is intermediate (see AMS, Chapter 6).

2.3.2.1 Microscopic Character of the Well-Banded Iron-Silica Bands

The microscopic study of these bands shows mostly iron oxides, quartz and graphite. The iron oxides are mainly magnetite and hematite arranged in bands alternating with silica rich bands (Figs 2.27 and 2.28). The hematite crystals show brownish colour and appear as elongated fibrous or granular shapes. Two types of quartz occur in these bands, the dominant ones are large, elongated, strained crystals with wavy extinction, which show twinning similar to the albite twinning in the plagioclase (but the microscopic character exhibit a uniaxial positive interference figure). The magnetite also occurs as large grains, sometimes with more than 3 millimetres in diameter (Fig 2.29). Fine-grained magnetite surrounded by very fine-grained matrix of silica-iron rich bands exhibit a mesh texture (Fig 2.30). The magnetite is altered to hematite as seen under the microscope in reflected light

(Figs 2.31 and 2.32). In general, the iron-silica bands show micro and mesobanding of different thicknesses due to alternation of iron rich and silica rich bands.

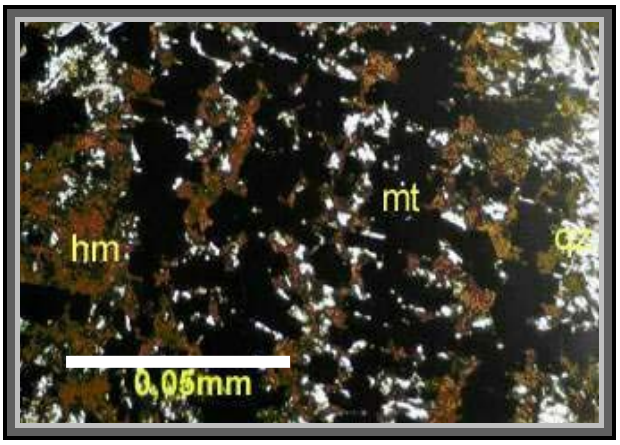

Fig 2.27

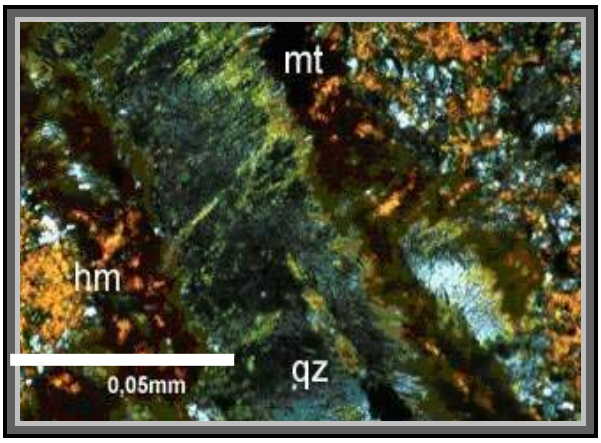

Fig 2.28

Fig 2.27 Microbanding in the magnetite (mt)-hematite (hm) rich bands showing the alteration of magnetite to hematite. The bands alternate with quartz (qz). Sample No. U-5, sub-area A, (PPL).

Fig 2.28 Iron-silica rich bands showing large quartz (qz) crystals and the alternation between magnetite (ematite (hm) (black and brown colour), the hematite shows varying brown to yellow colours and appears as fibers or granular crystals Sample No. U-5, sub-area B, (C.N).

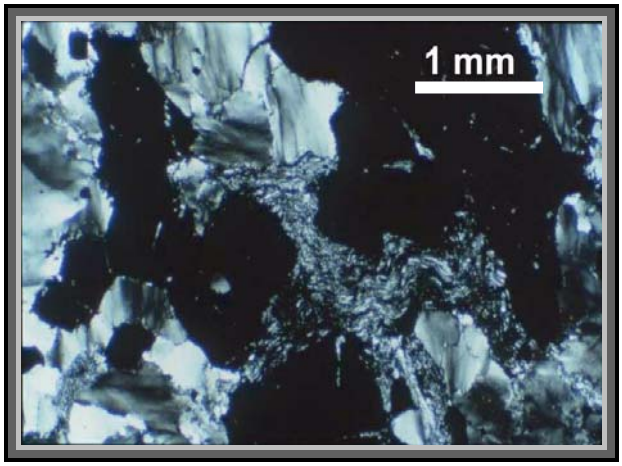

Fig 2.29

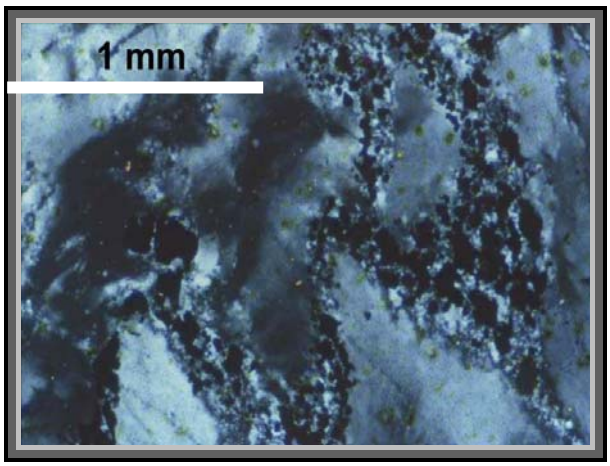

Fig 2.30

Fig 2.29 Deformed quartz grains with wavy extinction, large magnetite crystals, and very fine-grained iron-silica bands, which show minor folds. Sample No. U-3, sub-area B, (C.N).

Fig 2.30 Fine-grained magnetite developed in a very fine-grained matrix of quartz and iron oxides, exhibiting mesh texture. Sample No. U-2, sub-area B, (C.N).

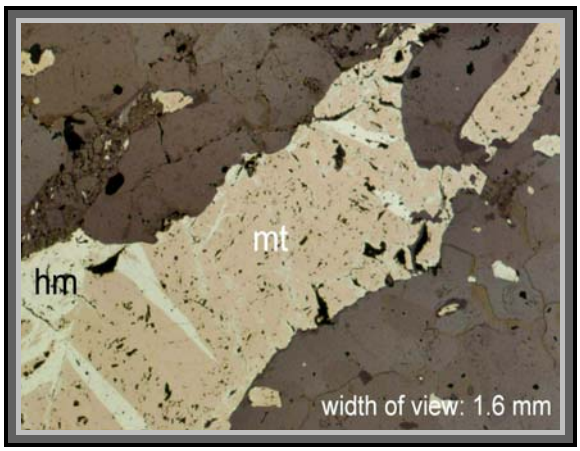

Fig 2.31

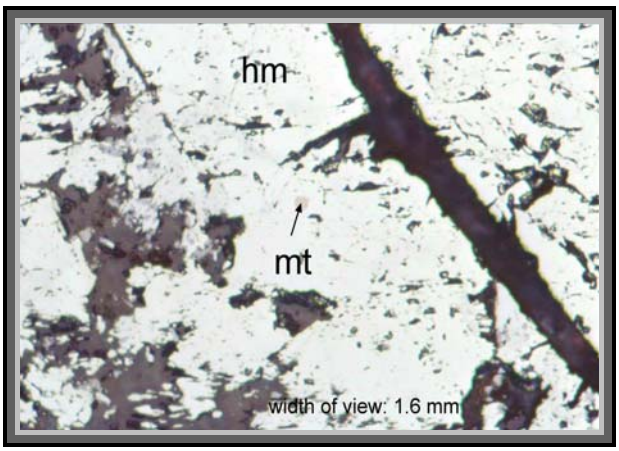

Fig 2.32

Fig 2.31 Photomicrograph under reflected light showing magnetite (mt) altered to hematite (hm). The dark brown colour is quartz (silica bands). Sample No. H-15, sub-area (B).

Fig 2.32 Photomicrograph under reflected light showing magnetite (mt) altered to hematite (hm). Sample No. H-16, sub-area (B).

2.3.3 Fuchsite-Bearing Quartz Bands

Fuchsite-bearing quartz bands often follow in the succession, overlying the iron-silica rich bands, but are exposed mostly in the extreme eastern parts of the study area. Generally, these bands have the same trend as the BIF bands and occupy large bands of up to 500 metres thick and 2-5 kilometres in length. They are white, grey, greenish grey or green fine to medium-grained in primary bands, few centimetre thick (Figs 2.33 & 2.34). The fuchsite-bearing quartz bands consist mainly of quartz, chlorite, fuchsite, altered feldspar minerals, clay minerals, and minor iron oxide. In these bands a penetrative foliation is parallel with the primary banding, and having the same trend as the BIF bands, mostly with 15° N and dips 60° to the west (Fig 2.34).

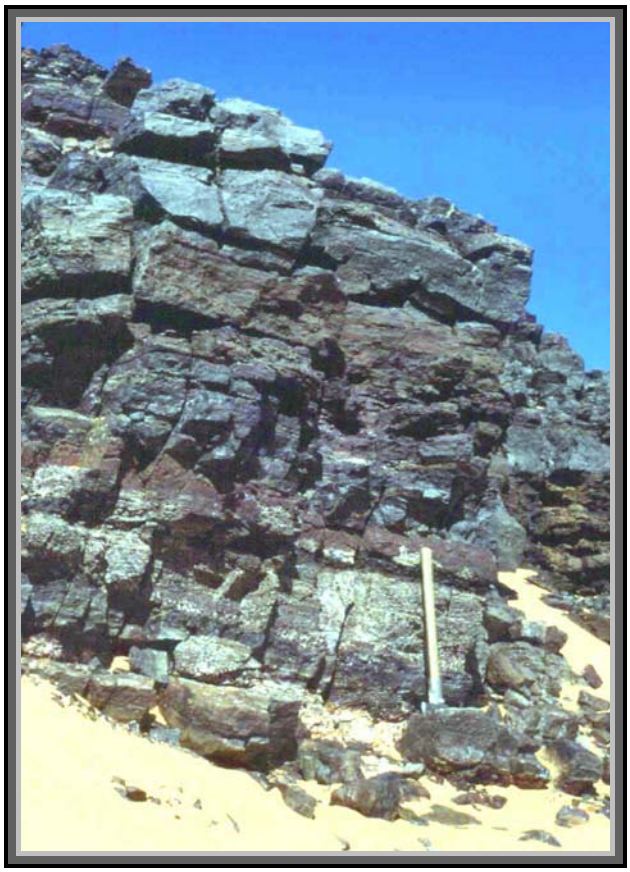

Fig 2.33

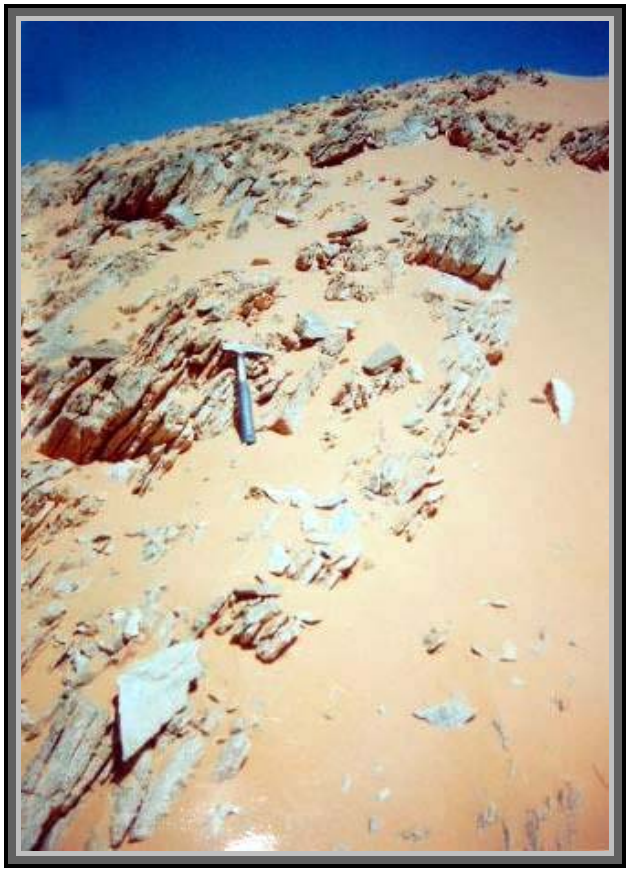

Fig 2.34

Fig 2.33 Quartz bands with greenish bands containing fuchsite, the photo shows nearly horizontal bands in Fold hinge (view to the west in sub-area A).

Fig 2.34 Primary banding in the fuchsite-bearing quartz bands dipping to 285°/ 65°, sand covers a large area of the exposures (view to the north in sub-area B).

2.3.3.1 Petrographic Study of the Fuchsite Bands

Microscopically, the fuchsite-bearing quartz bands consist of large quartz grains with ribbon structure and wavy extinction alternating with bands of fuchsite, chlorite, epidote, magnetite, hematite, graphite (Fig 2.35 & Fig 2.36). The bands contain sometimes inclusions of recrystallized quartz and minor zircon as accessory mineral.

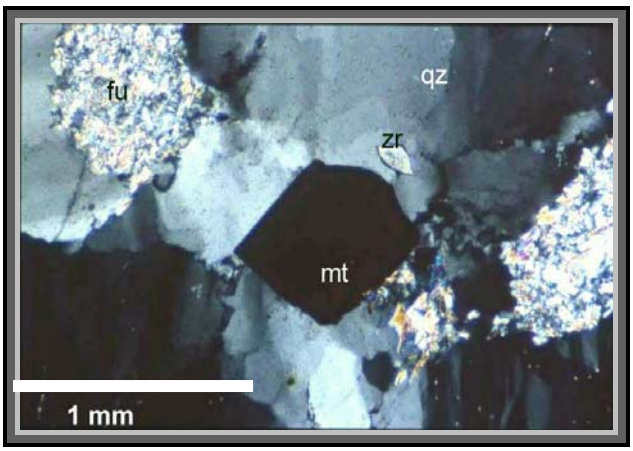

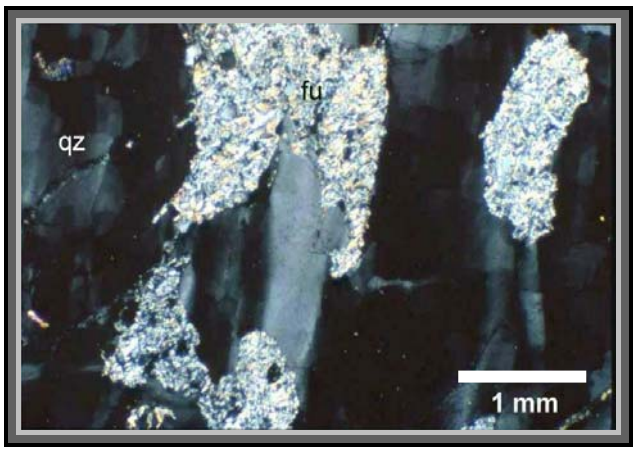

Fig 2.35 Fig 2.36

Fig 2.35 Fuchsite-bearing quartz (qz) bands showing large deformed quartz grains with wavy extinction, fuchsite (fu), magnetite (mt) and a small zircon (zr) crystal Sample No. U-4, sub-area B, (C.N).

Fig 2.36 The same bands with elongated quartz grains (qz) parallel with fuchsite (fu) grains. Sample No. U-4, sub-area B, (C.N).

2.3.4 Metapelitic Volcanosedimentary Bands Alternating with Iron-Silica Bands (Algoma-Type).

Metapelitic volcanosedimentary bands represent the base of the BIF sequence. They alternate with iron-silica bands (BIF), and vary in thickness between 1 and 5 metres and crop out for more than 100 metres along strike. They are fine to medium-grained, and white, brown and grey. These bands have the same trend as the BIF bands (10°/60° west). Lithic tuff bands, brownish grey to white and consist of very fine quartz and altered feldspar dominate these bands. They are 3 metres thick in average and alternate with quartz bands with thicknesses of up to 1 metre, BIF bands up to 0,50 metre and sometimes thin lamina of meta-chert with a few centimetres thick.

The iron-silica rich bands differ in composition with the higher part of the BIF sequence. They contain, sometimes, subordinate amounts of garnet, ortho-pyroxene, amphiboles, highly altered feldspars, chlorite, and relatively much magnetite. Graphite is rarely observed in these bands (Fig 2.37).

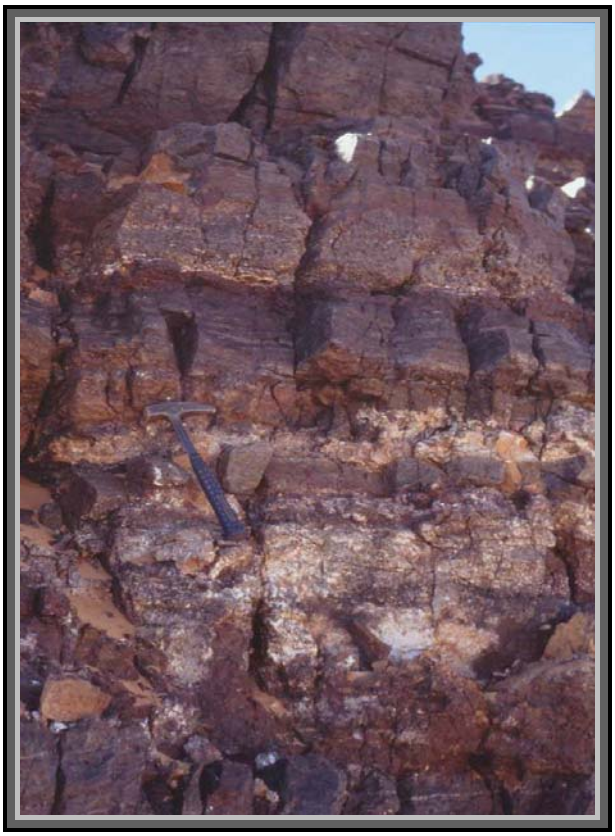

Fig 2.37

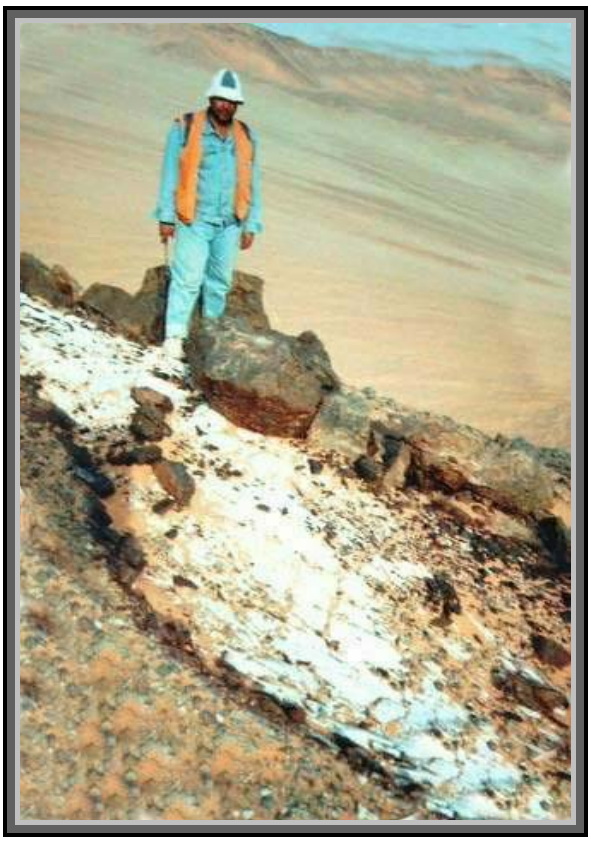

Fig 2.38

Fig 2.37 Metapelite Volcanosedimentary bands (white) alternating with BIF bands of the Algoma-type (view to the west in sub-area A).

Fig 2.38 Field photograph showing the Mylonitic band in the metapelite-volcanosedimentary bands (white) (view to north-east in sub-area C).

Within the BIF occasional mylonitic bands between 1 and 3 metres in thickness can be traced for a few hundreds of metres (Fig 2.38). These bands show reddish white colour or greyish red colour. Normally, they are fine- to very fine-grained, consisting mainly of crushed (mylonitized) quartz with subordinate amounts of magnetite, hematite and secondary goethite bands. The mylonitic bands are parallel to the BIF bands as well as to the foliation, and represent shear zones within the BIF. They show quartz porphyroclasts surrounded generally by foliated fine-grained groundmass of quartz-magnetite rich bands, which show earlier folding, formed during earlier deformations.

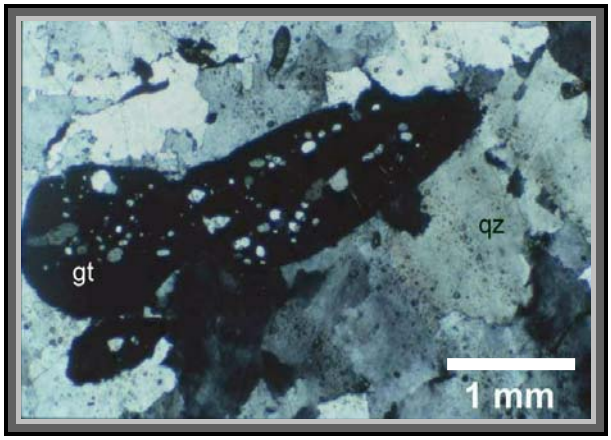

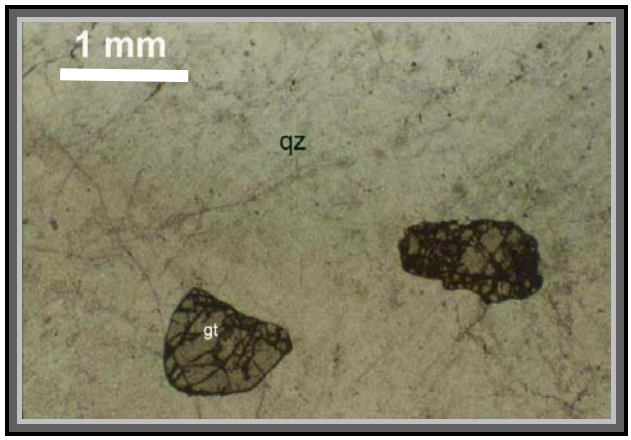

Fig 2.39 Fig 2.40

Fig 2.39 Iron-silica bands showing large garnet (gt) crystals with inclusions of recrystallized quartz (qz) show overgrown of earlier fabric, surrounded by granoblastic strained quartz. Sample No. H-4, sub-area C, (C.N).

Fig 2.40 Iron-silica bands showing two grains of highly cracked garnet (gt), surrounded by deformed quartz (qz) with some hematite (brown). Sample No. U-11, sub-area A, (C.N).

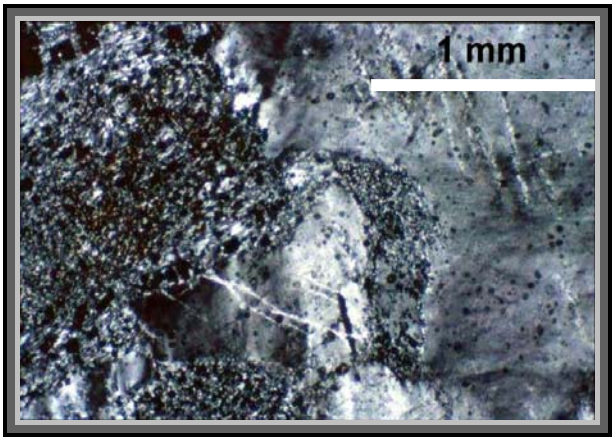

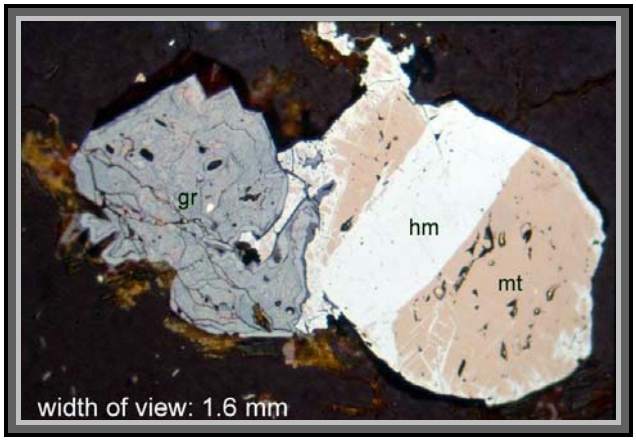

Fig 2.41 Fig 2.42

Fig 2.41 Photomicrograph showing large quartz-grained with wavy extinction and the fine grained quartz-magnetite bands. Sample No. U-2, sub-area B, (C.N).

Fig 2.42 Magnetite (mt) altered to hematite (hm) adjacent to graphite grain (gr), both surrounded by quartz rich in hematite. Sample No. U-6, sub-area A (Reflected light).

The bands in metapelite-volcanosedimentary rocks are generally parallel with the main thrusts and the fold axial surfaces in the area. Often, zones of fault breccia cut through the BIF bands. Some zones are welded by secondary goethite. These fault breccias generally prevail at E-W trending wrench faults, and can be considered as polyphase faults. In some areas they cut only through basement rocks, in other areas they cut through both basement and the overlying Tertiary sandstone.

2.3.4.1 Microscopic Study of Metapelitic Volcanosedimentary Bands Alternating with Iron-Silica Bands (Algoma-Type).

Microscopic study of metapelite-volcanosedimentary bands (Algoma-type) shows lithic tuff with very fine groundmass of altered minerals, mostly feldspar. The metapelite bands are composed mainly of highly altered feldspars, quartz, chlorite, epidote, garnet, graphite and some opaque minerals of hematite, magnetite and goethite with subordinate amounts of enstatite (ortho-pyroxene minerals) and amphiboles (Figs 2.39, 2.40 and 2.41). The quartz shows two types, the earlier one has large-grained with wavy extinction and the secondary is fine-grained recrystallized quartz. The garnet shows also two types, the earlier has large-grained with quartz inclusions, indicate an earlier fabric overgrown in the garnet (Fig 2.39). The other garnet is highly cracked without inclusion, which placed close to the N-S thrust surfaces showing cataclastic structure (Fig 2.40). Graphite occurs as a small plates and bundles of blades, contains some inclusion of iron oxide and adjacent to the alteration of magnetite to hematite as in fig 2.42. The quartz shows large crystals up to 3 mm in length with wavy extinction. Remnants of fine-grained quartz-magnetite-rich bands represent the old mylonite bands, which developed during the early deformation in the BIF. The fine-grained quartz-magnetite bands mostly show earlier folding, which formed during the earlier S-N maximum stress

The mylonite bands reveal quartz porophyroclasts surrounded generally by foliated fine-grained groundmass of quartz-magnetite rich bands.

2.4 Young Granite

There are several small granitic intrusions distributed in the investigated area. Their diameter is mostly not more than 150 metres. The granite is coarse to very coarse-grained and has rosy colour and consists mainly of orthoclase, quartz, plagioclase, biotite and muscovite. The granitic rocks are weathered and dissected by joints, fractures and exfoliation structure (Fig 2.43). The contact with other rock units is intrusive, and the granite has some xenoliths of the older gneisses (anatexite). In the middle of the area three granite intrusions are observed with diameters between 50 metres and 150 metres forming three points on one line extending from west to east.

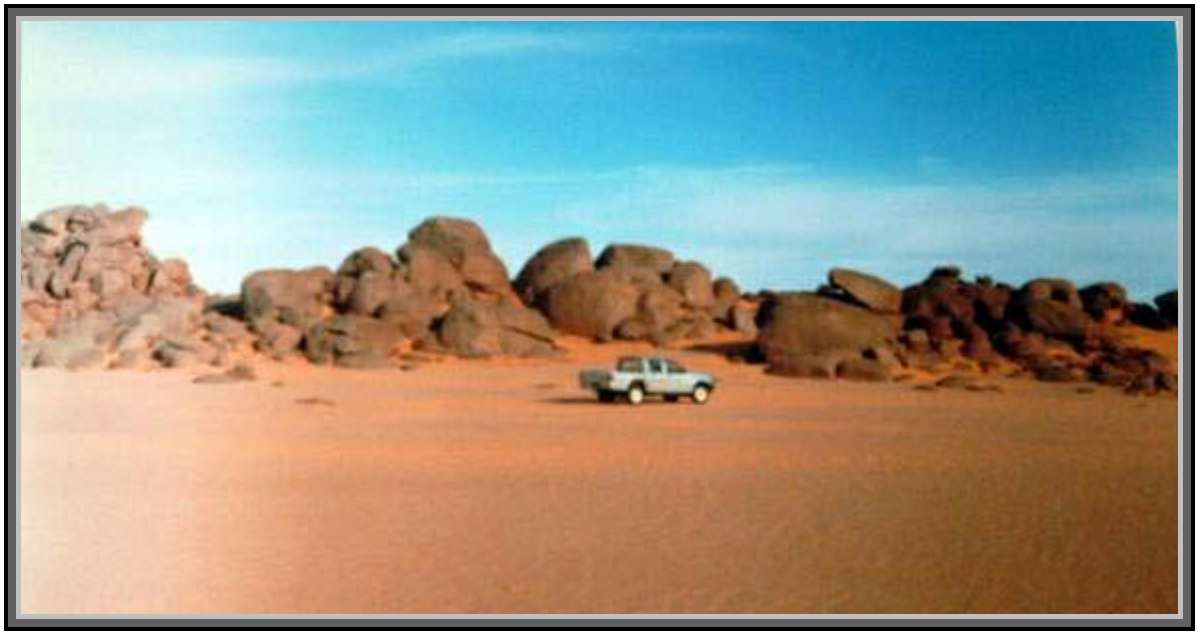

Fig 2.43 Outcrop of undeformed granite directly to the east of the investigated area. (View to the east).

2.5 Dykes

The investigated area is cutting by a number of acidic, intermediate, and basic dykes. Acidic dykes are represented by rhyolites and felsites, intermediate ones are dacites, trachytes and phonolites, basic dykes are basalts and dolerites. Their thicknesses vary from 1 to 10 metres and their lengths from 100 metres to more than 10 kilometres. In some areas they are covered with sand. They strike generally in NNE-SSW, NE-SW, NW-SE and E-W directions. The acidic and intermediate dykes are more abundant in the study area. They strike nearly NNE and extend parallel to the BIF and Anatexites bands or cut them at a low angle. These dykes are nearly vertical and very fine-grained. The basic dykes are less widely spread, and trend in the E-W, NW-SE or NE-SW directions. They

are fine grained, greenish grey to black in colour and show more alteration than the acidic dykes.

2.6 Phanerozoic Cover

The area is covered discordantly with sedimentary rocks, which occupy more than 25% of the rock exposures. The sedimentary rocks consist of yellowish brown, conglomeratic sandstone, composed mainly of quartz pebbles and gravels, rounded to sub rounded, cemented by fine grained sandstone The Mesozoic upper Jurassic – lower cretaceous Abu-Ras sedimentary Formation overlies unconformably the Precambrian in the middle and southern parts of the study area.

The stratigraphy of Panerozoic cover in the study area is as follow:

HOLOCENE

Quaternary

Sand dunes

Sand sheets

TERTIARY

Trachyte, basalt plugs and dykes

MESOZOIC

Upper Jurassic – Lower Cretaceous

Abu Ras Formation

The Phanerozoic rock unit are described from old to young as follow:

2.6.1 MESOZOIC

2.6.1.1 Abu Ras Formation (Upper Jurassic–Lower Cretaceous)

This term was first introduced by Issawi & Jux (1982) on the Geological Survey of Egypt, Dakhla Sheet on scale 1: 1,000,000 to describe a succession of conglomeratic sandstone, coarse grained sandstone and kaolinitic siltstone at the eastern part of Abu Ras Plateau, South-Western Desert, Egypt.

The rocks of Abu Ras Formation in the study area are described to be a succession of conglomerates, conglomeratic sandstone, sandstone and siltstone rich with ferns species and plant remains. The conglomeratic sandstone is yellowish brown to reddish brown, with fragments of quartz, gneiss, iron rich fragments and gravels, rounded to subrounded, cemented by fine to medium grained quartzitic sandstone. The thickness of this formation in the area is about 55 metres. The formation lies unconformably over the basement rocks with an uneven contact surface. Issawi & Jux (1982) attributed the environment of deposition of this formation to a fluviatile environment.

Fig 2.44 Abu Ras Formation (brown horizontal) discordantly overlying the Jaspar BIF (Looking west)

2.6.2 TERTIARY VOLCANICS

These rocks are recorded in southern part of the study area intruded into the Precambrian and Mesozoic rocks and represented by basalt and trachyte, in the form of dykes and plugs. Basalt is black, fine grained and shows columnar jointing. Vesicular and amygdaloidal textures are frequent. Trachyte is greenish grey, porphyritic with frequent nepheline crystals.

2.6.3 HOLOCENE

QUTERNARY DEPOSITS

The Quaternary deposits cover about 15% of present area. Their distribution controlled by the local geomorphology. The central and western parts of the investigated area with the relatively low topography have a thick accumulation of aeolian deposits in the form of sand sheets and sand dunes.

2.6.3.1 Sand Sheets

It is the most extensive unit all over the study area. It covers the low lands at the central part of the area. The sand sheets are composed of fine sands with grains mostly in the range of 0.1-0.2 mm, less frequently up to 0.5 mm large. The sand grains are mainly well rounded and well sorted quartz,. Well rounded pebbles may be present in addition to the fine grained sand.

The sand sheet belongs to the youngest Holocene deposits whose formation is currently under way.

26.3.2 Sand Dunes :

The sand dunes are present in narrow belts trending NE-SW at the western part of the study area, where the belts reach 1 km in width and extend for longer distance (5 km) from south to north. Their height ranges from 7 to 15 metres. During the work in the study area for three seasons it was noticed that the sand dune belts migrate westward at a rate of about 6 to 8 metres per year.

Two types of sand dunes, Seif and Barchans, dominate in the investigated area Said et al. (2000). The linear **seif dunes** form when two prevailing winds alternate, either daily or seasonally. When the supply of sand is limited, **barchan** shaped sand dunes are well developed. Some parts of the area are covered totally with huge sand dunes, which prevent any investigated work on some exposures of the different rock units.

All the dunes are composed of fine sands with grain size mostly from 0.1 to 0.2 mm, less frequently up to 0.5 mm large. They are composed mainly of rounded and well sorted quartz grains, , the reddish brown colour is due to a very thin limonitic film on the grains. In some areas the dune belts grade laterally into flat sand sheet.

CHAPTER 3

CHRONOSTRATIGRAPHY

In the study area radiometric age data are extremely rare. For this reason, correlations of the rock units are almost exclusively based on geochemical, structural and metamorphic similarities. However, there are sufficient available data to establish a preliminary chronostratigraphic sequence for the basement of SW Egypt (Table 2). Generally, the high grade gneiss and migmatite domain in the basement west of the Nile is interpreted as part of a pre Pan-African continental plate, e.g. by Meinhold (1979), Almond (1980), Vail (1983), El Ramly et al. (1984), Vail (1985), Kröner (1985), and El-Gaby et al. (1988). Apart from relatively unreliable ages derived from single sample Rb/Sr and K/Ar analyses (Hunting Geology and Geophysics Ltd., 1974; Schürmann 1974) the only evidence for Archaean crust in NE Africa comes from the Gabal Uweinat area in SE Libya. Rb/Sr whole rock ages on granulitic rocks and anatectic gneisses from the Uweinat area in SE Libya by Klerkx & Deutsch (1977) proved a Late Archaean age as well as a Mid-Proterozoic event which late affected these rocks.

These rocks include the Karkur Murr series, which exhibits high grade granulitic facies “Granoblastite Formation”. Because the effects of retrogression are difficult to evaluate, the age dating results are difficult to interpret. The age of 2.673 Ma is then a minimum age for the deformation producing tight isoclinal folding with fold axes oriented N-S to NNE - SSW during the granulite facies metamorphism. Cahen et al. (1984) recalculated the data of Klerkx & Deutsch (1977). Rb/Sr ages from the pyroxene granulite Karkur Murr Series yielded 2.656 +/- 71 Ma. This was the time of the amphibolite facies metamorphism, which affected the granulitic rock (Klerkx 1980). Granulite facies metamorphism might have occurred around 2.900 Ma ago as suggested by Rb/Sr model ages. The Archaean ages were confirmed by calculations on granulite samples.

Schandelmeier & Darbyshire (1984) determined a Nd-model age for a sample collected from the Gabal Kamil migmatite at 1.913 Ma. This rock suffered Late Proterozoic resetting of its Sr isotope system, so it give an age of 673 Ma. However, there is no indication for juvenile Pan-African material in the Gabal Kamil area which makes a mixed Archaean / Pan-African source very unlikely. The Nd model age reflects a source of Mid Proterozoic age. Homogeneous migmatitic gneisses, which were collected from Gabal El Asr and Gabal Um Shaghir areas yielded Nd model ages of 2.371 Ma and 1.670 Ma, respectively. Both data indicate pre–Pan-African crustal material contributing to the formation of the migmatitic gneisses.

Harris et al. (1984) reported Nd model age of 3.000 Ma and 3.200 Ma for two samples of the Karkur-Murr granulites. Nd values at the time of amphibolite facies metamorphism indicate that the 2.650 Ma event involved considerable crustal reworking.

Richter (1986), based on detailed petrological and structural investigations in the Gabal Kamil area, concluded that the Granoblastite Formation in the western part of Gabal Kamel area might be correlated with the Karkur Murr Series of Uweinat and the Anatexite Formation of the Gabal Kamil area with the Ayn Dua Series (Klerkx, 1980) of Uweinat. In particular, the poly-metamorphic history of the Gabal Kamil rocks was similar to that of the Uweinat area.

Schandelmeier et al. (1987) obtained model ages from the Gabal Kamil and Gabal El Asr areas ranging from 2.300 Ma to 1.900 Ma. These ages indicate the formation of new crustal material in Early Proterozoic times and adds new evidence to the proposal of Harris et al. (1984) that the late Archaean nucleus of Gabal Uweinat is rimmed by an Early Proterozoic fold belt.

Bernau et al. (1987) investigated the calc-silicate rocks of the Gabal El Asr and Gabal Um Shagir areas to determine their metamorphic conditions. Three stages of mineral formations occurred within these rocks: the first stage of metamorphism was one of granulite facies conditions at temperatures from 800° to 1000°C, and a total pressure of 8 to 9 kbar. The second stage, which was related to the migmatization of the granitoid country rocks, took place at temperatures of 650 to 700°C, and pressures probably just below 6 kbar. The third stage is represented by a LT-LP overprint under green-schist facies conditions. These three stages of metamorphic development could also be recognized within the metamorphic units of Gabal Uweinat (Klerkx 1980) and those of the Gabal Kamil area (Richer 1986).

Sultan et al. (1994), by using U-Pb (zircon) and Sm-Nd whole rock data for the hornblende-plagioclase gneiss at Gabal Kamil (pale pink to brown zircon), document the presence of pre-Pan-African crust by ^{207} Pb/ ^{206} Pb ages of ca. 2.629 Ma with normal igneous Th/U ratio at Gabal Kamil and Chephren quarries areas, some 400 kilometres to the east, close to the Arabian Nubian Shield.

Sultan et al. (1994) applied U-Pb (zircon) dating procedures for five samples collected from Libya encompassing gneissic and migmatitic granite, a post-tectonic granite, and a quartzite. Another four samples were collected from Gabal Kamil and one from Bir Safsaf. These include gneiss, migmatite, gabbro, quartzite, and post-tectonic granite. The granoblastic gneiss indicates an emplacement age of 2.828 +/- 14 Ma and

profound Pb-loss (with production of metamorphic zircon) at 1991 +/- 17 Ma. For the migmatite gneiss, crystallization at 2899 +/- 23 Ma and 2.227 +/- 237 Ma indicates this to be the oldest rock in the Uweinat area, and it clearly demonstrates the presence of Archaean crust in the region. The granite from the ring complex yields a crystallization age of ca. 578 + /-2 Ma. The Uweinat porphyroblastic granite indicates a crystallization age of ca. 580 Ma.

Schenk et al.(2002) applied U/Pb dating of 1974 $^{+}/_{-}$ 4 Ma for the time of granulite-facies metamorphism and orogenic reworking in Uweinat area.

	Rock type	Method	Age (Ma)	Reference
Bir Safsaf, Egypt	Grandiorite	Sm/Nd WR model age	1445	Schandelmeier et al. 1987
Bir Safsaf, Egypt	Grandiorite	Rb/Sr WR isochron	581+/-57	Bernau et al. 1987
Gabal El Asr Egypt	Migmatite	Sm/Nd WR model age	2399-1839	Schandelmeier et al. 1987
South of Gabal Kamil, Egypt	Migmatite	Rb/Sr WR regression line	673 +/- 56	Schandelmeier & Darbyshire 1984
South of Gabal Uweinat, Libya	Granodiorite gneiss	K/Ar biotite	1878+/-64	Hunting Geology & Geophysics Ltd.1974 (unpublished report)
South of Gabal Uweinat, Libya	Migmatite biotite gneiss	Rb/Sr WR isochron	1784+/-126	Cahen et al.1984, recalculated from Klerkx & Deutsch 1977
Wadi Wahech, Uweinat, Ayn Dua series, Libya	Mylonite	Rb/Sr WR, biotite regression line	2637+/-392	Cahen et al.1984, recalculated from Klerkx & Deutsch 1977
Gabal Kamil, Egypt	Anorthositic gneiss	U/Pb	2629-2063	Sultan et al. 1994
Gabal El Asr, Egypt	Anorthositic gneiss	U/Pb	2141-1922	Sultan et al. 1994
Gabal Umm Shagir, Egypt	Granite	U/Pb	626+/-4	Sultan et al. 1994
Il Passo mylonite, Uweinat, Libya	Granulitic gneiss	Rb/Sr WR, regression line	2556+/-142	Cohen et al.1984, recalculated from Klerkx & Deutsch 1977
Karkur Murr series, Uweinat Libya	Granulitic gneiss	Rb/Sr WR model ages	2919-2904	Cahen et al.1984, recalculated from Klerkx & Deutsch 1977
Karkur Murr series, Uweinat, Libya	Granulitic gneiss	Sm/Nd model ages	3200-3000	Harris et al. 1984

Table 2 Isotopic age determination for the basement complex of the Uweinat inlier, SW Egypt and SE Lybia, WR= whole rock.

CHAPTER 4

GEOCHEMISTRY

GEOCHEMISTRY OF BIF AND RELATED ROCKS

4. 1 Introduction

The geochemical characteristics of the different rock units encountered in the study area were determined from 25 selected samples representing the three main rock: the BIF, Anatexite Sequences and the Ultramafic- mafic rocks types. All samples were analysed for their major, minor and trace element contents.

Chemical analyses were carried out in the Laboratories of the Geological Survey of Egypt, by XRF technique for major and spectral analyses for trace elements.

The following major, minor and trace elements were determined quantitatively: Si, Al, Mg, Fe (total), Ca, Na, K, Ti, P, Mn ,Ag ,As ,Ba ,Be ,Bi ,Cd ,Ce ,Co ,Cr ,Cu ,Li ,Ga ,Hf, La, Mo ,Nb, Ni, Pb, Sb ,Sn ,Sr ,V ,W, Y ,Yb ,Zn ,and Zr. The results of the chemical analyses are listed in tables 3, 4 and 5. These samples are chosen as follow: fifteen samples from the BIF variety, eight samples from the Anatexite Sequences and two samples from the mafic-ultarmafic rocks.

4. 2- The Major Elements Analysis

4. 2. 1 BIF Chemistry

Nearly no clear significant variation could be distinguished from the major elements of the BIF samples. Generally the silica content in the BIF samples varies between 55,1% and 76,60%, while the iron oxides ranged between 20,34 and 39,02%.

12 BIF samples have silica content between 55,1% and 78,1%, while the iron oxide content ranges between 21% and 39,02%.

The Alumina contents in these samples can differentiated into two BIF types, one has higher Al_2O_3 ranged between 0,75% and 1,5% as in samples No. H-3, H-10 and H-16.

These three BIF samples belong to the lower part of the BIF (the Algoma Type) according to the field observation. Other 6 samples have Al_2O_3 between 0,25% and 0,66% and belong to the upper part of the BIF succession, based on the field observations.

From the tables (No. 3&4&5) it is to recognize that the samples No. H-19, H-20 and H-23 show some anomaly, related to the other BIF samples. The sample No. H-19 has a highly

silica content (91,4%) and very low iron oxide (3,2%), this sample is originally meta-chert including less amount of iron oxides. The other two samples show low silica content ranged between 40,25% and 46,40%, while the iron oxide is nearly the same as the rest of the BIF samples. The last two samples show extreme Alumina content comparing with the other BIF samples, which having amount of 14,65%-9,8%. These two samples (H-20 & H-21) were collected from highly mylonitized zones in the BIF.

4. 2. 2 Anatexite Sequences

Eight samples were analysed of the Anatexite Sequences, which can be divided into two groups due to the field observation and petrographic studies. Three of them belong to the melanosome bands. These bands are rich in mafic minerals, and their chemical analysis show low silica contents between 48,9% and 54,15%, while the other five samples represent the leucosome and have silica contents between 67,24% and 71,4%.
The major oxides as the Al_2O_3, Na_2O, K_2O and P_2O_5 have a higher content in the leucosome bands, while the TiO_2, MnO_2, MgO, CaO and the total FeO are higher in the melanosome bands.

Experimental studies showed that Ti, P, Cr, Zr, Y, Sr, V, and rare earth elements are among the least affected during metamorphism (Pearce and Cann, 1971 and 1973; Jakes and White, 1972, Garcia, 1978 and Stern 1981), whereas Al, Fe, Mg, Ca, and Si were found to be relatively sensitive to low to moderate grades of alteration (Pearce and Cann, 1983, Floyd and Winchester, 1975).

Tarney (1976) has shown that a plot of TiO_2 can discriminate affectively between gneisses of Igneous and sedimentary origin. Rocks derived from sedimentary plot consistently above a line of joining 1,85% TiO_2 at 40% SiO_2 with 0% TiO_2 at 81% Sio_2, while many igneous in the intermediate to acid range tend to plot below this line. Plotting the data of the anatexite and BIF on the diagram (Fig 4.1) shows clearly that the whole of the samples are located in the meta-igneous field with the exception of only one sample of BIF that was collected from an area close to highly deformed zone.

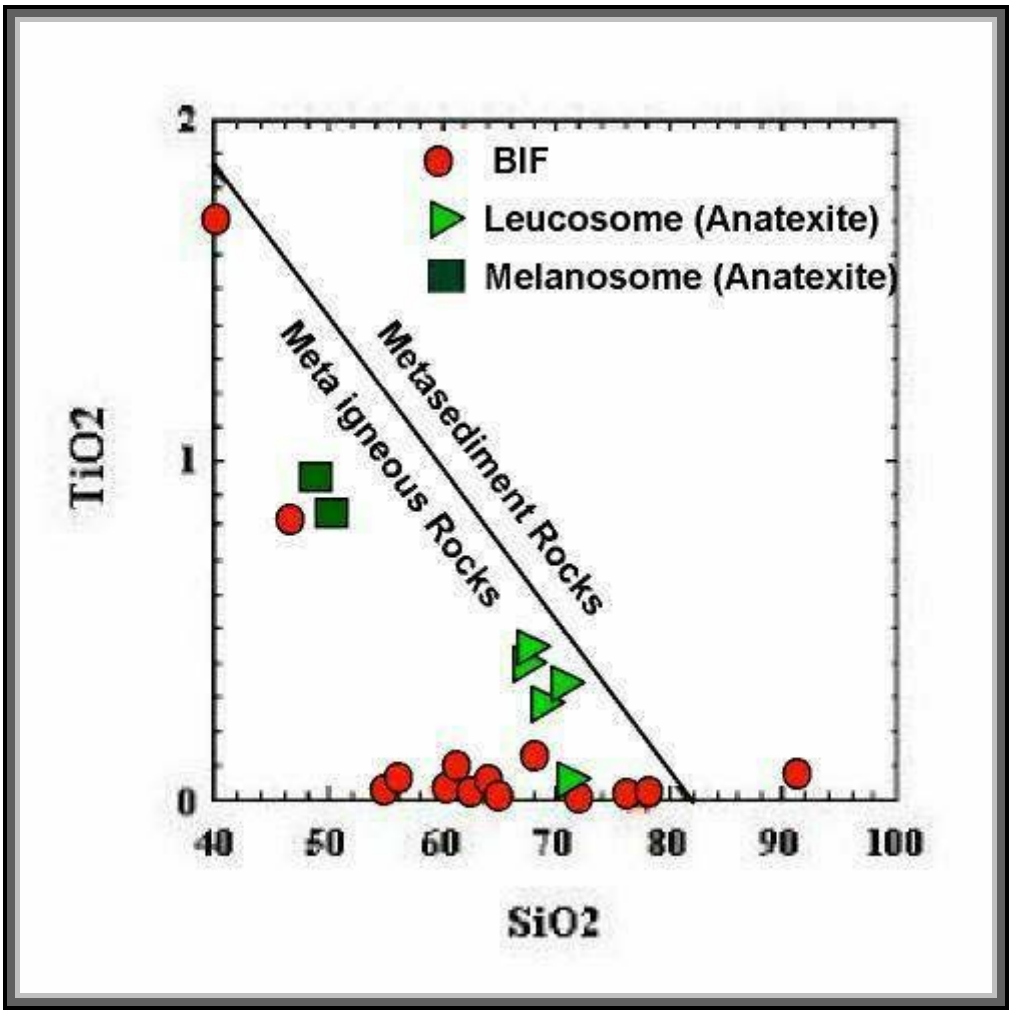

Fig 4.1 Plots of TiO_2 versus SiO_2 for the BIF and Anatexite on Tarney (1976) diagram. The same symbols through shown in the next diagrams.

In this study area neither rare earth elements analyses nor quantitative complete trace element analyses have been done for the studied sample. Major and some trace analyses are used to understand some chemical characteristics of the area.

However, the variation diagrams of the SiO_2 contents of these two rock types are plotted against the corresponding contents of MgO, Al_2O_3, CaO and the total iron oxides content. The relationships are shown on variation diagrams, Fig 4.2. Three distinctive clusters leucosome Anatexite and melanosome Anatexite and the BIF on the variation diagram demonstrate the following features:

1- On the Mg- SiO_2 variation diagram leucosome and melanosome Anatexite are located in two separate areas depending on their silica contents while the BIF samples are located on the line of least Mg content.

2- On the total Fe_2O_3- SiO_2 variation diagram the leuco and melanosome Anatexite exhibit tow separate clusters away from the BIF meanwhile the BIF samples show compositional line trends, except the highly deformed three BIF samples.

3- CaO versus SiO_2 contents show decreasing CaO with increasing SiO_2 contents in both leucosome Anatexite and BIF

4- Al_2O_3 versus SiO_2 contents show very slight decrease with decrease SiO_2 of the melanosome then the leucosome Anatexite. The BIF samples show lower silica contents than Anatexite.

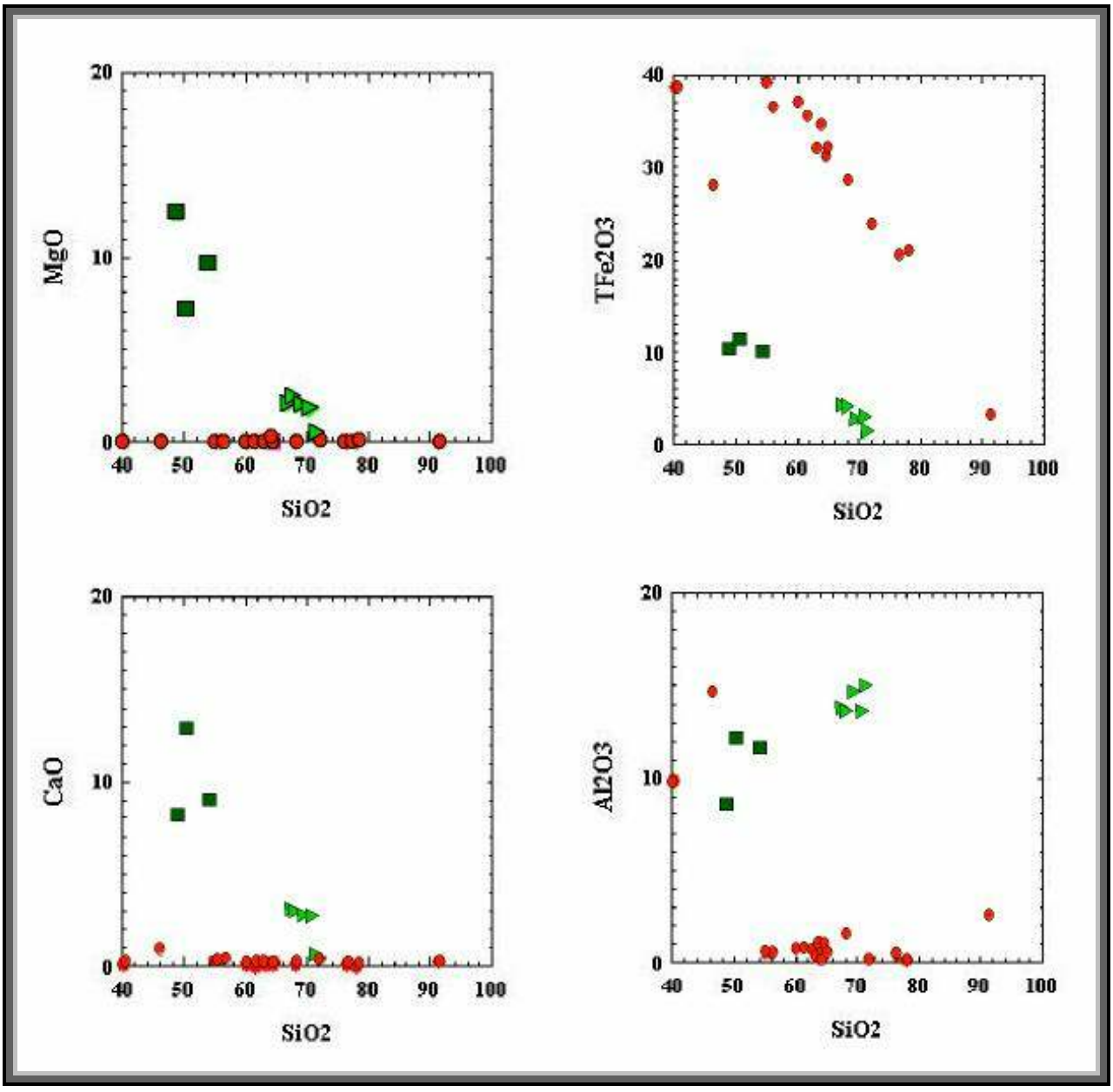

Fig 4.2 SiO_2 versus major oxides for the Anatexit and BIF.

BIF samples

Sample No.	SiO_2	TiO_2	Al_2O_3	MnO	MgO	CaO	Na_2O	K_2O	P_2O_5	TFe_2O_3	Lost of ignition
H3	64.7	.06	1,05	.68	.01	.12	.01	.01	.01	31.1	2,78
H4	56.1	.06	.57	.48	.01	.4	.01	.01	.17	36.4	5,38
H7	63.2	.04	.66	.21	0	.07	0	0	.06	32	3,51
H8	76.6	.01	.48	.19	0	.12	0	0	.07	20.34	1,57
H10	60.1	.04	.75	.25	0	.09	.02	0	.06	36.8	1,31
H11	64.7	.04	.5	.17	0	.23	.06	0	.11	32	1,7
H13	72.1	.01	.31	.6	.12	.43	0	0	.22	23.75	2,07
H14	61.7	.09	.7	.21	0	.02	0	0	.06	35.5	2,19
H15	78.1	.01	.15	.12	0	0	0	0	.02	21	0,27
H16	68.3	.13	1,5	.19	0	.06	0	0	.08	28.5	0,67
H17	55.1	.03	.56	.24	0	.4	0	0	.12	39.02	4,07
H18	63.8	.02	.25	.22	0	.12	0	0	.09	34.4	0,56
H19	91.4	.07	2,52	.13	0	.26	0	0	.13	3,2	1,63
H20	40.25	1,7	9,8	.12	0	.08	0	0	.94	38.5	8,15
H23	46.4	.82	14.65	.05	0	.97	.03	.07	.43	27.9	8,21

Anatexite Sequences samples

Sample No.	SiO_2	TiO_2	Al_2O_3	MnO	MgO	CaO	Na_2O	K_2O	P_2O_5	TFe_2O_3	Lost of ignition
H1	68	.43	13.67	.11	0,11	3	4,7	1,2	.15	4,08	1,88
H2	67.24	.41	13.79	.11	2,03	3,11	4,55	1,49	.17	4,73	1,74
H5	69.5	.28	14.7	.08	2,01	2,85	4,8	1,15	.07	2,95	0,95
H6	50.6	.84	12,12	.25	7,21	12,92	1,35	.62	.01	11,4	1,87
H9	71.4	.06	14.95	.06	.51	.89	3,4	5,95	.03	1,4	0,73
H12	70.78	.34	13.65	.09	1,82	2,81	2,98	2,91	.15	3,05	0,78
H21	54.15	.4	11,6	.19	9,66	9,03	2,35	.54	.04	9,88	1,52
H22	48.9	.94	8,55	.16	12,4	8,09	.64	1,39	.09	10,32	7,89

Ultramafic-mafic samples

Sample No.	SiO_2	TiO_2	Al_2O_3	MnO	MgO	CaO	Na_2O	K_2O	P_2O_5	TFe_2O_3	Lost of ignition
H24	8,6	.03	.26	.3	19.5	28.24	0	0	0	2,78	39,47
H25	36.59	1,36	24.5	.07	0	26.38	0	0	.41	10,12	0,38

Table 3 Chemical analysis of the major elements.

BIF samples

Sample No.	Ag	As	Ba	Be	Bi	Cd	Co	Cr	Cu	Li	Mn	Mo	Nb	Ni
H3	32.41	8,76	48.21	--	27.08	1,57	6,75	34.15	--	1,099	--	--	--	32,65
H4	9,29	8,43	87.86	--	38.98	--	4,01	--	--	4,21	443.1	--	39.49	26,49
H7	32.15	7,48	71.13	--	33.66	--	6,85	19.71	.23	6,69	354.7	15.9	.03	7,97
H8	16.82	9,66	42.7	--	54.81	38.81	--	--	--	95.9	--	20.78	22.88	--
H10	37.4	23.54	44.96	--	1,43	--	20.12	70.71	--	--	--	--	--	79,16
H11	2,65	29.24	15.46	--	--	--	20	254.3	3,82	--	212.9	--	--	783,6
H13	4,99	22.6	14.89	13.57	7,73	15.36	20.75	131.4	10,39	--		--	--	21,65
H14	4,35	27.3	8,68	18.2	5,41	3	21.95	33.69	39.12	--	415.5	--	--	145,7
H15	6,36	19.53	13.52	3,82	1,95	11,4	73.7	268.1	8,45	--	449.4	--	--	25,99
H16	5,28	23.88	19.97	29.65	5,48	--	--	--	13.3	--	59.7	--	6,64	0,89
H17	5,72	18.84	18.37	15.71	4,3	27.31	20.08	246.8	6,42	--	608.1	--	--	42,89
H18	3,78	30.38	32.94	31.63	.7	--	19.94	572.7	8,76	--	572.4	--	--	40,53
H19	1,43	12,87	103.3	37.59	1,85	4,34	--	64.91	25,8	--	543.2	--	--	79,19
H20	2,86	15.18	25.76	57	13.07	6,64	23.67	666	13.13	--	65.78	--	--	61,45
H23	6,62	18.98	27.93	--	15.1	36.56	31.38	444.4	46.29	--	--	--	--	117,9

Anatexite Sequences samples

Sample No.	Ag	As	Ba	Be	Bi	Cd	Co	Cr	Cu	Li	Mn	Mo	Nb	Ni
H1	8,25	8,3	633.9	--	--	52.1	1,29	12,39	--	--	--	--	50.53	24,39
H2	7,59	8	637	--	--	33.15	1,17	--	---	--	--	17.08	45.89	16,31
H5	5,08	3,66	468	--	20.64	.94	1,97	--	--	1,35	367.2	--	48	17,2
H6	5,34	4,41	739.4	--	5,3	--	1,61	--	--	8,48	--	--	47.78	--
H9	.08	9,06	34.7	--	--	12,46	--	7,84	1,43	--	150.6	--	--	40,89
H12	5,75	12,82	792.9	3,63	--	16.78	20.24	152.4	5,51	--	241.7	--	--	106,9
H21	5,38	13.22	35.32	--	10,82	12,84	32.1	--	13.44	--		--	--	61,45
H22	6,88	14.43	96.48	--	6,24	13.44	30.88	--	6,6	--	485.5	--	--	387.5

Ultramafic-mafic samples

Sample No.	Ag	As	Ba	Be	Bi	Cd	Co	Cr	Cu	Li	Mn	Mo	Nb	Ni
H24	0	12,47	19.64	30.22	44.86	14.69	--	--	74.04	--	23.77	--	--	15,59
H25	7,09	15.26	2,7	--	.96	--	24.17	576.1	12,74	--	--	--	--	64,6

Table 4 Chemical analysis of the Trace elements.

BIF samples

Sample No.	Pb	Sb	Ce	Sn	Sr	Ti	V	W	Y	Zn	Zr	La	Yb
H3	--	36.07	14	168.7	--	--	--	15.17	--	204.9	--	--	--
H4	--	5,29	6,54	5,84	--	--	--	7,46	--	--	--	160.3	--
H7	--	--	21.49	52.36	--	--	--	15.77	--	387.1	--	68.93	--
H8	--	--	4,87	198.3	--	--	--	10,3	--	243.6	--	--	--
H10	36.27	135.7	--	--	--	--	--	--	--	--	14.45	--	--
H11	51.66	--	--	--	--	--	--	--	--	--	13.83	--	--
H13	180	--	--	--	--	--	197.4	--	--	415.2	10,53	--	17624
H14	141.8	--	--	87.14	--	--	159.2	--	--	183.7	11,29	--	37172
H15	273.6	--	--	--	--	--	23.46	--	--	307.4	11,6	--	.55
H16	--	--	--	--	.74	--	--	--	--	426.3	11,67	--	16
H17	130.6	--	--	--	--	78.31	457.3	--	--	247.4	9,67	--	14305
H18	--	--	--	--	--	--	404.1	--	--	643.5	10,91	--	21.52
H19	202.8	--	--	255.3	--	--	--	--	259.4	253.1	5,2	--	--
H20	--	--	--	118.2	--	--	--	--	53.52	509.5	4,48	--	--
H23	248.3	--	--	157.8	19.36	--	--	--	--	245.2	4,42	--	--

Anatexite Sequences samples

Sample No.	Pb	Sb	Ce	Sn	Sr	Ti	V	W	Y	Zn	Zr	La	Yb
H1	--	37,46	17.4	271.8	--	249.9	49.25	--	--	330.9	--	--	--
H2	--	50.51	33.87	178.9	--	403.9	51.07	--	--	359.4	--	152.3	--
H5	--	--	11,02	--	--	--	--	20.34	--	603.1	--	105.6	--
H6	--	28.34	6,86	14.02	--	--	--	36.38	--	--	--	33.49	--
H9	--	31.27	--	156.5	--	1,76	--	--	48.11	232.4	8,54	--	--
H12	--	--	--	339.9	--	270.1	18.36	--	--	288.7	--	--	--
H21	--	0	--	205	--	--	--	--	--	266.2	5,92	--	--
H22	--	08,05	--	388,9	36,44	--	--	--	--	403,1	0,13	--	--

Ultramafic-mafic samples

Sample No.	Pb	Sb	Ce	Sn	Sr	Ti	V	W	Y	Zn	Zr	La	Yb
H24	158	22.96	--	55.42	32.19	--	101.2	--	--	163.3	7,01	--	--
H25	--	28.99	--	--	--	--	--	17.27	--	239.3	--	--	--

Table 5 Chemical analysis of the Trace elements

CHAPTER 5
STRUCTURES

5.Structure

The crystalline basement rocks around Gabal Uweinat represent a complexly deformed part of the south-western Desert of Egypt, being strongly folded, refolded and faulted. The area is characterized by regional lineament features in NNE-SSW direction, which holds for both main units, the BIF and the Anatexite sequence. A map shows the location of field photograph in this chapter (Fig.5.1).

5.1.Major Structures:

The detailed geological map (Fig 2.1) of the area explain the main rock units with large-scale structural elements. Two sections across the study area are shown on Figs 5.1 & 5.2. The structural analysis indicates that tectonic deformation produced major and minor folds, faults or overthrusts and shear zones, particularly in the BIF and Anatexite successions

The area includes several thrust slices of the BIF and Anatexite. The BIF lies on top of the Anatexite Succession that is turn covers the Ultramafic-mafic unit. The widths of each slice range between 3 and 5 km. A putative basal thrust (sole thrust) cross cut the area for about 20 km from west to east and most probably extends outside the study area in both sides. The thrust slices are separated by a series of nearly parallel thrust faults that are approximately equidistant and have been derived from east vergent folds. They have nearly the same transport (displacement) direction and are inclined to the northwest. The thrusts strike in general to the NNE (10°: 25°) and dipping to the WWN (280°: 315°) with average ranged between 35° and 75°.

Several of these thrusts strike all over the area with a length of about 25 km, while others extend only for 5 to 8 km converging into other thrust, especially in the southern part of the area. The northern part of the study area shows evidence of four regional thrust slices while in the southern part recorded eight regional thrust slices (Fig 5.2 & 5.3).

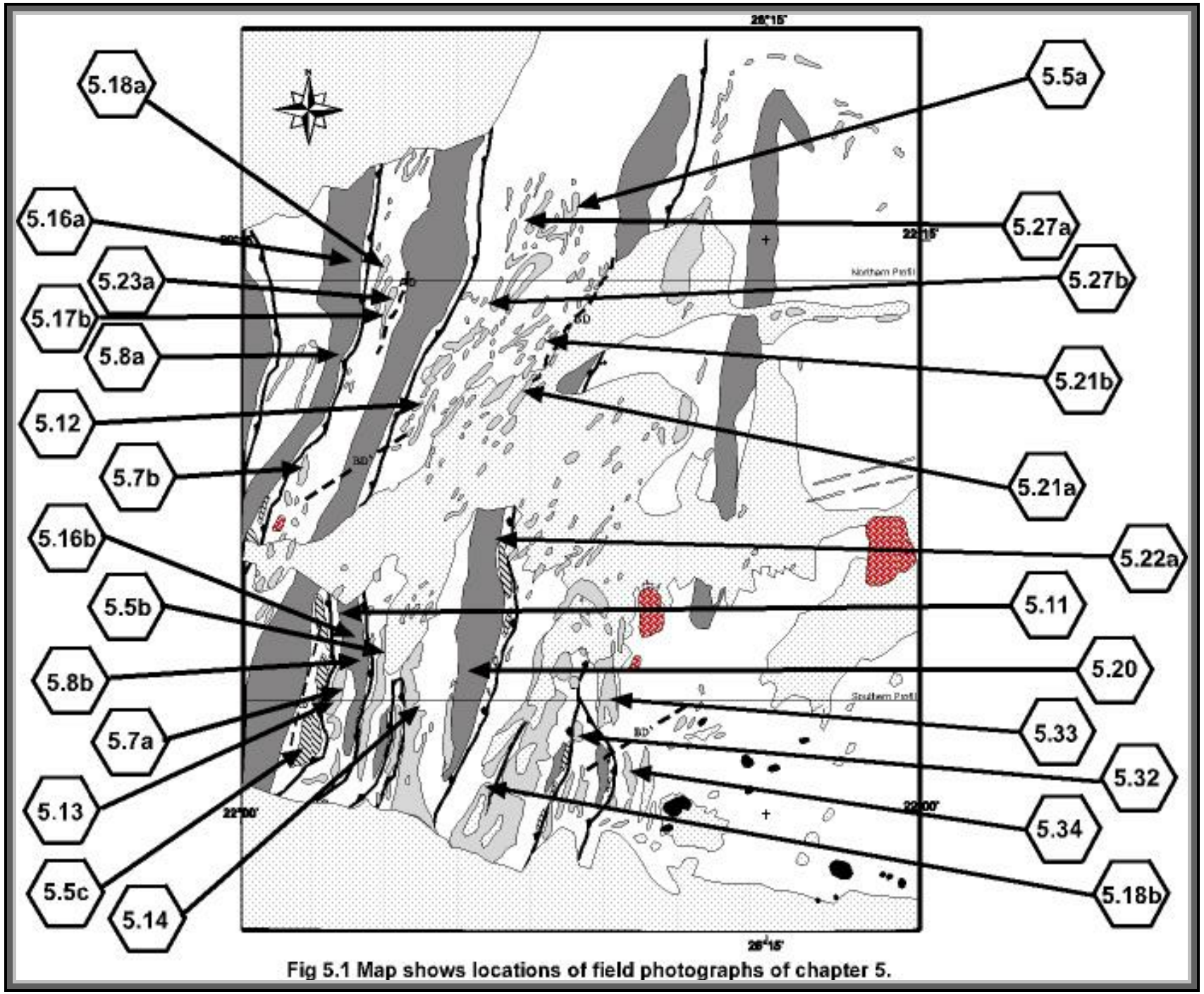

Fig 5.1 Map shows locations of field photographs of chapter 5.

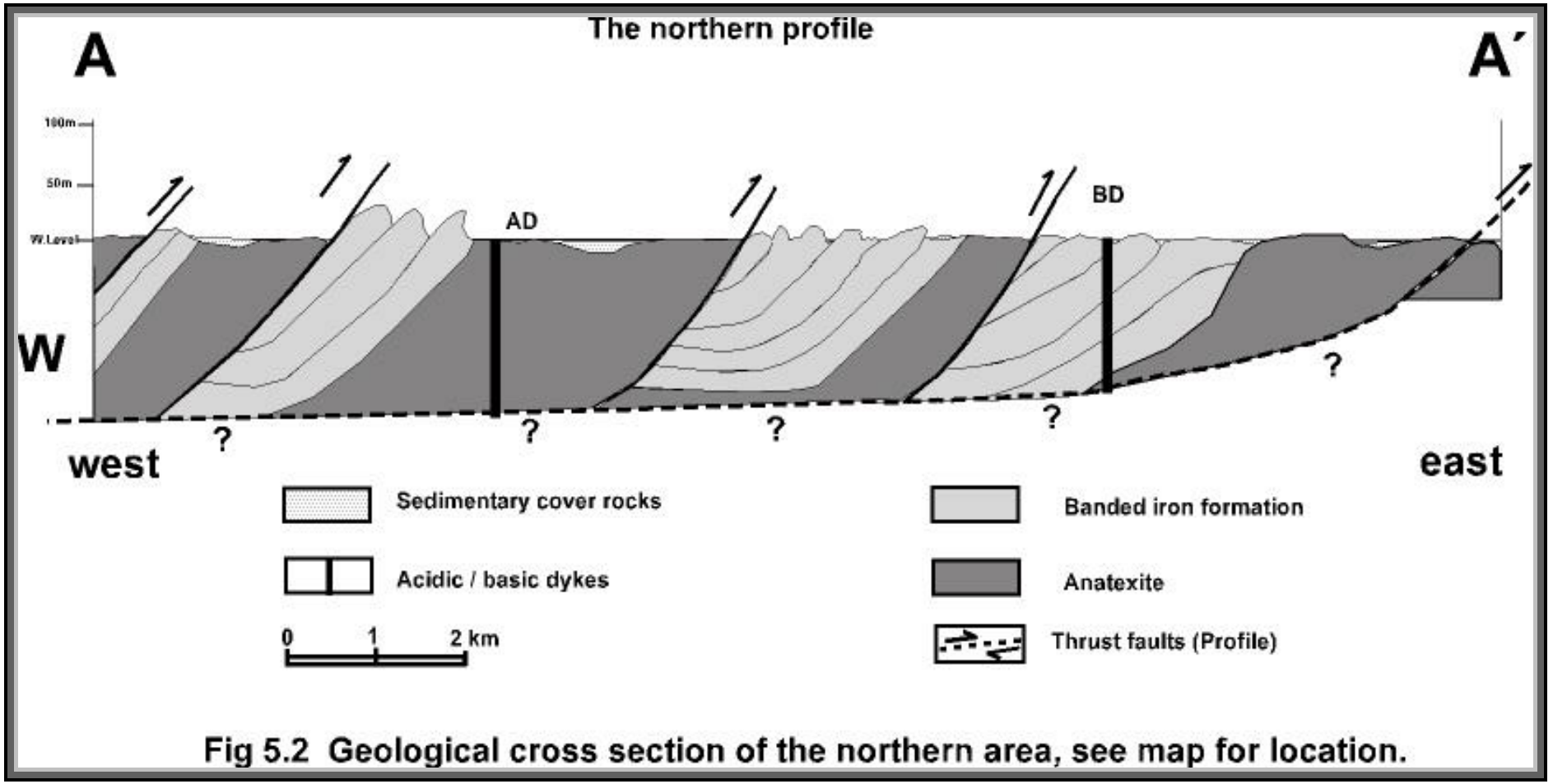

Fig 5.2 Geological cross section of the northern area, see map for location.

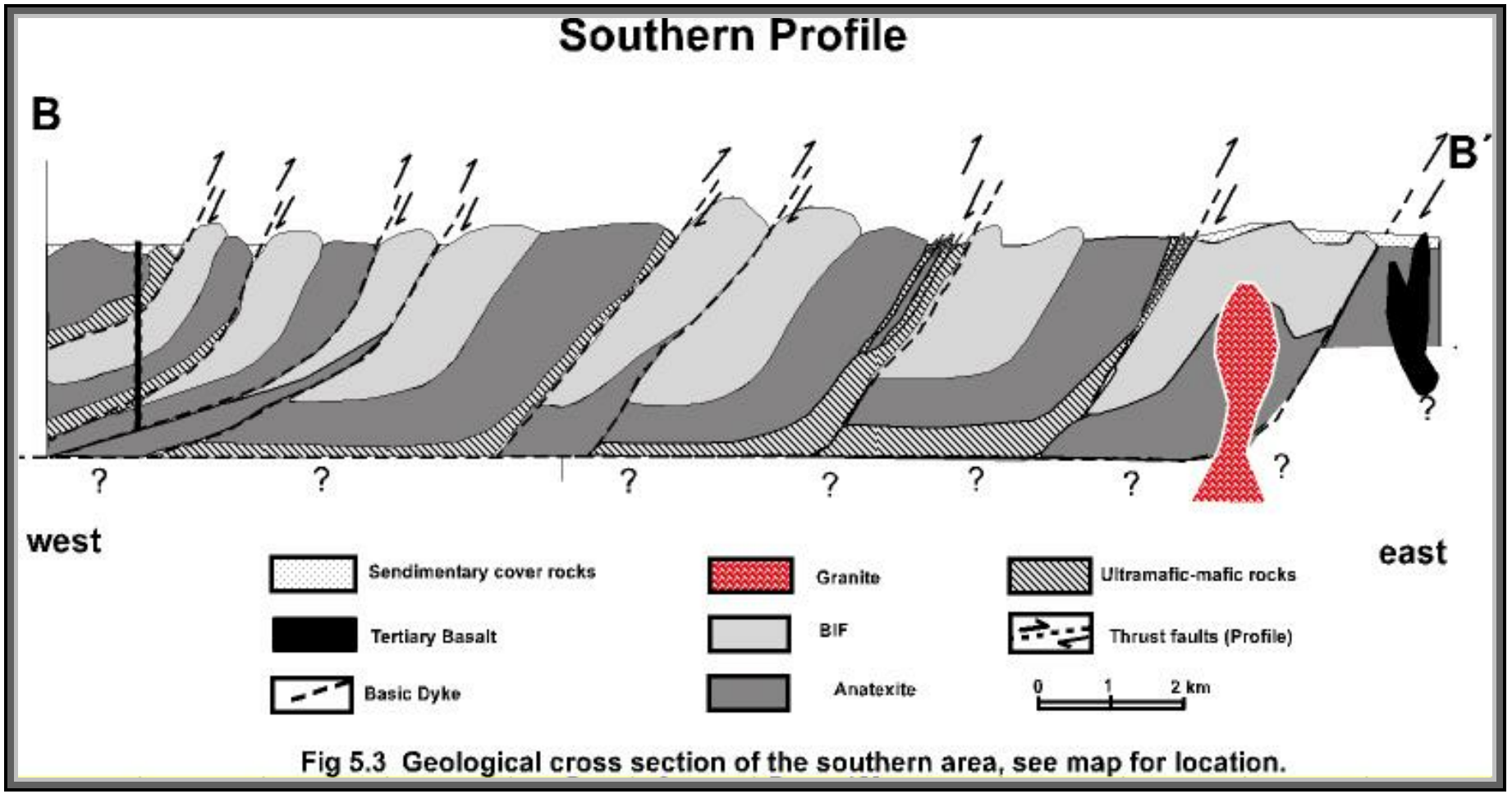

Fig 5.3 Geological cross section of the southern area, see map for location.

Major Structural Elements

5.1.1. Folds

Two generations of fold dominate the present area, represented by F2 and F3 showing different parameters. The older one, F2, was refolded by F3 and exhibits almost steep to vertical fold axes. It was observed generally in the BIF rocks, and rarely observed in the lower parts of the succession as the Anatexite sequences and Ultramafic-mafic rocks.

The (older) Folding Phase F2

F2 folds appear in the field in different scales from a few centimetres in some places to several tens or more than a hundred metres in other places. Micro folds observed in the oriented thin section also with the same characters as the field observations with steeply plunged fold axes (Fig 5.4). The F2 folded the Anatexite and BIF bands, which folded the primary bands or bedding in the BIF as in figures 5.5 a & b, while in the Anatexite sequences and Ultramafic-mafic, the F2 folded the light and dark bands with minor isoclinal and tight folds (Fig 5.5 c).

F2 indicate an old fold deformation developed during nearly south-north transport as a maximum stress from south to north. The upper part of the succession (BIF) was deformed by pure shear, due to its higher position in the old crust, and its less competency as the lower Anatexite sequences and Ultramafic-mafic bands, which imprint by pure and simple shear.

The fold axes had an E-W trending, north vergent folds and accompanied with low angle thrusts and shear zones, parallel with the fold axial surfaces, an illustrated sketch in Fig 5.6 represent the development of the F2. These E-W folds were refolded by F3, and can be now observed after about 90°, anticlockwise rotation, around a horizontal axis, in the limbs of F3 folds.

The Second Fold Phase F3

F3 folds can be seen in all of the three basement units (Ultramafic-mafic, Anatexite Succession and BIF), and resulted in a syncline-anticline belt that generally has NNE-SSW trending 15° fold-axes with plunge angles 15°. A development from east vergent folds to overturned and reverse faults parallel to the fold axial surface, dipping to the west (azimuth 285°) with angles between 35° and 70°. As a result of the reverse faulting, only the western anticlinal limbs can be observed at a regional scale, these limbs contain the refolded F2 as a minor folds with steeply fold axes.

Minor tight-isoclinal folds with east vergent, and asymmetrical folds, parallel with the main (F3) folds and thrusts surfaces are also exposed, (Figs 5.7 a&b) and (Figs 5.8 a&b). The F3

phase refolded the earlier folds F2 in the BIF from the old position with E-W horizontal fold axes to the observed position with nearly vertical fold axes.

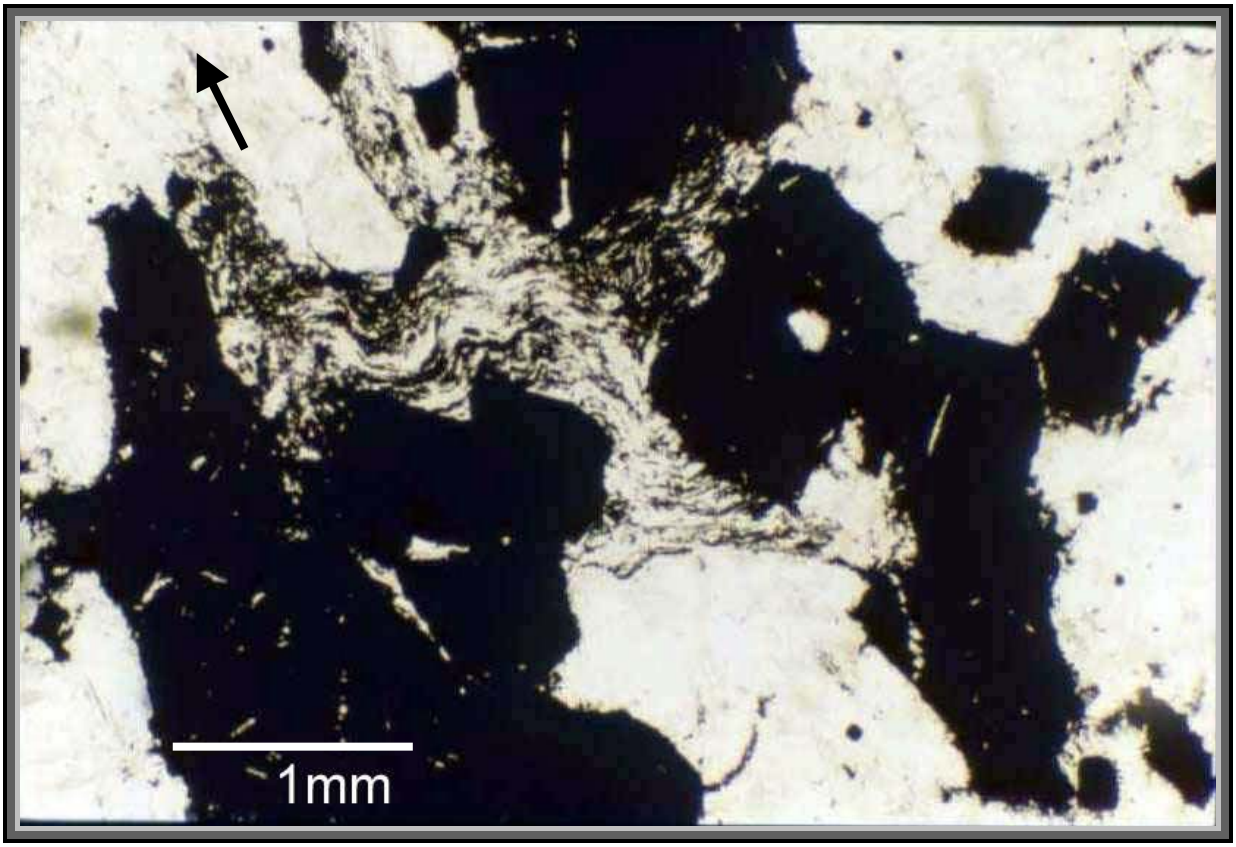

Fig 5.4 Photomicrograph in the BIF showing the F2 folds, which folded the earlier banding in the BIF, arrow shows North direction (PPL).

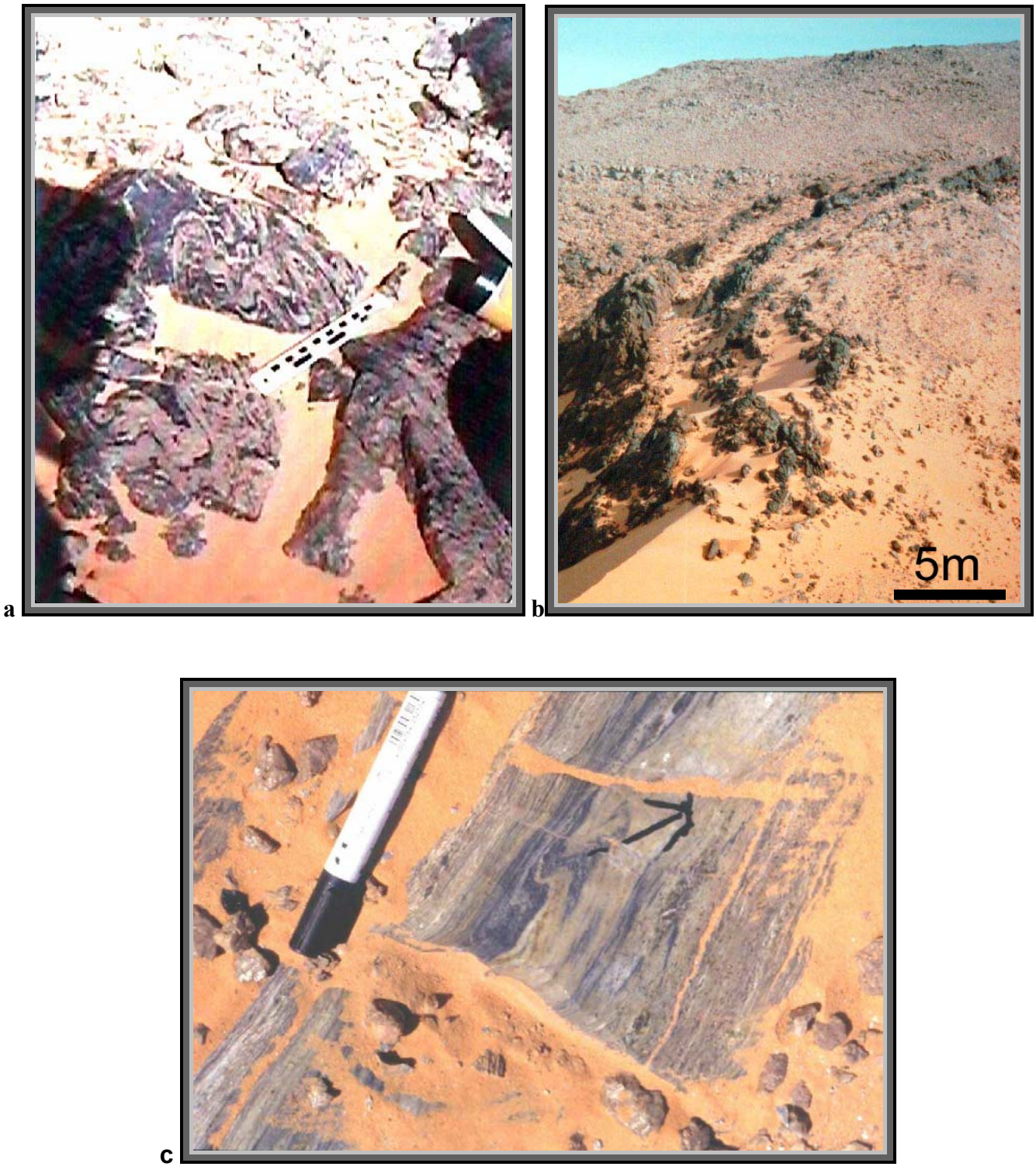

Fig 5.5 (a, b & c) F2 deformation results in (a) small scale from sub-area B, (b) large scale vertical folds from sub-area C, (view to the north) of the BIF and (c) from the UM bands show minor tight fold with steeply fold axes to the west. of sub-area (C).

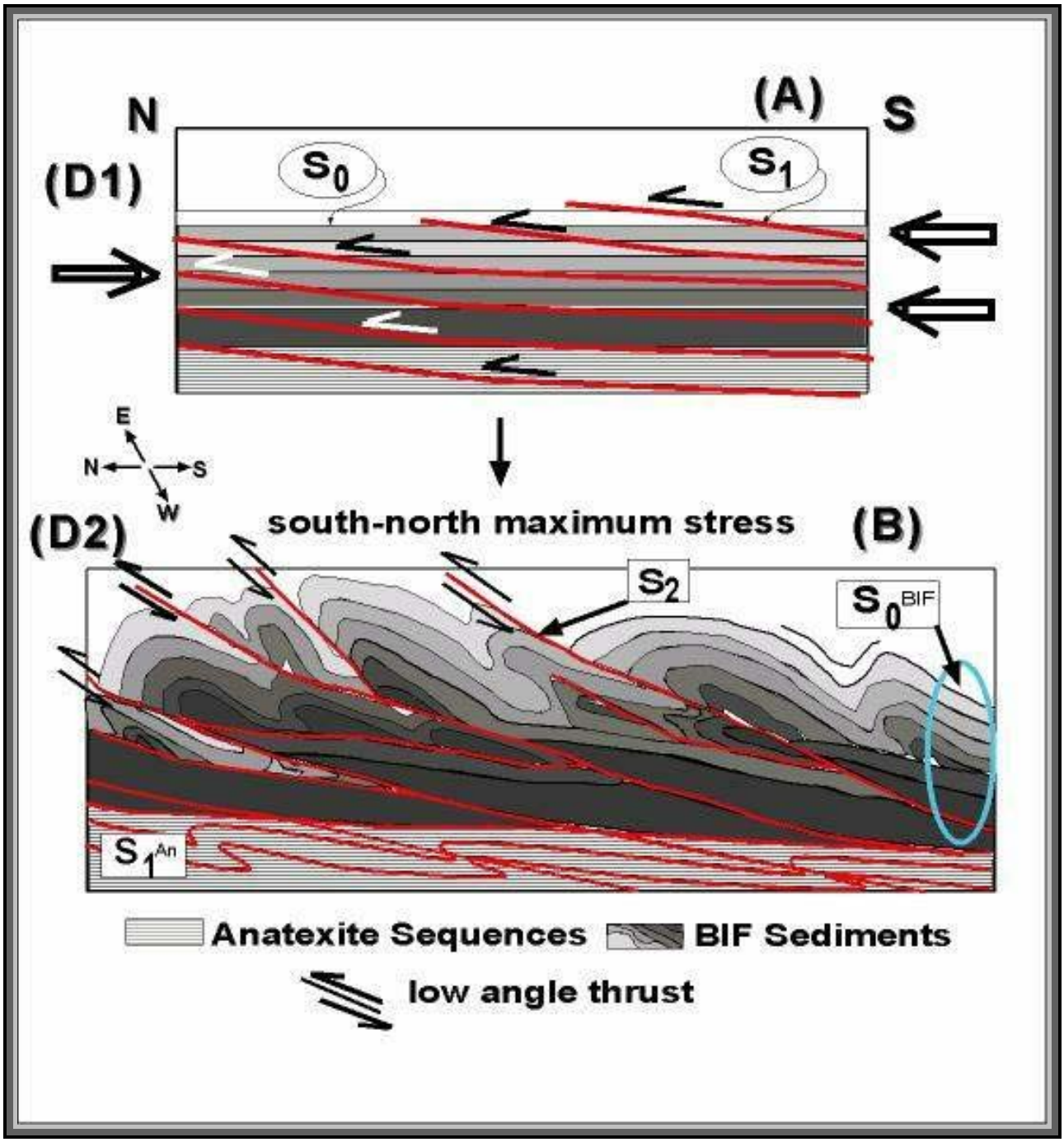

Fig 5.6 (A) BIF deposited horizontal over the old crust. Early deformation (D1) affected the higher unit (BIF) with simple shear mylonitization while the lower units overprinted with anatexis processes (S1). **(B)** The second deformation phase (D2) leading to E-W folding (F2), that is parallel to low angle thrusts. Foliation has (S2) E-W trend. It is notable that D2 slightly affect the Anatexite sequences.

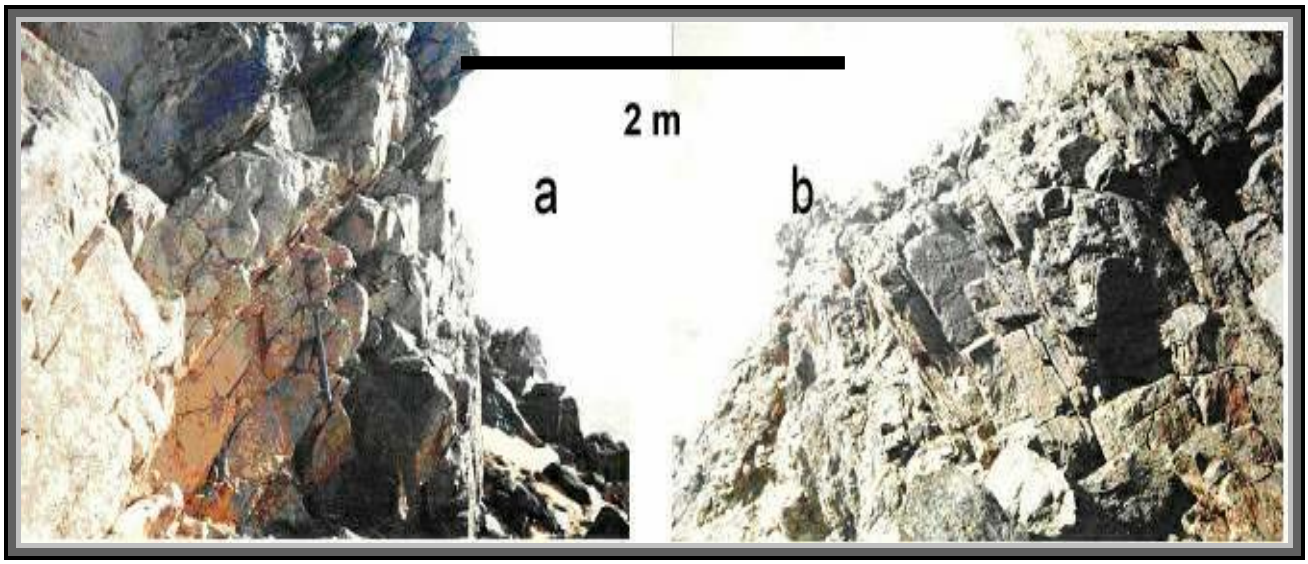

Fig 5.7 (a & b) Detail of the western limb of F3 fold (a- looking north) (b- looking south).

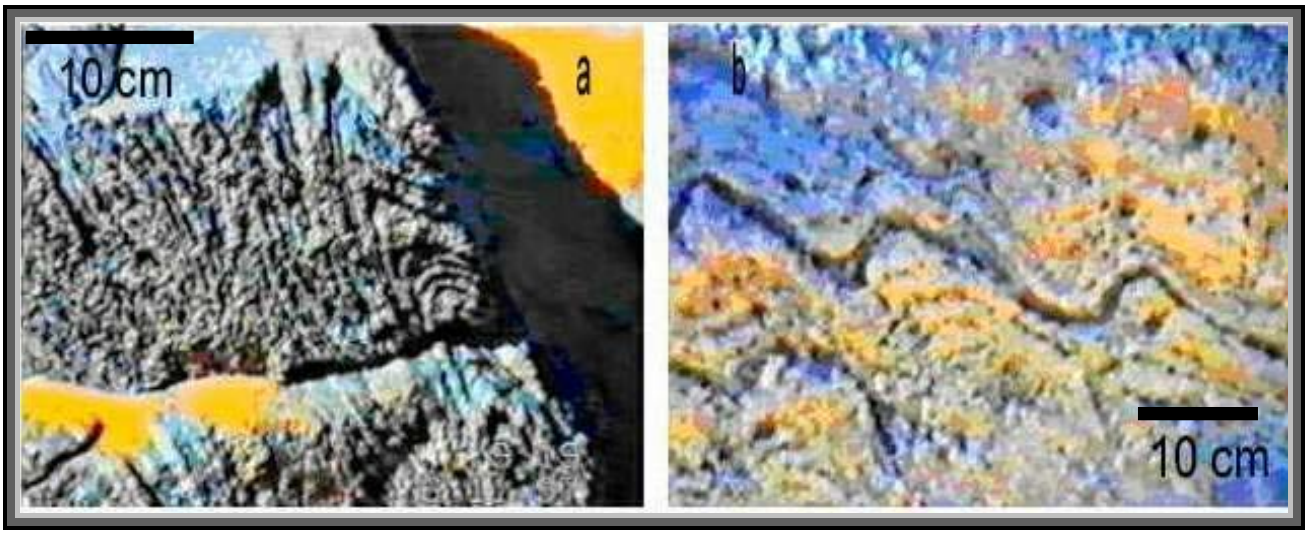

a **b**

Fig 5. 8 (a & b) Minor F3 folds in the Anatexite Sequences (a) from sub-area (A) shows tight isoclinal folds, and (b) from sub-area (C) shows asymmetric folds (both view to the south).

The stereogramm in (Fig 5. 9) shows the average of the measured fold axes of F2 and F3 in the whole area, F2 is nearly steep and plunging to the west with average 00°/86°, while F3 is shallow and plunged to the NNE or SSW with average 16°/12°. Some randomly distributed points (fold axes) represent F2 with intermediate fold axes during the refolding by F3.

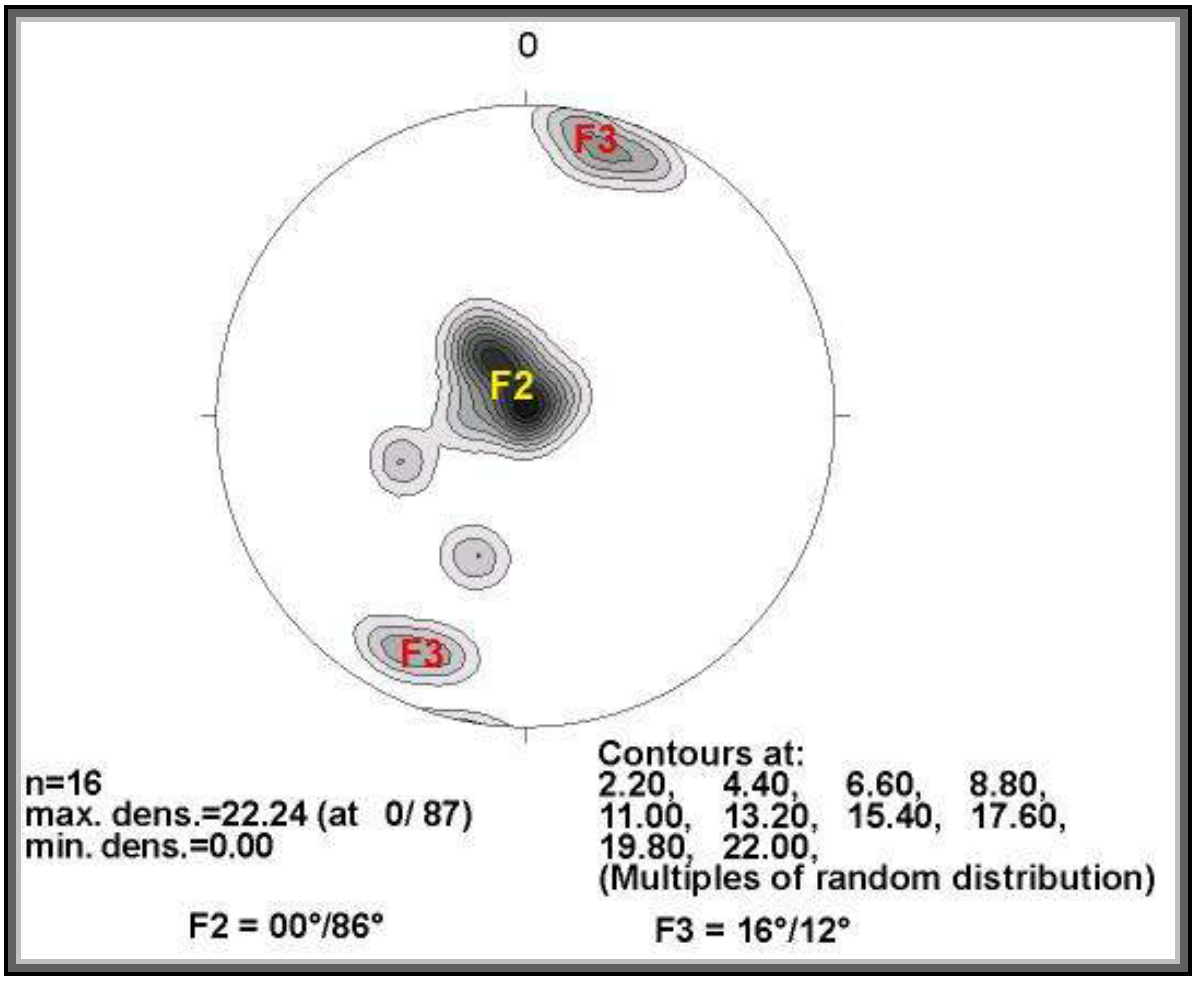

Fig 5. 9 Equal area projection, lower heispere showing the fold axes of F2 and F3.

5.1.2. Faults and Shear Zones

As a result of extensive tectonic and metamorphism events, the study area was deformed by numerous shear zones and faults. These shear zones and faults can be classified into four spatial and chronologic phases as follow:

1- NNE-SSW to NNW-SSE nearly 90° anticlockwise rotated thrust faults accompanied with shear zone.

2- N-S reverse faults (thrusts).

3- East-West wrench faults

4- East-West Normal faults.

5.1.2.1- NNE to NNW Nearly 90° Anticlockwise Rotated Thrust Faults Accompanied with Shear Zone:

This type of thrust faults and shear zones (rotated 90°, after E-W low angle thrust) dominate in the central part of the northern area and traced also in the southern area. This type of faults observed only in the BIF. The origin of these faults and shear zones are belonging to low

angle thrusts, which accompanied the F2 folding phase and due to the rotation during F3 (about 90° anticlockwise around a horizontal axis) appear as dextral strike slip faults (Fig 5. 10).

These faults extend for about 100 to 200 metres with less than 5 metres thicknesses and show a few metres displacement they appear now as a minor apparent-dextral strike-slip faults.

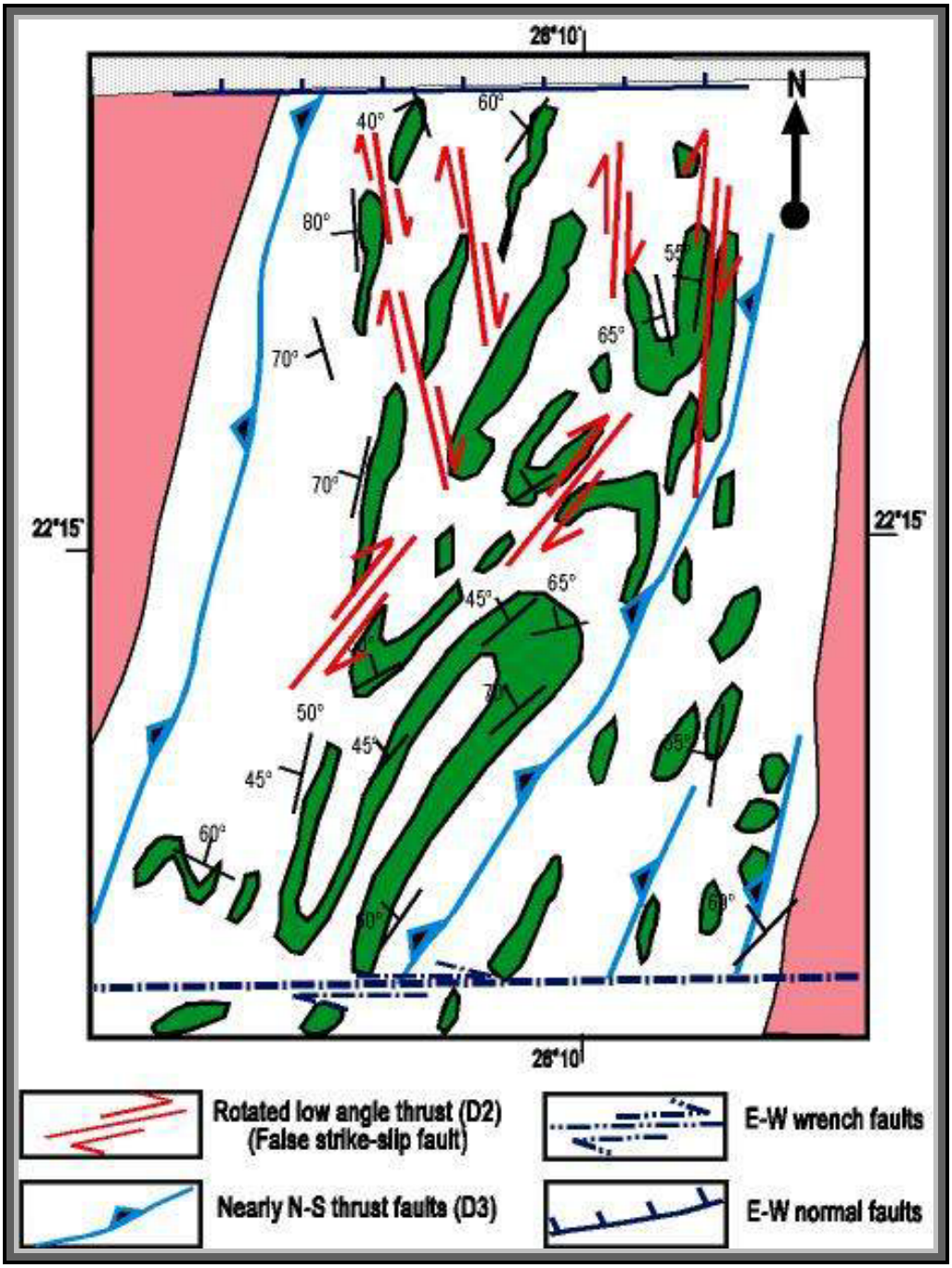

(Fig 5.10) Exemplar map shows the different fault system, in the northern central part of the study area.

5.1.2.2- N-S Reverse Faults (Thrusts)

The N-S reverse faults originated during east-west crustal shortening with nearly NNW-SSE to NNE-SSW strike and dipping to the west with angle ranged between 35° and 70°. These thrust faults dominate allover the area and affected the major three rock units. The thrusts form an imbricate belt, which contains several slices of the BIF overlaying the Anatexite sequences. These slices are composed mainly of the BIF as the upper unit and the Anatexite as the lower unit and sometimes yield some ultramafic rocks at the contact between the slices. The thicknesses of the slices range between 500 metres and 5 kilometres, with the length varying between 5 and 20 kilometres, whereby the slices are mostly parallel to each other (Figs 5.11 & 5.12). However in some locations the thrust belt shows an imbricate fan, especially in the BIF, which appear the BIF as a western fold limb thrusted over other western fold limb and showing fold surface parallel with fault surface.

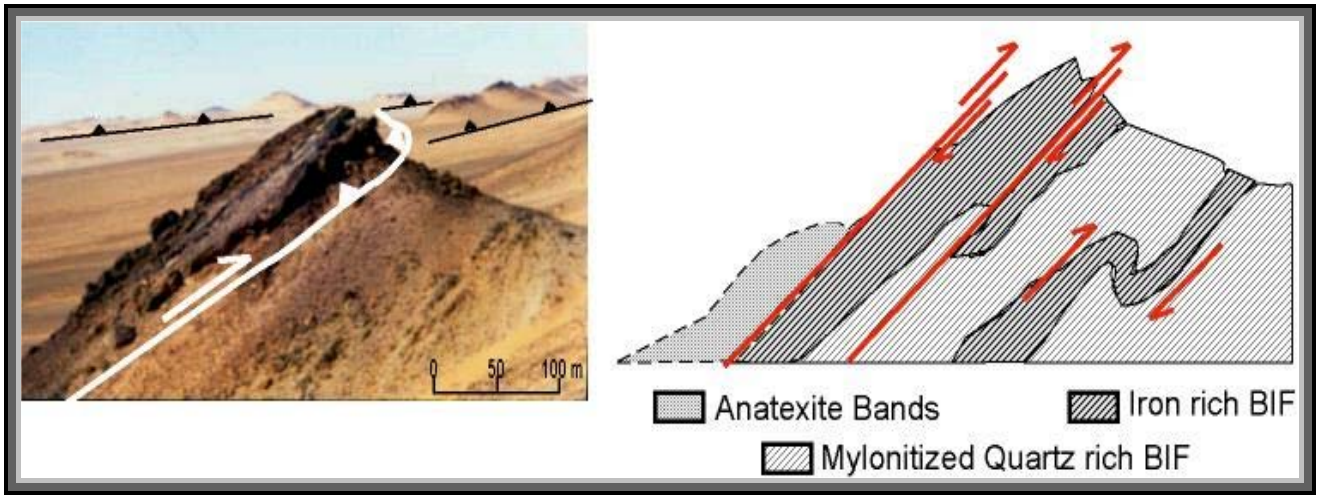

Fig 5.11 Field photograph and explanatory sketch of a thrust fault with drag folds in the hanging and footwall within the BIF of the southern sub-area C (view to the north)

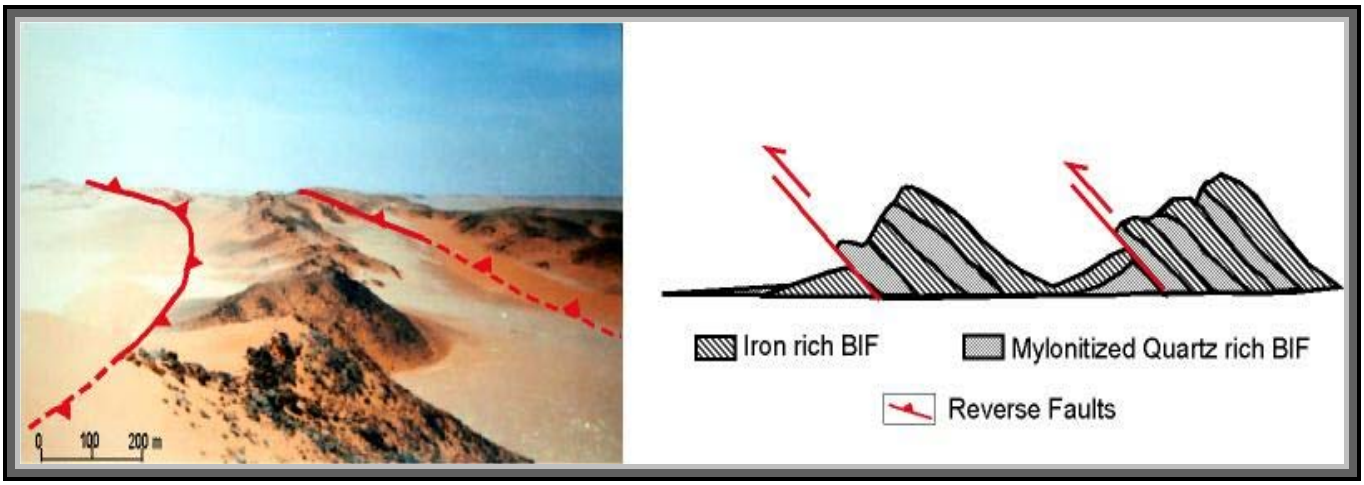

Fig 5.12 Field photograph and explanatory sketch of two ridges comprising two thrust slices within the BIF in the northern sub-area B (view to the south)

5.1.2.3- East-West Wrench Faults

The wrench fault system cuts through the all rock units, including the sedimentary cover rock, in nearly E-W direction, often accompanied by major extrusion of rich iron mineralization. In some places these faults show more than one generation having the same trend. The first one is probably older than the normal fault system, because the fault breccia in the old one is welded by goethite, being confined to the BIF, while in the younger one the fault breccia is welded by rich iron mineralization of mainly hematite and occurs in the basement and in the sedimentary rocks (Fig 5.13 & 5.14)

Exemplar map shows the different fault system, in the north central part of the study area (Fig 5.10).

Fig 5.13 Wrench fault affecting the sedimentary rocks in the northern area (view to the east)

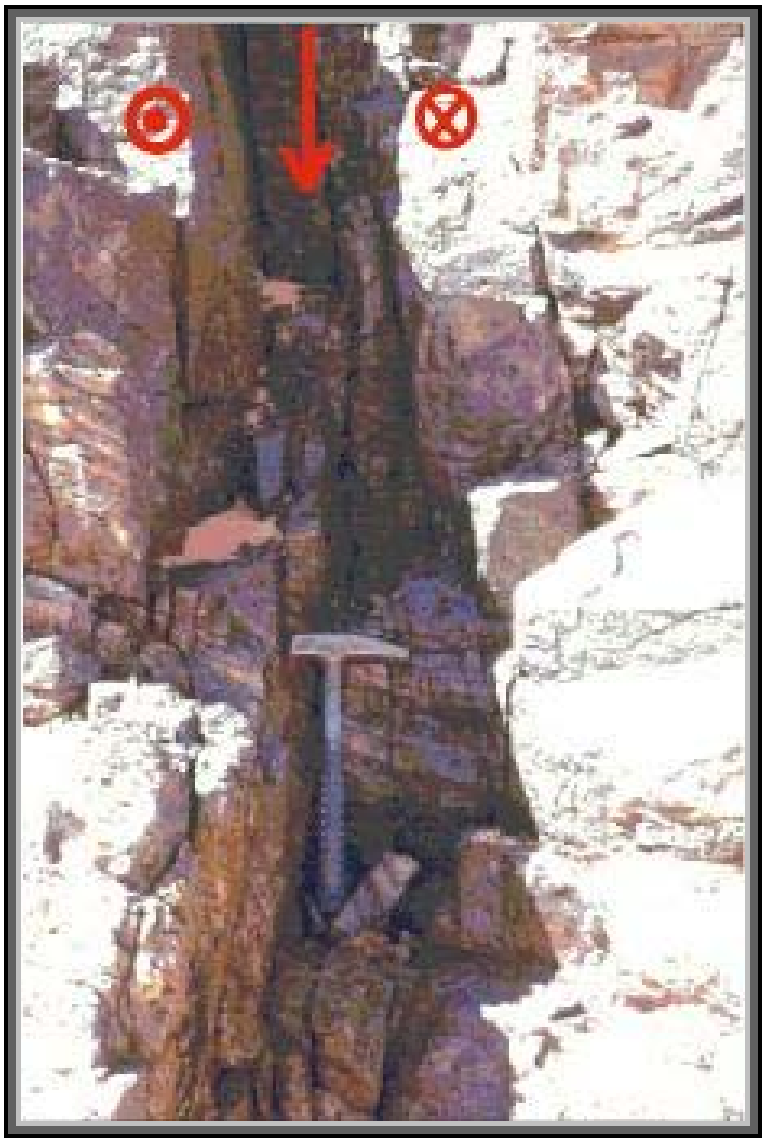

Fig 5.14 Wrench fault affecting the BIF rocks in the southern part of the area (view to the west)

5.1.2.4- East-West Normal Faults

The final fault types are normal faults resulted of N-S crustal extensions as a wide graben in the middle of the present area traversed the middle part of the area from east to west. This graben exhibits, a sedimentary horizontal succession of more than 20 metres thickness, of Carboniferous age. Locally, it is deeply eroded uncovering windows of the BIF (Fig 5.15). The graben is flanked by two horsts of the BIF, to the south and the north respectively, which are often covered with the same banded sediments having less than 2 metres thickness. Further to south and to north of these two horsts the basement rocks are fully covered by the flat lying sedimentary succession, some tertiary volcanics outcrops or sand dunes, which indicate the down throw on the normal fault.

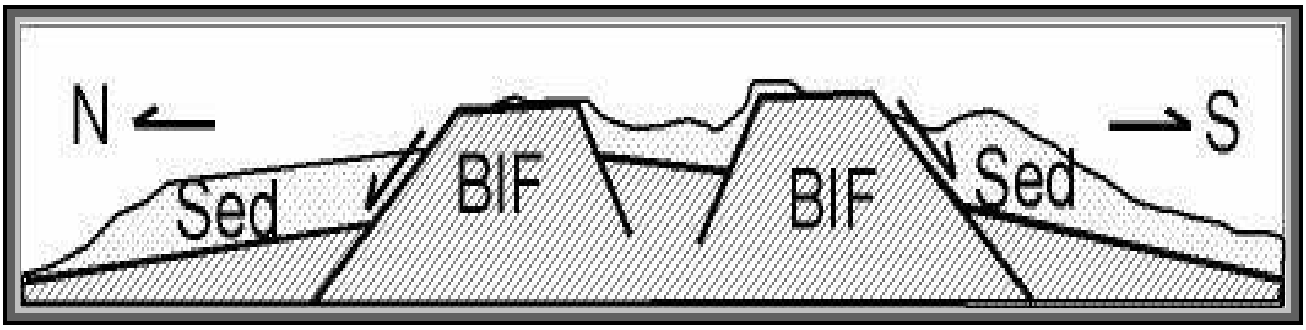

Fig 5.15 Profile showing the N-S extension producing graben and horsts (normal faults).

5.2. Minor Structural Elements

5.2.1. Banding:

Both the BIF and the Anatexite Succession show clear banding, distinct changes in grain size, colour and lithology. The main trend of the banding in both units is NNE-SSW with a mainly dip angle ranged between 10° to 70° to azimuth mainly 280°.

The Anatexite Sequence shows light and dark bands that vary in thickness and lithology. The thickness of these bands ranged between a few centimetres and a few metres in alternation of light and dark bands of highly mobilized migmatic bands.

The migmatitic structures are represented by schlieren, ptygmatic folds, lit par lit structure and others. The strike of the anatexite bands range between 350° and 25°, dipping to west with an average ranged between 35° and 70°.

No relics of primary structures or parent rocks remained. The primary structures of the parent rocks were destroyed during early deformations (D1 & D2), due to the shearing and migmatitization processes. Migmatitization resulted in nearly shallow dipping south banding in the Anatexite sequence until they were folded and affected by the second deformation phase (D2) which formed the minor asymmetric and tight-isoclinal folds parallel with the major folding of F3 fold phase (5.5a & b and 5.16 a & b and 5.17a).

Fig 5.16 (a & b) Field photographs showing Anatexite with pronounced banding (view to the south).

The BIF shows banding as a primary layering with layers composed of chert, primaryly laminated magnetite-quartz bands, quartz bands and metapelitic bands. The banding has nearly the same trend as in the Anatexite succession, with thicknesses ranging from a few centimetres to more than 10 metres (Figs 5.17b and 5.18a & b). This suggests that both units were deformed during the same deformation. In addition, the BIF shows earlier structures due to south-north maximum stress with an earlier E-W folds accompanied with low angle thrusts and shear zones have vary thicknesses between a few centimetres and more than one metre. The earlier folds, thrust and shear zones were rotated with about 90° anticlockwise around a horizontal axis during the F3 folding phase and appear now inside the BIF bands. The early shear zones can be observed in a few metres to a few hundred metres along the strike, which have nearly N-S direction with steep dip angle to the west.

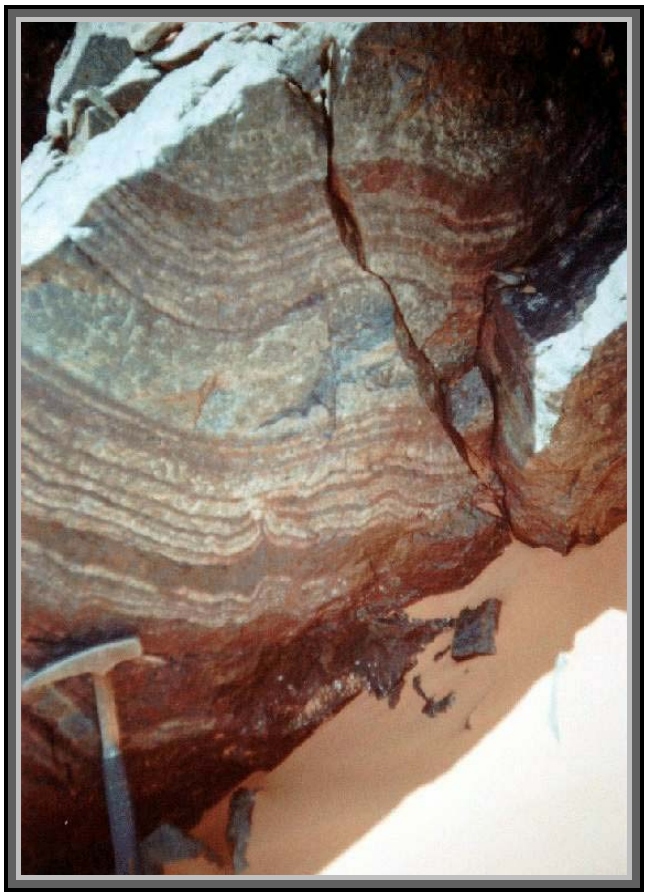

Fig 5.17a Fig 5.17b

Fig 5.17a show the banding in the Anatexite sequence in polished surface of alternation between dark and light bands.

Fig 5.17 b Field photograph shows the primary banding in the BIF, alternation between iron bearing bands with pure slica bands, the bands imprint with the earlier folds (view to the south)

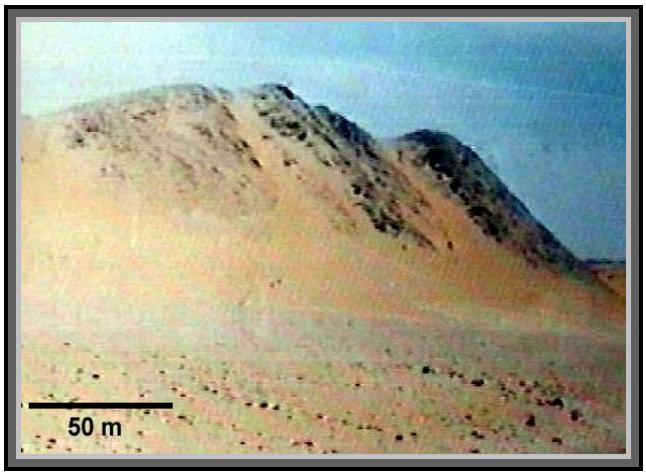

Fig 5.18 a Fig 5.18 b

Fig 5.18 (a &b) Field photographs showing the BIF with pronounced primary banding (view to the south).

5.2.2. Foliation:

All rock units show penetrative foliation, which generally discuss joints parallels banding. Most of the foliation is related to shearing processes, which affected the banding surfaces, but in places, where closed to the thrust surfaces, dominate narrow penetrative foliations parallel with the bands (Figs 5.18 a & b).

Often minor folds (asymmetric or tight-isoclinal) with vertical axial surfaces or east vergent, folded the Anatexite bands, which gradually change into overthrusting and reverse faults that parallels the foliation plane.

The foliation in the BIF hills varies between the lower part and the top of the hills. The hills often represent the western limbs of anticlines, therefore the foliation at the top is parallel with the banding. The general dip is 10° to the west, while near the Wadi level the angles reach 70° to the west.

The main attitude of the foliation in the investigated area is 15° / 65° to the west, with the strike between 335° and 25° with dip angles between 15° and 75° to the west. The stereogram in (Fig 5.19 a & b) shows the average of foliation poles in the whole area and the average value of the field foliation, which may be represented by a great circle with 294° / 45°.

The penetrative foliation in the Anatexite sequences is shown in Fig 5.20, while the narrow penetrative foliations in the BIF are shown in Fig 5.21 (a & b).

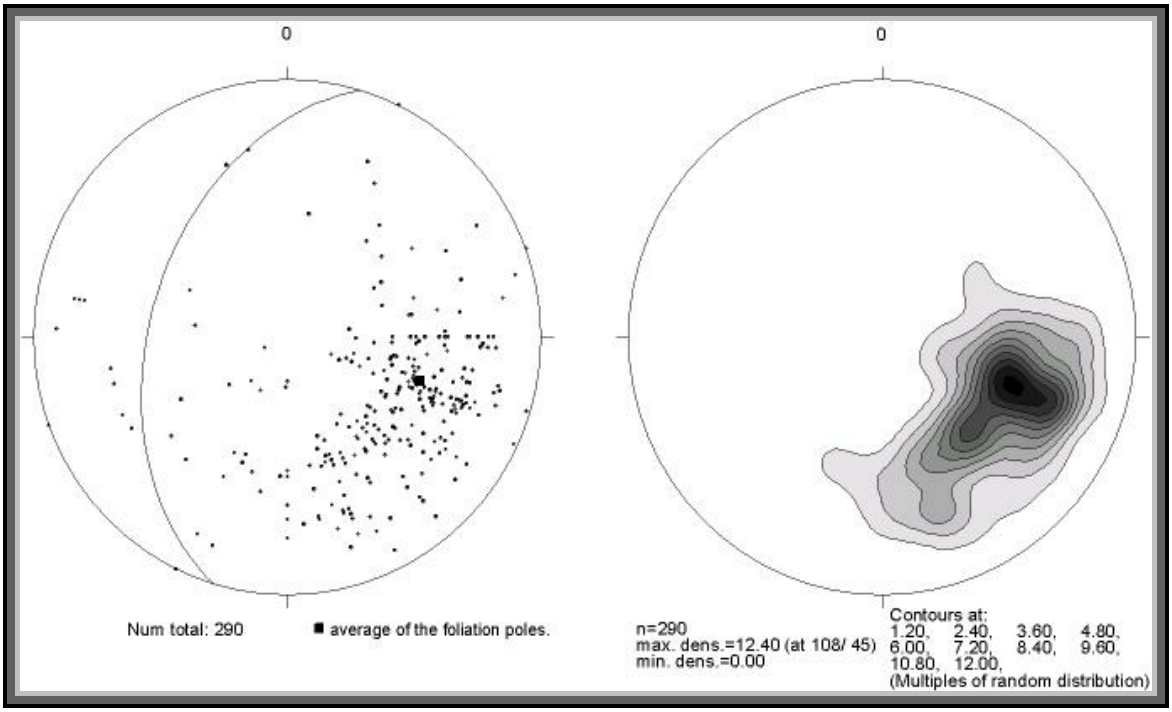

Fig 5.19 (a & b) Equal area projection, lower hemisphere poles of foliation from the whole area

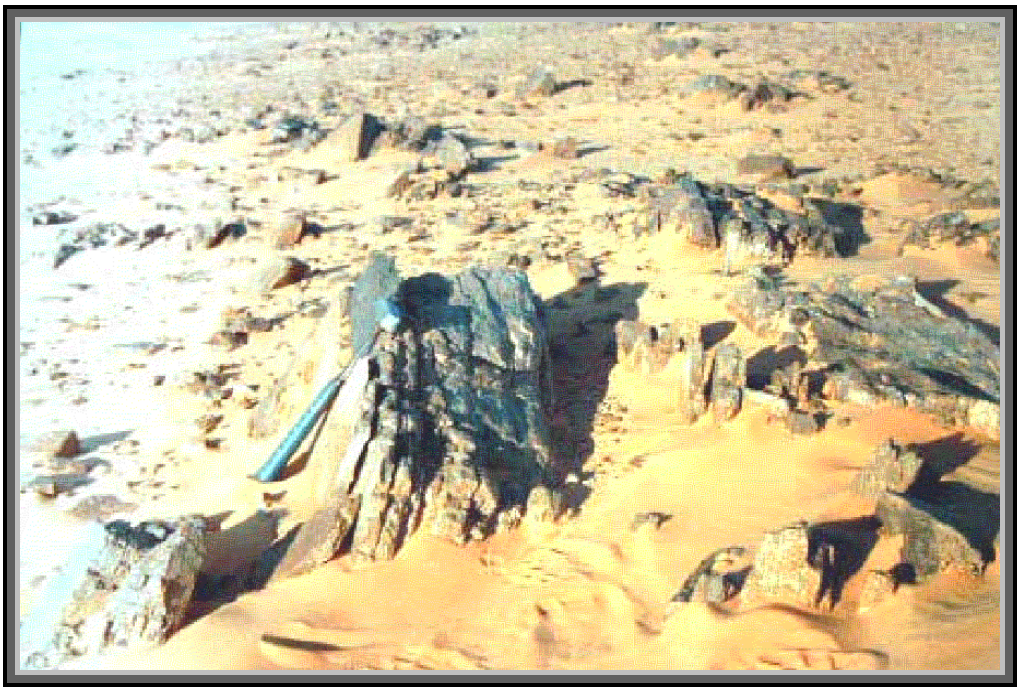

Fig 5.20 Foliation in the Anatexite Sequence (view to the north).

Fig 5.21 a

Fig 5.21 b

Fig 5.21 Foliation in quartz rich bands (a) and iron rich bands (b) of the BIF (view to the N).

5.2.3. Lineation

Several linear elements can be recorded from the deformed rock units of the study area. These are:

1- Mineral lineations,
2- Slickenside lineations
3- Fold axes

5.2.3.1. Mineral Lineation

Mineral lineation occurs as stretching of some mineral grains such as plagioclase, biotite and hornblende in the Anatexite Succession (Fig 5.22 a & b). Sometimes stretching mineral lineations are observed parallel with the fold plunging in the BIF.

The mineral lineations have an average attitude of 013°/ 06° in both of Anatexite and BIF, which indicates the extension direction as a result of east-west shortening.

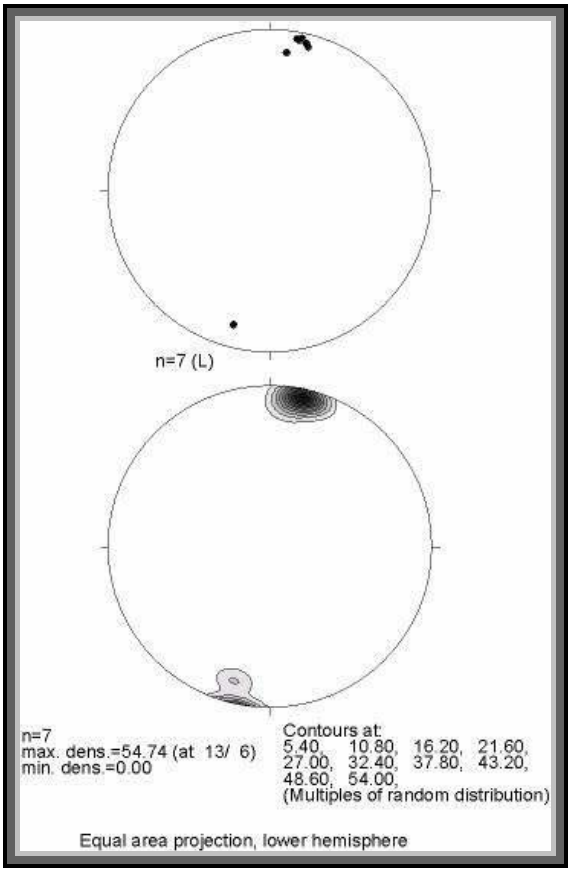

5.22a 5.22b

Fig 5.22a Mineral lineation in the Anatexite, derived from oriented growth of plagioclase, biotite and hornblende (view to the east).

Fig 5.22b Equal area projection, lower hemisphere diagram of mineral lineations in the Anatexite Sequences with a maximum at 13°/6°.

5.2.3.2. Slickenside Lineations

The slickenside lineations are observed in some places on fault surfaces of BIF or Anatexite sequence. Where measured, the slickensides represent a movement on the fault surfaces have a strike of 10° and dipping to the west with 50°. Figs 5.23 a & b show slickenside on a nearly N-S oriented fault surface dipping to the west, representing the footwall of a minor reverse fault. The general slickensides trend between 260° and 290° with plunge angles from 30° to 65°.

Fig 5.23 a

Fig 5.23 b

Fig 5.23 (a) Field photograph (looking east) in the BIF (chert-jaspilite bands) and **(b)** explanatory sketch showing the slickensides in the footwall of a minor reverse fault (260°/50°).

5.2.3.3. Fold Axes

Fold axes are measured or calculated for the major and minor folds. Two sets of fold axes can be recognized in the present area, F2 and F3.

F2 is observed generally in the BIF rocks with steeply fold axes dipping to the west or in some places exhibits shallow fold axes plunging also to the west, mostly in minor recumbent folds, which appear in the BIF bands with low angle of dip, nearly 10° to the west. (In the fold crest). F2 occurs in the Anatexite sequences as ptygmatic folds, while in the Ultramafic-mafic bands as minor tight folds. F2 shows in both units fold axial surfaces parallel with the banding extension (see Figs 5.5 a, b &c).

The F3 dominate in the BIF and Anatexite, with the general attitude of 020°/20° (see Figs 5.7 a&b and 5.8 a&b in this chapter). The fold axes (F3) in the regional folds in the investigated area are frequently parallel with the fold axes of the minor folds in the in both of BIF and Anatexite sequences.

5.3. Detailed Geology and Structure

For better understanding of the geology and structure of the study area, it should be divided into smaller sub-areas, each of which shows unique and certain detailed structure features. The combination of the study of sub-areas can be give complete structure evolution. The following are four sub-areas arranged from north-west to south-east (Fig 5.24)

These Sub-Areas are:

1- Northwestern sub-area (A).

2- Northern central and eastern sub-area (B).

3- Southwestern sub-area (C).

4- Southern eastern sub-area (D).

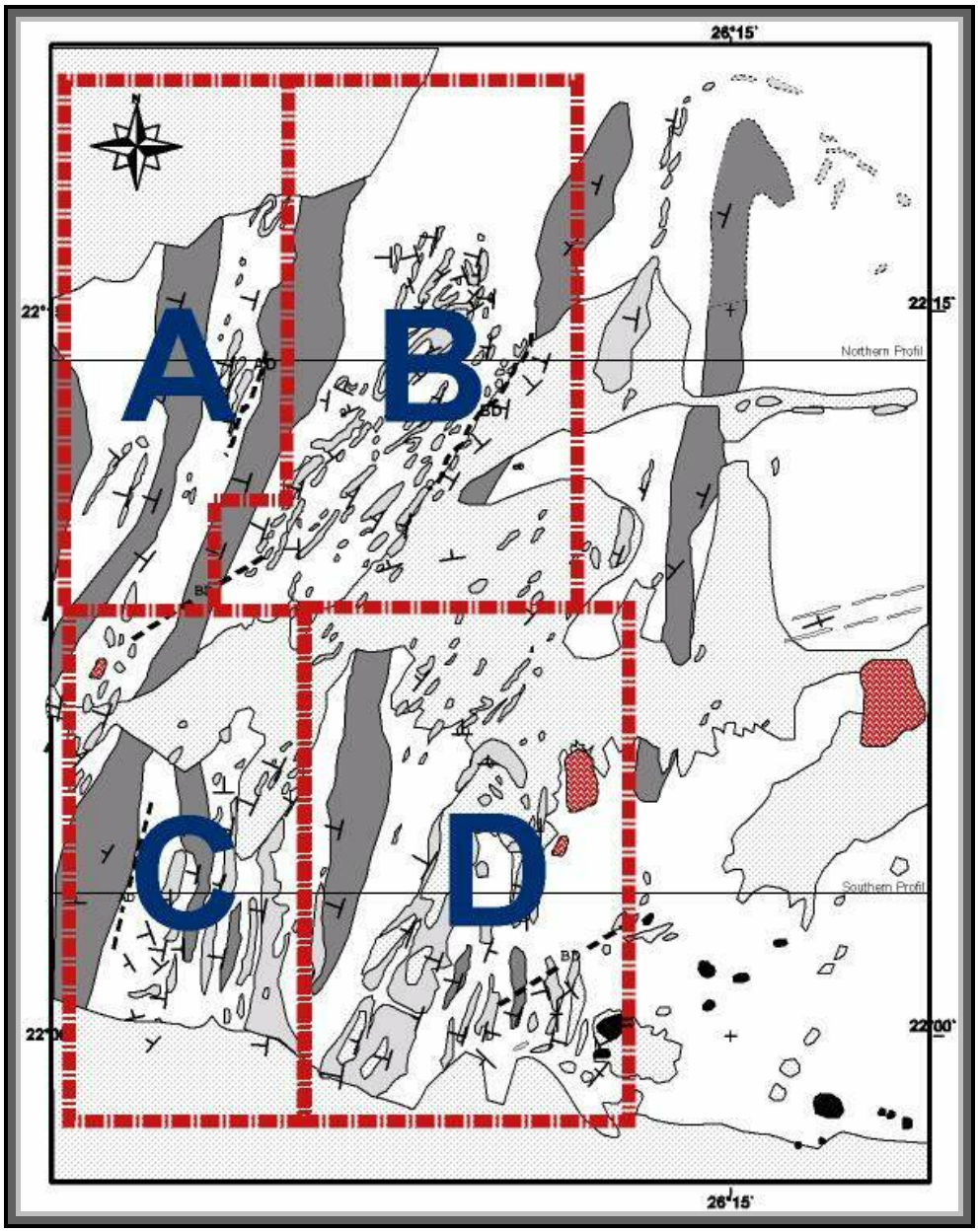

Fig 5.24 Shows location of the sub-areas

5.3.1-The Northwestern Sub-Area (A)

Sub-area (A) occupies about 120 km^2 (10 x 12 km) (Fig 5.26). Two regional thrusts are running through this area, each one having four km width and more than ten km length (slice No. 1& 2 in Fig 5.26). The upper unit in these thrusts is the BIF, which unconformable overlies the Anatexite. The contact between these units is always covered with sedimentary rocks or sand dunes. At the western side of the sub-area (A) there are thrusts sets in, where the Anatexite is thrusted over the BIF e.g. thrust 1 (Fig 5.26). The thrusts affected the BIF by development of a mylonitic zone of about 3 metres width. The trend of this zone is azimuth 20° dipping with an angle of 55° to the NW. This sub-area is characterized by NW dip directions for the foliation and banding of the BIF and Anatexite, the angles of dips range between 40° and 70°. The foliation is nearly parallel to the thrust surfaces and sometimes varies in its dip.

Following below the BIF toward the east are anatexite rocks consisting of a repetition of narrow leucosome and melanosome bands that crop out in low lands at the wadi level. The leucosome bands always contain minor asymmetric east vergent folds, which normally have asymmetry (Z) sense. The fold axes plunge 15° to the NE.

The width of the BIF is less than two km while the Anatexite has more than 2 km width. Further to the east follows the next thrust zone e.g. thrust 2, being nearly parallel with the first one. The BIF exposures crops out in the wadi level, covered by sand dunes for about 200 metres toward east, there are a three separate hills of the BIF. Each hill represents the western limb of an anticlinal fold, the dip angle at the lower part of the limbs at wadi level is rather steep, while it is becomes nearly horizontal on top of the hill. The three hills are separated by minor thrusts, which together form an imbricate fan (Fig 5.26 profile). On the western hill, a mylonitic zone parallel with the thrust surface is more than 3 metres wide and a few hundred metres long. The foliation cutting through these hills is nearly parallel with the banding in the BIF with dip angles of 65°, while the shear zone or mylonitic zone is inclined to the bands (with about 40° dipping to the west) and only occasionally parallel. The average thickness of the mylonitic zones is about two metres. Some minor isoclinal refolded folds with steep fold axes, or sometimes with shallow fold axes dipping to the west, are obvious at the surface of these hills. Generally, the foliation in this sub-area ranges between azimuth 340° and 20° dipping between 20° and 70° to the west. Stereographic plots of the poles of field foliation indicate the average of foliation as great circle with attitude 290°/60°. The density of contours shows two poles represents two regional thrusts in the sub-area (A) as shown in (Fig 5.25).

Locally younger foliation has nearly E-W trend with a vertical dip, parallel to a minor dextral strike slip fault to be recognized by a fault breccia, which is welded by goethite (gossan). This zone extends for more than 100 metres, the thickness ranging from 3 metres to a few decimetres. Displacement is noticeable. This fault zone is parallel to a major dextral strike slip fault, which cuts almost the whole northern part of the area, but is only recorded in the BIF parts.

The sub-area (A) was affected by the intrusion of several acidic and intermediate dykes, which cut nearly parallel to the banding, while a younger basic dykes having a trend of azimuth 70°.

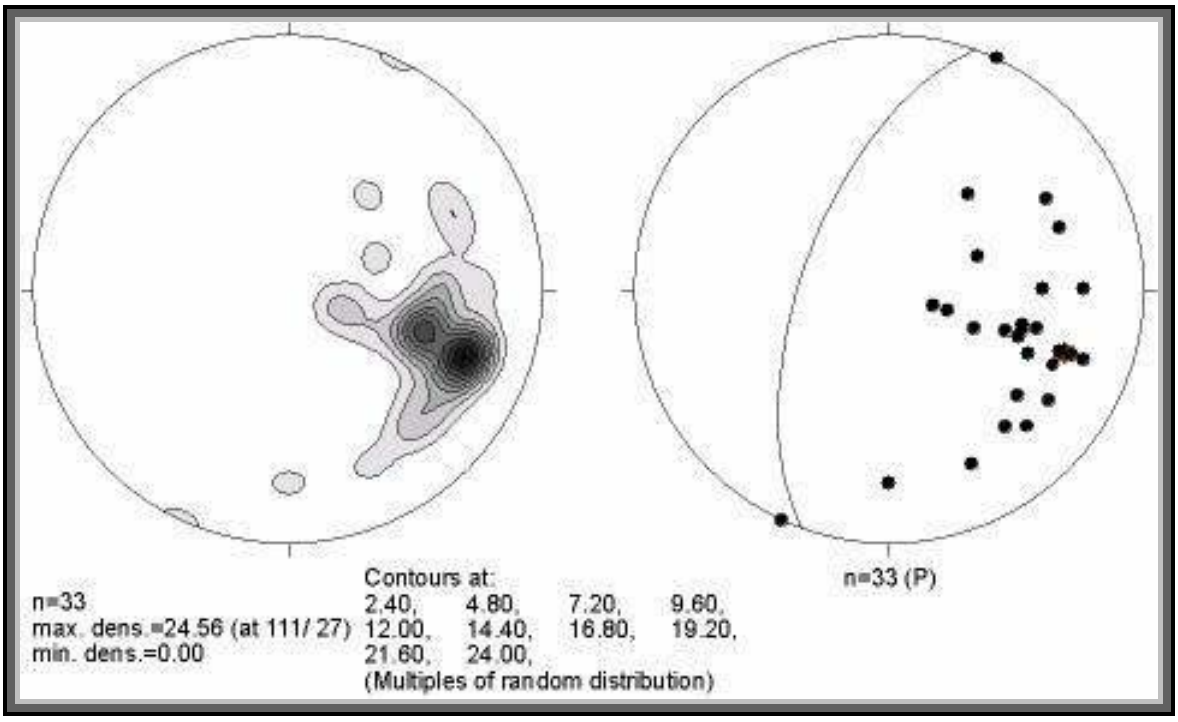

Fig 5.25 Equal area projection, lower hemisphere poles of foliation in sub-area (A)

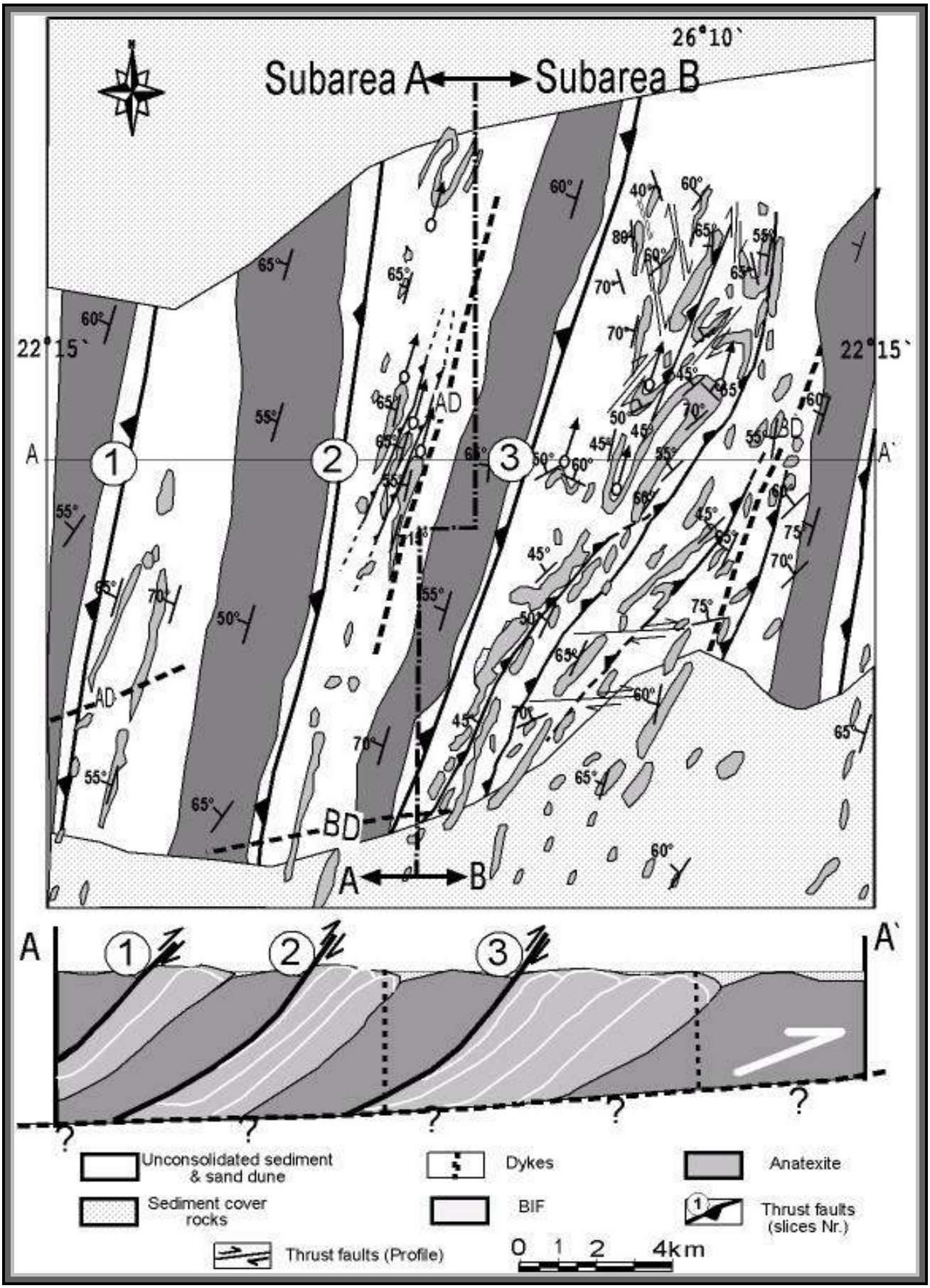

Fig 5.26 Structural and geological map of the northern sub-areas (A & B)

5.3.2. Northern Central and Eastern Sub-Area (B)

The sub-area B covers an area of about 120 km^2 (10 x 12 km) from the central eastern and northern part of the investigated area. It adjacent to east sub-area (A), (Fig 5.26). The area is dissected by major thrust e.g. thrust No 3 (Fig 5.26). Some other minor thrusts are parallel to the major one, and run only in the BIF.

On the western side of the sub-area (B) there is an Anatexite Sequence thrusted over the BIF in similar relation to sub-area (A). The Anatexite has the same properties as in sub-area (A). At the contact between the Anatexite and the BIF, toward the east, the area is covered by sand dunes. The BIF is highly deformed, whereby highly sheared chert is stained with goethite. Highly folded and refolded bands characterize the BIF in this area. The general strike is azimuth 15° dipping 50° to the NW. All the BIF in this area belongs to the western limbs of anticlinal folds (F3), which developed during the D3 (E-W shortening) phase. In these limbs many macro- and micro-folds with steep fold axes are developed (F2), with scales ranging between a few centimetres and a few hundred metres. F2 appears in the center of this area as some macrofolds while in the northeastern part appears as microfolds, all exhibiting steep fold axes. These fold structures belong to D2. The microscopic study of BIF samples in this area show remnants from earlier simple shear mylonitization zones, which developed during crustal thickening.

The earlier simple shear bands folded by F2, that is supposed an earlier deformation phase (D1) which partially overprinted with the later intense deformations of D2 and D3.

The BIF in the northern part on sub-area (B) shows some NNE-SSW to NNW-SSE nearly 90° anticlockwise-rotated thrust faults accompanied with shear zone. They exhibit an apparent dextral strike-slip faults. They extend for a few hundred metres to more than one kilometre and show a few metres displacement, as the result of early S-N shortening during the formation of F2 folding in the D2.

The southern part of this sub-area exhibits some repetition of the BIF bands due to minor thrusting. These slices are bounded by reverse faults, which are parallel to the major thrusts in the area. Normally the BIF bands in this part are parallel to the main foliation, which strikes 10° to 45°, dipping to the west with 55°.

Several dextral strike slip faults are observed at a scale of 2 to 4 kilometres with almost E-W trend run through all the rock types. At the fault surfaces a fault breccia well developed independently of the different rock types, welded by hematite (Figs 5.27 a & b). The southern and eastern parts of the sub-area (B) are covered with Carboniferous sandstone and sand dunes. On the eastern part of this sub-area the BIF overlies another Anatexite sequence

again, the contact is mostly covered with sand dunes, especially in the southern part. The Anatexite has a width of 2 to 3 kilometres with the same lithological, morphological and structural characters as on the western side of the same sub-area. The following Anatexite Sequences was thrusted to the east, over the BIF, which is exposed in several windows emerging in the sandstone plateau and wide sand dune sheets, which mostly cover the eastern side of the investigated area. This makes it difficult to access, sampling and mapping this part of the present area.

The contact between the Anatexite and the BIF exhibits a highly sheared zone as a result of reverse faulting. Stereographic plots of the foliation indicate the average of foliation as a great circle with attitude 316°/42°. The wide pole distribution is due to the different band trends at F2 and F3, also several minor fault slices in the sub-area (B) and due to the curvature of folding in F3. Most of the poles represent the western limb of regional anticline fold (Fig 5.28).

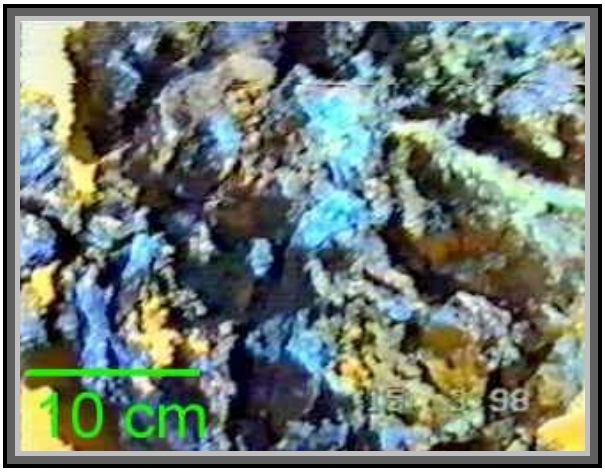

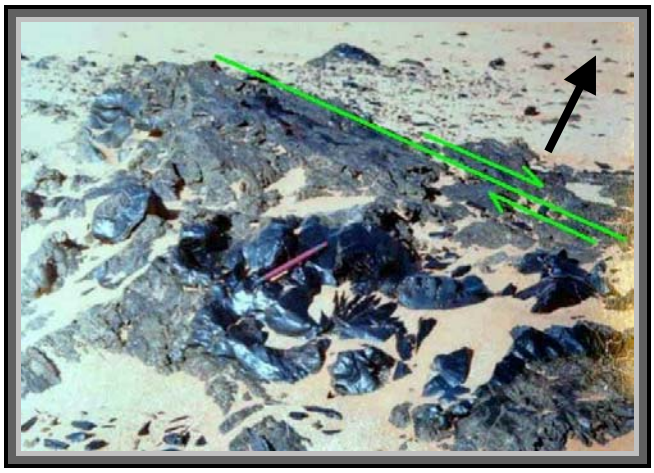

Fig 5.27 Fig 5.27 b

Fig 5.27 Field photographs **(a)** fault breccia welded by goethite in the BIF in the northern part of the sub-area (B). **(b)** Minor right lateral fault and fault breccia in the BIF welded by goethite, in the middle part of sub-area (B), arrow to the north.

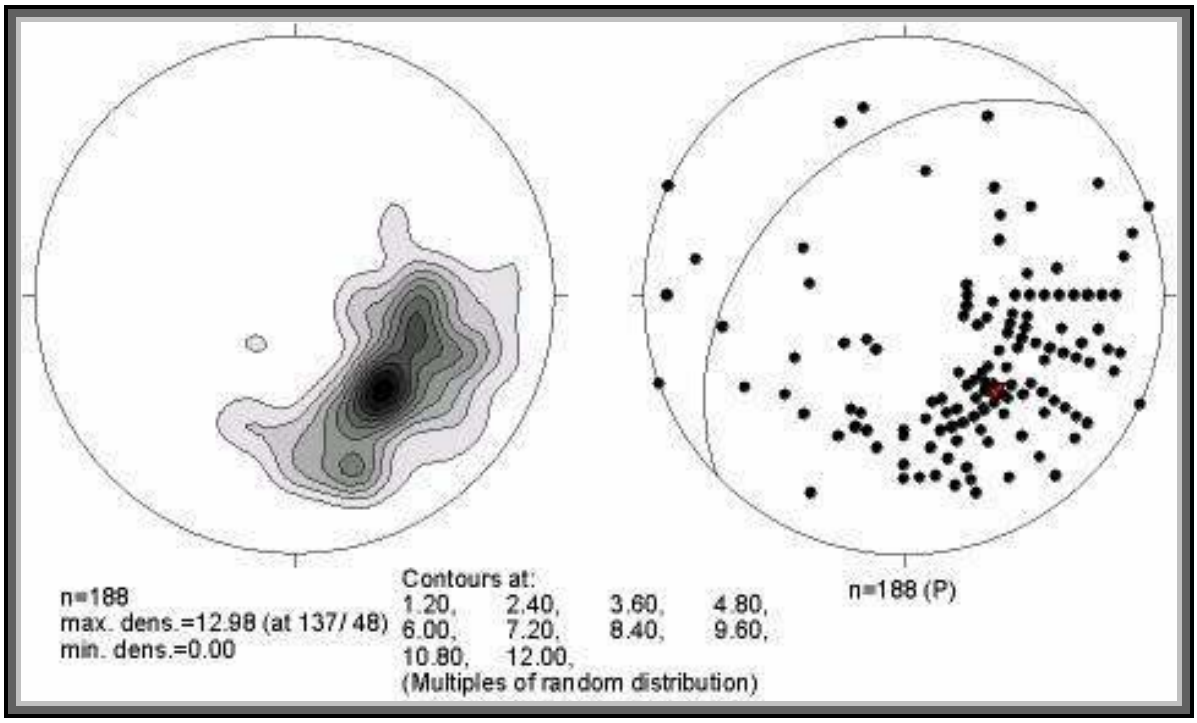

Fig 5.28 Equal area projection, lower hemisphere poles of foliation in sub-area B

5.3.3.The Southwestern Sub-Area (C)

The area occupies 96 km^2 (8 x 12 km) (Fig 5.29). The area is dissected by four thrusts nearly follow the same trend of the major thrust in the area. They are numbered as 1, 2, 3 and 4 (Fig 5.29). The southern and northern parts of this area covered by sedimentary sheet of Carboniferous sandstone. The remaining parts covered by BIF, Anatexite Sequences and small Ultramafic-mafic bands. At the western side of this sub-area the Anatexite Sequence crops out in small isolated exposures.

The Anatexite Sequences has about 4 kilometres width and extend to the north for about 20 kilometres, being covered with sandstone or sand dunes in some places. The bands trend between 340° and 20° and dipping to the west with nearly 55°. A penetrative foliation is mostly parallel with the banding.

To the east of the Anatexite sequences exposed some bands of Ultramafic-mafic rocks, which consist of forsterite marble, calc-silicate rocks, serpentine, talc-carbonate and highly deformed gabbroic rocks. The ultramafic-mafic bands have about 100 metres width and extend for more than 5 kilometres in north-south direction. They are covered in places by carboniferous sandstone, sand sheet and sand dune. The contact between the Anatexite and Ultramafics is hardly to recognized being covered by sand. However, most probably, there is a gradational contact as watched in sub-area (D) to the east, where the Anatexite Sequences

lies on top of the ultramafic rocks and both exhibit same orientation for banding and foliation, especially near the contact zone.

Toward the east, the Ultramafic-mafic bands are covered with sand, about 200 metres further to east highly sheared BIF bands of low topography are outcropped.

The contact between the ultramafic-mafic bands and the BIF has clearly tectonic contact, whereby the ultramafic-mafic rocks with the overlying Anatexite are thrusted over the BIF to the east. The thrust surface (thrust No.1 in Fig 5.29) is parallel to the fold axial surface in the BIF toward east, which has N15° E / 55° to the NW direction. This thrust extends to north, which runs also through the sub-area (A).

Further to east, the BIF emerges as a chain of small hills with low elevation between 5 and 50 metres over wadi level with about 500 metres width. The BIF is composed of yellowish brown colour chert bands turn into brownish black with increasing hematite and magnetite contents. The BIF bands gradually change in their iron bands according to quartz rich bands. Often, mylonitic zones of 1 to 2 metres of thickness cut the different BIF types parallel with the banding and foliation. Toward east, the Anatexite Succession becomes the lower unit beneath the BIF with discordant contact. This Anatexite Sequences has the same characteristics as in the western outcrop. It extends for about 400 metres eastward, about 5 kilometres north-south, and hidden under the sandstone rocks.

The BIF and the Anatexite exhibit a thrust slice No. 2 (Fig 5.29) and appear as a western limb of an east vergent anticline, which has an almost horizontal fold axis trending to the azimuth 15°. The foliation in both the BIF and the Anatexite is parallel and ranges from 340° to 20° dipping to the west with 55° at the steeper parts and 10° to the west according to the position related to the fold crest.

Further to the east, another two thrust slices are exposed No. 3 & 4 (Fig 5.29), all the four slices have the same characteristics and exhibit the western limbs of an east vergent anticlines, the eastern limb being suppressed during the thrusting. The BIF in each slice is exposed in hills of 60 metres elevation over wadi level while the Anatexites crop out only at the bottom or sometimes as small blocks in the wadi floors. The eastern thrust slice in this area e.g. No. 4 (Fig 5.29) runs only through the BIF.

Often the BIF bands show minor asymmetrical folds with nearly vertical fold axes (F2), representing deformation phase D2. The second deformation phase D3 is characterized by NNE thrusts and folds with east vergent (F3). The thrust No.3 conjoins the thrust No 2 in the south and curved to the east and adjoins the thrust No. 4 in the north.

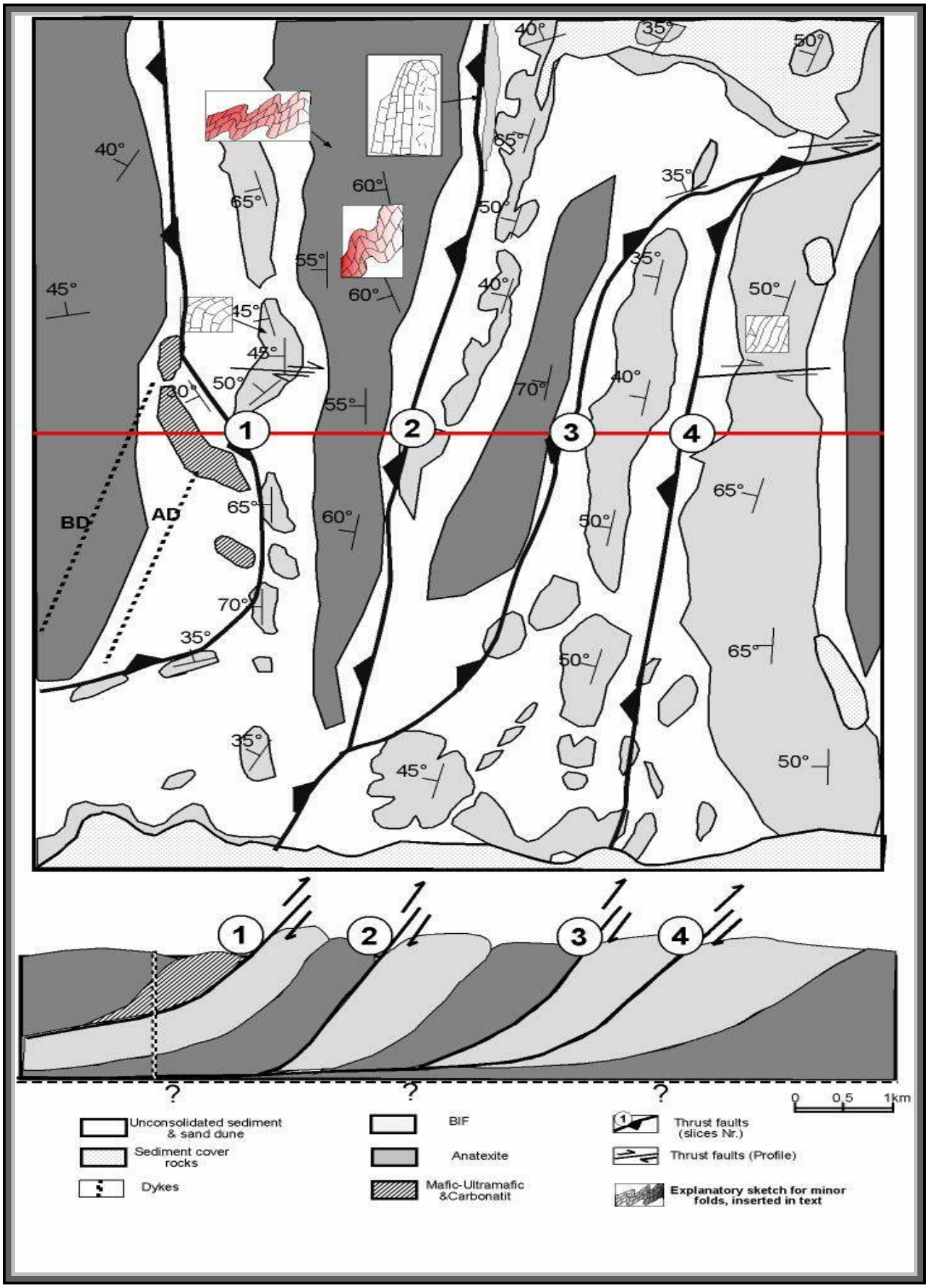

Fig 5.29 Structural and Geological map of sub-area (C)

The Anatexite Sequences in this sub-area (C) show only minor F3 folds, whereby the bands often exhibit a minor tight-isoclinal folds or asymmetric folds with fold axial surfaces inclined to the east (east vergent) as well as enclosed minor thrusts between the folds. Normally the attitude of the fold axes is azimuth 15° with a plunge of 10° to north. The minor thrust surfaces are often parallel with the fold axial surface, attitude 285°/55°.

Toward south of this sub-area all rock units and the thrust slices curved to the west to form a regional synclinal fold plunging to 300° with 45°, this may be due to regional E-W dextral strike slip faulting.

The Anatexite can be followed for more than 20 km in this sub-area thereby with a thickness of up to 5 km. Locally, it is covered with sand or other sediments. These bands are more or less parallel and extend mainly in NNE direction with varying dip angles between 40° and 70° to the WNW direction. Foliation is parallel to the banding. In the Anatexite Sequence different types of minor folds with Z-shape (sometimes developed to minor thrusts parallel with the main thrusts in the area) and with M-shape dominate. These minor folds have fold axes plunging 15° in azimuth 15°.

Slickensides were measured in the foot-walls of the BIF bands. They have general attitudes of 280° / 70° whereas mineral lineations recorded in the Anatexite in the plagioclase, hornblende and biotite trending generally with 010° / 10°.

The BIF hills in sub-area (C) exhibit western fold limbs at the regional scale (in every slice). These limbs represent macro folds plunging in 15° to azimuth 15°, and parallel to the minor folds in the Anatexite Sequence. These major fold limbs have always dip angles more than 65° to the west at wadi level and sometimes less than 20° to the west on top of the BIF hills. The BIF bands often contain different types of minor folds as isoclinal or disharmonic folds at centimetre scale. These folds have mainly sub-vertical fold axes or are dipping steeply to the west. In the other areas folds can be observed at the scale of some tens of metres also with vertical fold axes. Folds at kilometre scale may show the same fold characteristics. This type of folds characterized the BIF only and rare in the Anatexite.

The foliation in both, the Anatexite and the BIF, is nearly parallel to each other.

The BIF bears additionally several shear zones, which generally parallel the foliation and bedding surfaces. The rocks in the shear zones are mylonitic to ultramylonitic and show several kinematic indicator. The thicknesses of these zones are more than 3 metres and extend at the surface for more than 100 metres. Rock fragments in these zones are often stained with goethite.

Younger foliation has trend of 100° with vertical dip, parallel to minor dextral strike slip fault easy recognize by fault breccia, that welded by goethite (gossan). This zone extends to the east for more than 500 metres tell sub-area (D). Its width ranging from 50 metres to 100 metres, displacement is noticeable. This fault zone is parallel to a major dextral strike slip fault, which run through several outcrops of the present area, but is only observed in the BIF bands. The BIF in the eastern side of sub-area (C) is composed mostly of quartz bands with high amount of fuchsite giving rise to a greenish white colour. Highly foliated, these bands have the same trend as in the western part of sub-area (D).

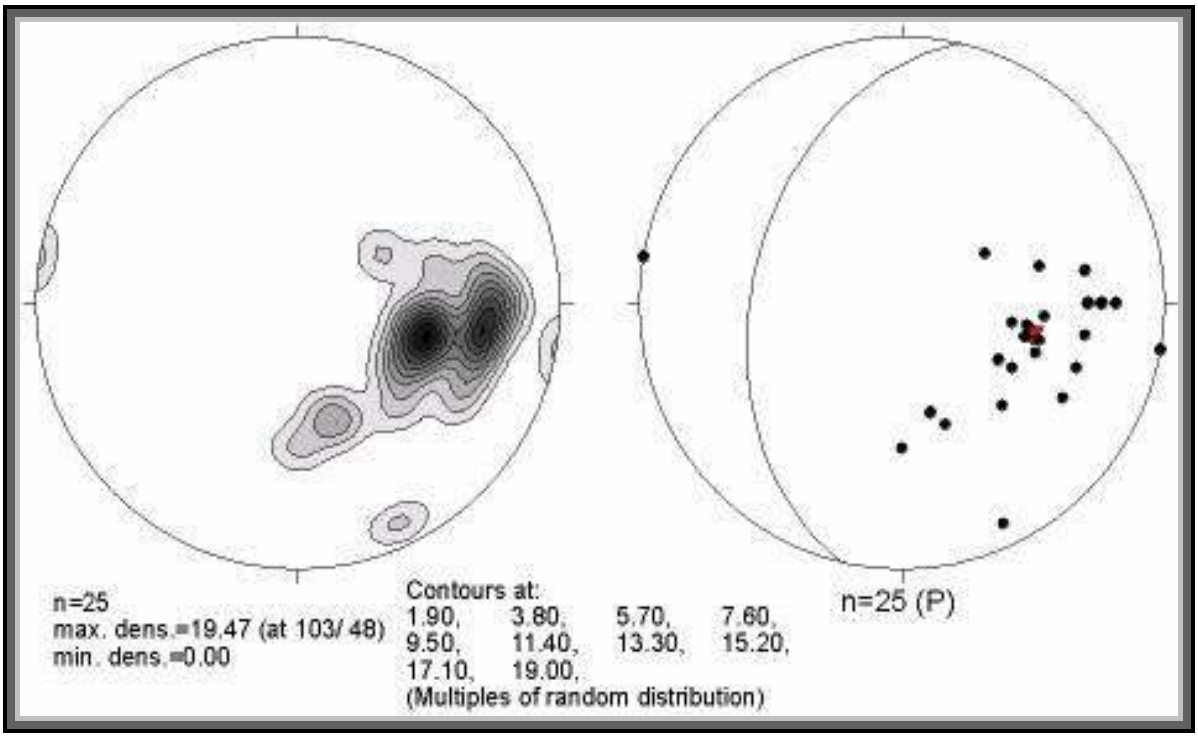

Fig 5.30 Equal area projection, lower hemisphere poles of foliation in sub-area C.

Stereographic plot of the field foliation indicates average foliation as great circle with attitude 283°/42° in the sub-area (C). A somewhat scattered distributions due to faults in (sub-area C) (Fig 5.30). The field foliations indicate the western limb of the regional anticline fold.

5.3.4. The South-eastern Sub-area (D)

The sub-area D, adjacent to the east of sub-area (C). It occupies 120 km^2 (10 x 12 km), the southern and northern parts of this sub-area is covered by Carboniferous sandstone and whereas the eastern part is also covered with the same sediments that intruded by a big mass of granite intrusion (Fig 5.31). The area is dissected by five thrusts nearly parallel to the major thrust in the area, they are numbered as 1, 2, 3,4 and 5 (Fig 5.31).

On the western side, there is a quite large exposure of Anatexite Sequence crops out as lower unit beneath the western BIF in sub-area (C), at the wadi floor or in small blocks in the middle and east of the mapped area. They exhibit the same characters and trends as in the western sub-area (C). The Anatexite Sequence has about 1500 metres thickness and extends into the northern area for altogether more than 20 kilometres mainly with azimuth 10° and a dip of more than 50° to the west. It covered locally with sandstones and sand dunes. The small blocks in the wadi floor often show minor east vergent folds and thrust faults, which are parallel to the fold axial surfaces and the main structure in the area.

East of the Anatexite Sequence there are several small hills in the wadi include lenses or bands of ultramafic-mafic rocks, which are composed of strongly altered gabbroic rocks, serpentinite, talc carbonate, calc-silicate and forsterite-marble. These bands are highly deformed and foliated parallel to the main foliation in this sub-area.

The contact between the ultramafic-mafic rocks and the overlying Anatexite shows a highly deformed (secondary) transitional contact with an azimuth of almost 340° and a concordant dip to the west. It can also be observed at several localities. For about 500 metres toward east of the contact, only wadi sediments cover the area, followed by BIF that crops out with high relief. The contact between the ultramafic-mafic rocks and the BIF lies nearly at the wadi level, which shows a thrust criteria in low land exposures of the highly sheared BIF and the Ultramafic-mafic rocks e.g. thrust No 1 (Fig 5.31). Further to the east, the BIF is covered locally with sandstone.

The BIF is composed of thick chert and jaspilite bands followed by magnetite-hematite rich bands and quartz bands. Together, they constitute the western limb of an anticlinal fold (F3) or thrust slice of azimuth 10° and dips at the wadi level of 60° and at the top of hills of 25° to the west. In this limb a number of minor folds (few tens of metres scale) have mostly steep fold axes (F2). The width of this limb is about 900 metres with length. About 8 kilometres. Some mylonite zones within this limb represent thrust, which mostly parallel the BIF bands.

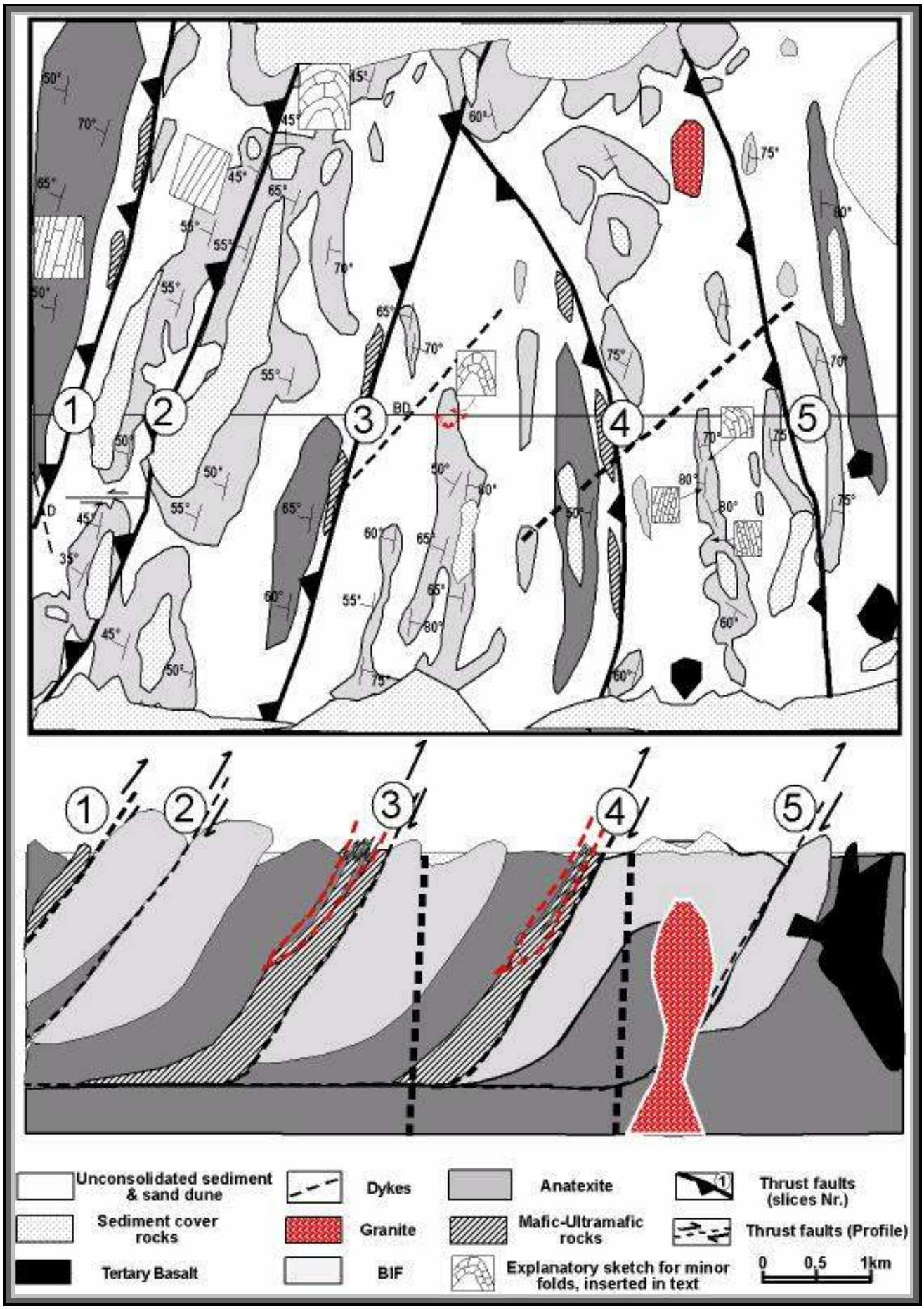

Fig 5.31 Structural and Geological map of the sub-area (D)

Further to the east, there is a repetition of the BIF bands, which represents another western limb of an anticlinal fold. The width of this limb is about 500 metres with the length of about 8 kilometres. It extends parallel to the above described western limb.

The latter limb has the same characteristics and trend as the earlier one, but it is mostly covered with sandstone. The contact between these two BIF limbs is highly sheared, foliated, and represents a thrust parallel to the fold axial surface e.g. thrust No.2 (Fig 5.31). The foliation and banding in both of BIF limbs are parallel with the major band extension, but they show varies dip angles and also have same trend as the regional fold axial planes and the thrust faults.

Toward east the BIF bands ended with high scarp, which borders the wadi to the east, the wadi is parallel to the BIF bands and extends to the NNE direction.

Sedimentary rocks and sand dunes cover most of the wadi floors. In some parts of the area, the Anatexite Sequences crop out again, on wadi floor and as small blocks exhibiting the same characteristics as in the western area. The Anatexite Sequences can be recognized with 500 metres thickness and extends for about 4 kilometres in north-south direction as well as small isolated bands, beneath the overlaying sediments.

Toward east of the Anatexite Sequences some bands and lenses of highly deformed NNW trending ultramafic-mafic rocks emerged into wadi floor with about 70 metres thickness and 300 metres length. They have the same characters as the western ultramafic-mafic band in the sub-area (C). Further east, there are a several minor thrust slices with less than 20 metres thickness. They are composed of highly deformed ultramafic-mafic and Anatexite rocks, which indicate the next thrust over the BIF following to the east e.g. thrust No. 3 (Fig 5.31).

This BIF is highly deformed in the first 100 metres below the thrust. It comprises a mixture of all types of BIF bands with high amounts of magnetite, garnet, goethite and calcite. The BIF has brownish grey colour, it is very hard, its bands are mostly crushed, and often contain cavities filled with very fine quartz crystals, that surrounded by a zone of goethite (Fig 5.32). This BIF represents the lower part of the succession that represent Algoma type of the BIF.

Further east, the BIF succession changes in that the BIF bands contain more jaspilite bands. The upper surface is mostly covered with horizontal beds of sandstone. The BIF extends for about 1000 metres to the east, with lower topography than the western part of this sub-area. Generally, the bands have mostly N-S strike and vertical or steep dips, ranging between 55° and 80° toward west or east. The variation in the dip angles define an anticlinal fold, the fold axis of which plunges 015°/15°. This fold developed as a result of the granite intrusion, about 5

kilometres east of the area, where is a small granitic intrusion outcrop in the northeastern part of this sub-area. Due to the granitic intrusion the foliation was rotated in various directions. In the northeastern part near the contact with the granite, the BIF show pattern of vertical joints at 70° and 340°.

These fracture were filled with iron oxide minerals (Fig 5.33). These joints are accentuated by iron mineralization, which is more resistant to weathering than country rocks.

Fig 5.32

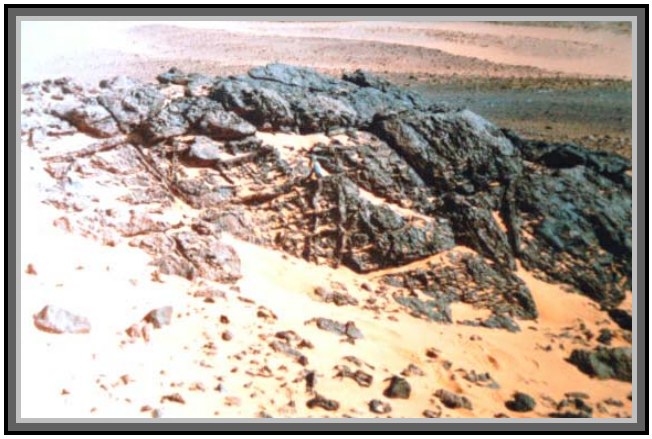

Fig 5.33

Fig 5.32 Cavities filled with very fine quartz crystals surrounded by a zone of goethite in highly deformed BIF.

Fig 5.33 Joint pattern in the BIF close to the contact to a granitic intrusion eastward, (view to the north).

Continued toward east, there are two thrusts in the BIF is followed by the Anatexite Sequences e.g. thrusts No. 4 & 5 (Fig 5.31), they have same characteristics as in the western thrust slices. They totally have about 4 kilometres thickness and about 10 kilometres length. The thrust No. 4 is curved toward west and conjoins with the thrust No.3.

The most eastern part, the whole area is covered with sandstone and sand dunes. Some Tertiary basaltic extrusions cut through the BIF, Anatexite, and also the sedimentary rocks.

Generally the structure pattern in the eastern part of this sub-area differ from the western part in that, the western part shows nearly vertical F2 fold axes whereas the eastern part shows the F2 fold axes are locally plunging into NW directions with nearly 60° angle, while in other location the fold axes are again vertical (Fig 5.34). The second fold generation, F3 is generally conformable with the western part.

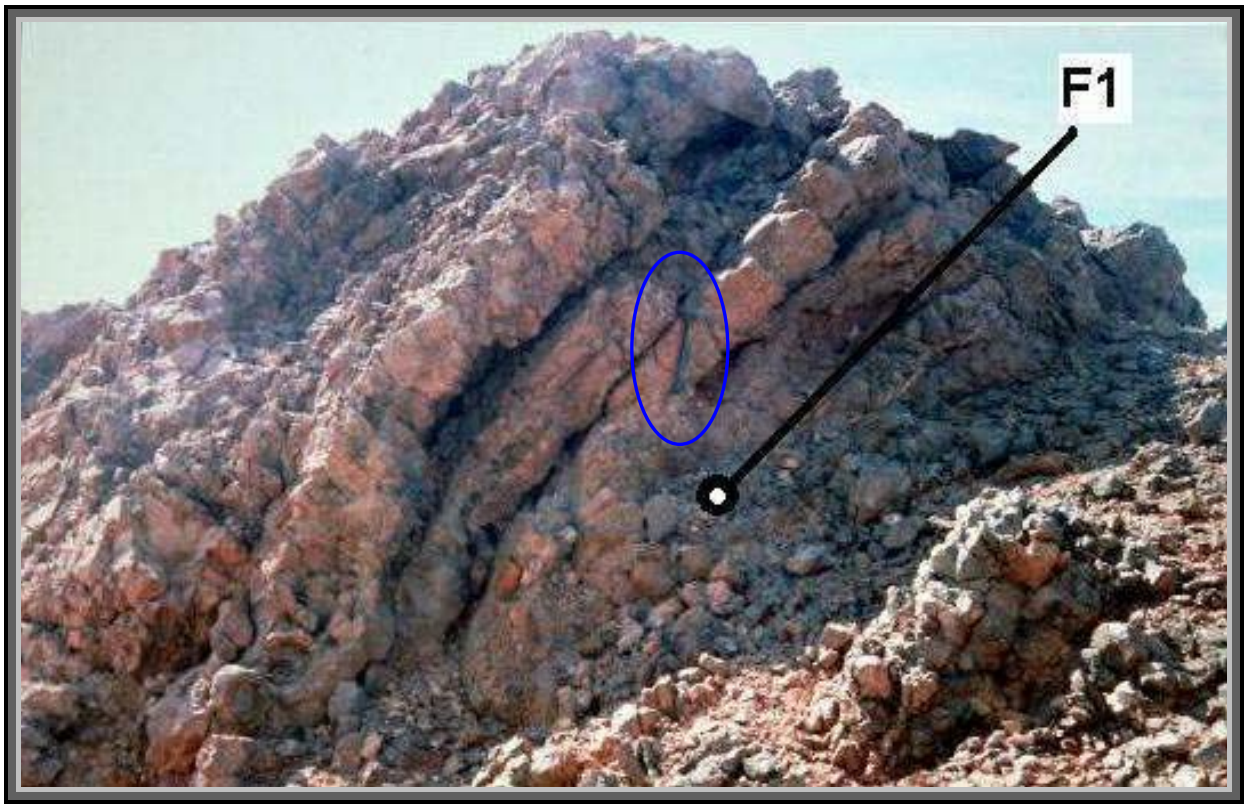

Fig 5.34 F2 fold in the western limb of a F3 fold (view to the north).

Foliation and Lineation

The average foliation trends in this sub-area are generally between 340° and 25° with a dip angle from 25° to 60° mainly to the west. Mineral lineations plunge with maximum 10° to the north. The observed slickensides at the thrust surfaces have trends of 272° / 65°.

A stereographic plot of the field foliation indicates average of foliation with attitude 291°/50 (Fig 5.35). The field foliation indicates the western limb of regional anticline with some scattering points due to different dip directions and fold curvatures.

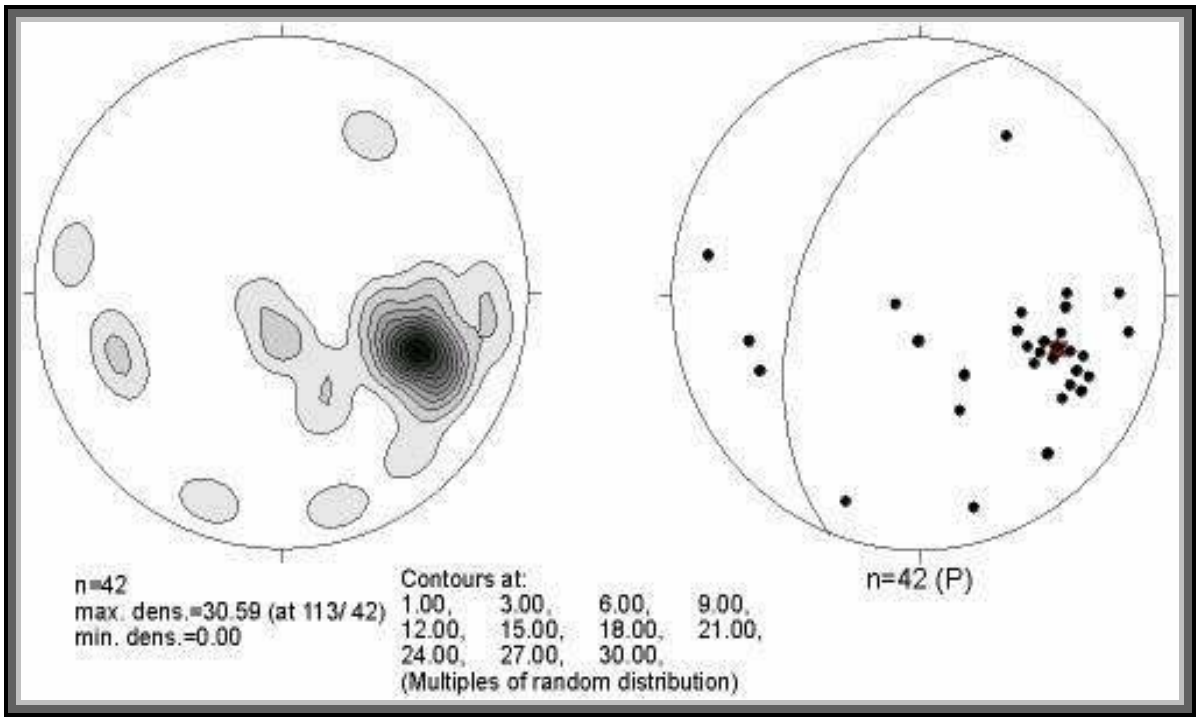

Fig 5.35 Equal area projection, lower hemisphere poles for the field foliation in sub-area (D), the scattering represent the various dip direction, particularly in the eastern part of this sub-area.

5.4 Deformation Phases

Three deformation phases can be discerned in the study area (D1, D2 and D3), the three phases D1, D2 and D3 affected, only the basement rocks and followed with Phanerozoic brittle deformation affected the basement and the overlay sedimentary rocks in the investigated area.

The D1 structures indicate a crustal thickening followed by crustal thinning and developed the melano- and leucosome in the Anatexite sequences, and observed in the thin section of the BIF as simple shear mylonitization zones (S1).

The D2 structures dominate in the BIF as a micro and macro folding (F2) associated with low angle thrust or shear zones (S2), while observed in the Anatexite sequences and the Ultramafic-mafic as a minor folds with the same characters as in the BIF.

The D1 overprinted with D2 deformations, and both of them overprinted by the D3 structures, which refolded the F2 at a perpendicular direction of the fold axes by F3. The D3 affect by refolding and thrusting at the BIF, Anatexite sequences and Ultramfic-mafic bands as F3 and S3. (Table 6)

5.4.1. D1 (Crustal Thickening or Thinning)

The D1 considered as earlier objected deformation in this region occurred during the Early to Middle Proterozoic as a crustal thickening followed by crustal thinning, there are not enough criteria to distinguish the origin of this deformation. This phase started after the deposition of the BIF between 1800-2.900 Ma, the worldwide deposition of the BIF (Windly, 1979), and succeeded by a regional migmatization (anatexis) event around 1.800 Ma, age dating of the Anatexite sequences around the study area (Schandelmeier et al. 1987 give age of 2.399-1.839 Ma by Sm/Nd). In this phase developed the melano- and leucosome in the lower units (Anatexite and UM), while developed a mylonitic shear Bands (simple shear) in the upper unit (BIF).

During the early crustal thickening or thinning all the old structures in the particularly deeper crust (Anatexite and UM rocks) were erased or flattened and formed the leucosome and melanosome. The primary bands in the BIF (nearly upper crust) are particularly surviving this (migmatization) deformation and affected only with some mylonitic shear zones, which observed now as remnants in thin sections of the BIF. Generally in (D1) the Anatexite bands had E-W strike and dipping shallow to the south (S1) and parallel with the mylonitic shear zones in the BIF.

5.4.2. D2 (South-North Crustal Shortening)

The D2 deformation phase has a maximum stress with nearly S-N direction. The south-north shortening resulted the F2 folding, which dominated in the BIF and less observed in the Anatexite sequences and Ultramafic-mafic rocks. The F2 appear as ptygmatic and tight-isoclinal folds, folded the Anatexite and the UM bands. The BIF primary bands were folded by F2 and formed an imbrication of isoclinal and asymmetrical folds (F2) with north vergent and have nearly E-W horizontal fold axes, the folds are separated by some shear zones parallel with the fold surfaces (S2).

Generally in (D2) the Anatexite bands had E-W strike and dipping shallow to the south (S2), and contain minor folds (F2) with E-W axial surfaces.

5.4.3. D3 (East-West Shortening)

The D3 deformation phase was documented in all Precambrian rock units, characterized by NNE-SSW fold axes developed to east vergent, overturned folds and thrusts (reverse faults). A thrust slices are derived from the overturned limbs of anticlinorial structures. The axial surfaces of these folds (F3) is parallel with (S3) and trend to azimuth 15°, dipping to the WWN

with dip angle between 55° and 70°, they are parallel to the thrust surfaces. Zones of intense deformation appear closed to the thrust surfaces between the slices show transition from open, upright folds with weak cleavage to inclined, tight isoclinal folds with strong axial surface foliation. F3 affected F2 by refolding thereby rotating the F2 folds around a horizontal surface in anticlockwise direction.

The resulting foliation, S3, is parallel to the thrust surfaces, however, the dip angle ranges between 20° and 70° to the WWN (285°).

5.4.4. Phanerozoic Brittle Deformation

5.4.4.1 East-West Wrench Faults

The wrench faults run in some places only through the basement rocks. The resulting fault breccia was welded with goethite. In other places, exhibiting the same trend, cut through the basement and the overlying sandstones, thereby resulting also in large zones of fault breccia welded with hematite. In some places extends for a few tens of metres and in other places for a few hundred metres.

5.4.4.2 East-West normal faults

These faults heralded a N-S extension that gave rise to a series of parallel E-W striking normal faults and associated graben and horst structures (fig-5.15).

Displacements by normal faults in the southern and northern margins of the study area are larger than in the central part.

Deformation phase	Folding	Faulting	Foliation	Banding	Rock type and affect
D1	??	??	**S1** unknown trend, due to poly-deformations phases	The leuco-melanosome bands dominate in the Anatexite, while remnants of mylonitic shear Bands in BIF.	Anatexis bands in Anatexite, and mylonitic bands in the BIF
D2	E-W, north vergent with horizontal axes: **F2** The fold axial surfaces dipping with shallow angle to the south	Low angle thrust with E-W trend and nearly parallel with the fold axial surfaces.	E-W foliation in the BIF and the Anatexite bands, dipping with low angle to the south**:** **S2**	The leuco-and melanosome in the Anatexite, the primary bands in the BIF were refolded.	Affected all basement units, due to its position in the old crust, with ductile or brittle deformation.
D3	N15°E folds, east vergent, plunging with 15° to the NNE. Normally only the western limbs of these folds are present: **F3**	High angle reverse fault, parallel to the fold axes, attitude 285°/65°	Penetrative foliation nearly parallel to the thrust surfaces attitude 285°/50° **S3**	--	BIF and Anatexite
Late brittle deform-ation	--	E-W wrench faults, with displacement of a few cm to a few metres	Shear zones, show locally E-W vertical foliation	--	2 generations, the older one cuts only the basement, the later one cut also the sediments
	--	E-W Normal faults,			All rock units

Table 6 Shows the different deformation phases in the study area.

Sub-area A	Sub-area B	Sub-area B	Sub-area B	Sub-area C	Sub-area D
315°/65°	290°/60°	80°/60°	310°/75°	270°/45°	305°/60°
305°/65°	310°/50°	160°/60°	340°/60°	315°/40°	280°/35°
285°/45°	270°/65°	190°/40°	330°/55°	325°/35°	290°/60°
285°/50°	290°/50°	230°/40°	340°/60°	345°/35°	300°/65°
290°/65°	290°/45°	320°/80°	25°/50°	00°/45°	295°/50°
290°/45°	290°/35°	250°/90°	20°/40°	290°/45°	00°/15°
290°/60°	290°/20°	300°/35°	340°/60°	325°/45°	290°/50°
310°/55°	280°/20°	320°/45°	330°/50°	310°/35°	295°/60°
335°/65°	290°/45°	340°/60°	340°/35°	00°/15°	295°/60°
00°/65°	305°/65°	305°/60°	350°/60°	270°/40°	290°/50°
220°/40°	260°/20°	295°/40°	00°/55°	270°/55°	295°/50°
320°/60°	270°/35°	290°/60°	340°/60°	280°/65°	290°/35°
240°/60°	290°/55°	315°/45°	340°/50°	290°/60°	295°/50°
270°/65°	305°/40°	325°/30°	00°/43°	305°/40°	295°/65°
95°/60°	320°/45°	317°/38°	330°/70°	260°/40°	295°/40°
90°/60°	325°/40°	315°/40°	340°/70°	270°/40°	280°/75°
295°/50°	330°/45°	310°/45°	320°/70°	220°/45°	320°/70°
270°/50°	315°/35°	292°/25°	340°/70°	205°/65°	20°/75°
295°/30°	290°/40°	285°/27°	320°/40°	168°/63°	345°/75°
285°/45°	280°/40°	315°/40°	290°/50°	285°/70°	290°/45°
287°/45°	310°/35°	040°/18°	345°/45°	282°/52°	270°/70°
290°/65°	285°/35°	240°/35°	310°/35°	274°/28°	340°/40°
250°/60°	340°/40°	60°/60°	340°/45°	290°/20°	330°/30°
270°/50°	280°/40°	60°/40°	320°/40°	025°/73°	295°/40°
295°/60°	270°/35°	240°/35°	40°/50°	097°/30°	295°/45°
290°/70°	280°/40°	315°/40°	50°/50°	051°/24°	295°/45°
290°/65°	310°/35°	100°/70°	325°/45°	027°/19°	290°/50°
290°/40°	340°/50°	280°/40°	350°/50°	335°/80°	285°/50°
250°/30°	300°/35°	270°/50°	340°/60°	290°/45°	290°/50°
290°/65°	335°/40°	260°/40°	320°/60°	255°/45°	300°/45°
290°/20°	25°/40°	290°/50°	340°/60°	240°/30°	210°/60°
290°/15°	335°/45°	305°/75°	00°/55°	345°/35°	100°/75°
025°/90°	350°/50°	305°/60°	00°/60°	270°/70°	065°/8°
25°/40°	295°/50°	240°/75°	00°/45°	300°/35°	075°/60°
20°/45°	355°/60°	290°/65°	285°/35°	300°/0°	275°/50°
310°/60°	330°/50°	325°/44°	305°/55°	340°/40°	65°/60°
270°/50°	350°/40°	00°/55°	320°/50°	280°/35°	270°/50°
320°/50°	305°/40°	015°/45°	315°/47°	285°/45°	290°/60°
270°/40°	320°/40°	270°/70°	340°/40°	280°/90°	280°/35°
	320°/50°	290°/60°	320°/35°	280°/40°	290°/55°
	290°/50°	295°/50°	310°/50°	280°/60°	300°/60°
	310°/60°	260°/50°	290°/40°	280°/60°	275°/45°
	345°/65°	290°/60°	320°/45°	270°/65°	255°/80°
	340°/65°	270°/60°	285°/40°	285°/40°	270°/45°
	345°/55°	270°/70°	285°/60°	290°/60°	310°/60°
	335°/40°	260°/75°	280°/35°	280°/60°	270°/45°
	350°/60°	235°/50°	305°/55°	270°/60°	90°/80°
	310°/45°	115°/35°	295°/40°	260°/60°	285°/75°
	10°/50°	305°/50°	290°/75°	300°/60°	00°/45°
			295°/90°	315°/45°	

Table 7 Structural field measurements of the Dip (direction/amount) in the Sub-areas

General Lineation in the whole area	Mineral Lineation	F2 Axes	F3 Axes	Slickensides	Fault Types
					Apparent-dextral Strike Slip Faults (S2)
195°/15°	012°/04°	330°75°	00°10°	295°/50°	330°
15°/09°	011°/06°	347°85°	020°15°	300°/45°	340°
11°/06°	015°/09°	330°65°	200°15°	270°/40°	350°
12°/04°	195°/15	00°87°	345°6°	277°/55°	00°
272°/35°	009°/07°	320°70°	340°5°	255°/60°	010°
208°/13°	190°/12°	55°80°	00°15°		025°
07°/15°	008°/11°	350°75°	020°10°		015°
210°/15°		270°75°	040°15°		030°
07°/15°		330°75°	020°25°		045°
00°/20°		00°88°	040°25°		**N-S Thrust** (S3)
270°/15°		00°10°	00°30°		
260°/20°		020°15°	030°30°		00°/55°
80°/15°		200°15°	025°10°		340°/60°
208°/40°		270°0°	10°15°		310°/50°
200°/30°		020°70°			010°/50°
268°/39°		00°15°			025°/40°
237°/40°		215°75°			350°/50°
231°/34°		340°80°			340°/60°
148°/05°		020°75°			320°/60
146°/06°		040°15°			340°/55°
152°/03°		020°25°			025°/50°
029°/12°		040°35°			020°/40°
218°/04°		015°90°			005°/55°
210°/24°		00°30°			015°/55°
154°/06°		030°35°			**Phanerozoic S.S.Fault**
162°/01°		040°90°			090°
		010°80°			110°
		070°35°			100°
					105°
					095°
					Phanerozoic Normal Faults
					090°
					095°
					085°

Table 8 Structure field measurements of lineation, mineral lineation, fold axes and different type of faults in the whole area.

CHAPTER 6

ANISOTROPY OF MAGNETIC SUSCEPTILITY (AMS)

6.1 Background

Magnetic fabric techniques are one group of many that can be used to measure the petrofabric of rocks so that their origin and structural evaluation can be determined, but their speed, precision, cheapness and range of applicability make them unique. The method principally involves the collection of oriented samples followed by determination of the strength of the magnetization that a sample acquires when a magnetic field is applied at different orientations. Any differences can then be interpreted in terms of the net shape of the grains and degree of their crystalline alignments, which, in turn, can be interpreted in the same way as in all other petrofabric techniques. There is thus no need for a rock to contain specific strain markers as these are provided by its own mineral constituents. This, with their speed and precision, allows magnetic fabric methods to be applied on a greater scale and to much wider range of geological problems than most conventional methods. There can obviously be problems with interpretation, particularly of the magnitude of strain, but these are not significantly greater for magnetic fabrics than for other methods as they all depend on an understanding of the deformation mechanism that operated under the conditions pertaining when the fabrics where acquired (D.H.Tarling et al 1993).

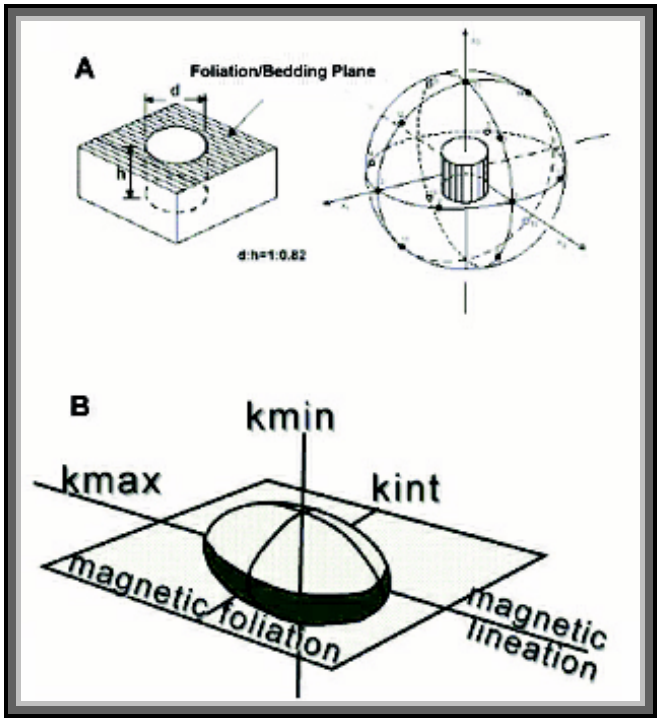

(Fig. 6.1) A. Geometry of measured parameters of Anisotropy of Magnetic Susceptibility (AMS), (after JELINEK 1977), **B**. The AMS ellipsoid (after De WALL 1991)

AMS stands for **A**nisotropy of **M**agnetic **S**usceptibility. The magnetic susceptibility is the physical property, which reflects how the magnetization of a material responds to an applied magnetic field and is mathematically as

K= M / H, where

K= Magnetic susceptibility (unitless, SI)

M= Induced magnetization (A/m)

H= Applied magnetic field strength (A/m)

The susceptibility is not an isotropic (or constant) parameter. It responds differently to different directions of the applied field, it is anisotropic. Therefore it cannot be described by a "single value", but has to be written as a symmetric 3 x 3 tensor. By the use of linear algebra it is possible to calculate the (own values) eigenvalues and the eigenvectors of the tensor. The eigenvectors are termed principal directions (p1, p2, p3) and the eigenvalues are termed principal susceptibilities (K_1, K_2, K_3), where $K_1 > K_2 > K_3$. Graphically the principal susceptibilities define the so-called AMS ellipsoid, with K_1 representing the long axis, K_2 the intermediate and K_3 the short axis (Fig 6.1A).

6.2 DATA ANALYSIS

6.2.1 Measurement:

The AMS measurement was carried out with a Kappabridge KLY-2 at room temperature, using the ANISO 10-14 programs for calculations (JELINEK, 1977; 1980). The KLY-2 Kappabridge has a sensitivity of $5x10^{-6}$ SI in detected anisotropy as low as 1 mT (static field). Samples for the AMS measurement were standardized to a constant size in cylinder shape of 2.5 cm diameter x 2.2 cm length; the proportions ensuring the best approach of a spherical sample geometry. The cylinders or cores drilled from the samples were marked to match with the field orientation in the field and was subsequently used. This marking is used for sample orientation in the AMS measurement correlated to the stereo plots in the lower hemisphere. The samples were drilled in laboratories of the Egyptian Geological Survey of Egypt and measured in the AMS laboratory of the Geological Institute of Heidelberg University. The AMS was measured in 15 different positions on the cylinders (Fig 6.1B). The description of the AMS was suggested by Hrouda (1982) in different parameters, which are derived from using principal axes ratio and different susceptibility.

The calculations of the program ANISO 10-14 are used following analysis by the Kappabridge KLY-2. Total anisotropy H depends on (OWENS 1974)

$H = K_1 - K_3 / K_m$

The character of the magnetic fabric is indicated by the shape factor T:

$(T) = 2 (\ln K_2 - \ln K_3) / (\ln K_1 - \ln K_2) - 1$ (JELINEK, 1981)

If T **< 0 (-),** the magnetic ellipsoid is prolate (cigar shape)

If T **> 0 (+),** the magnetic ellipsoid is oblate (disk shape)

The intensity of the preferred orientation of magnetic minerals in a rock is indicated by the anisotropy factor **P**:

$P = K_1/K_3$ (HELLER,1973; JANÁK, 1972; HROUDA et al., 1971).

The corrected anisotropy factor **P`** is determined by :

$(P`) = \exp (2 (\ln K_1 - \ln K)^2 + 2 (\ln K_2 - \ln K)^2 + 2 (\ln K_3 - \ln K)^2)^{1/2}$ (TARLING & HROUDA; 1993)

The magnetofabric is defined by the following geometric elements: K_1 and K_3 are the magnetic lineation and the pole of magnetic foliation, respectively. Intensities of lineation, **L**, and foliation, **F**, are determined by:

$L = K_1/K_2$

$F = K_2/K_3$

6.3 AMS in Study Area

For the AMS study the author collected 33 oriented samples, which represent the different types of lithology and structure from all over the area. Two samples are excluded, because they are out the limit of detection. About 6 cylinders were obtained from each sample making a total of about 200 cylinders to measured. For systematic analysis and interpretations the AMS data, obtained on these cylinders and categorized into two main groups: BIF (Banded Iron Formation) and Anatexite Sequences. The complete AMS data is given in Table 7.12 at the end of this chapter. The AMS data are treated in different diagrams such as equal area stereograms, T-P´ and T-Km diagrams.

6.3.1 Magnetic Susceptibility of the BIF

The AMS investigations in the BIF show strong variations in the averages of the mean susceptibility values for the different BIF bands (Table 7). The general features of BIF are already outlined in the chapter 2.

Rock type	Metachert and jaspilite bands	Well-banded iron-silica bands	Fuchsite-bearing quartz bands	Pelite-volcanosediments alternating with BI
Averages of the mean susceptibility x 10^{-6} SI	316 - 632	5,607; 25,816	4 : 1,273	1,119 : 108,752

Table 9 Shows the magnetic susceptibility values in the different bands of the BIF.

The well-banded iron-silica bands and the pelitic bands show very high values in mean susceptibility pointing to ferrimagnetic carriers, while the metachert and quartz bands exhibit lower magnetic susceptibility values. They are dominated by diamagnetic and paramagnetic minerals. Accordingly, the BIF samples are divided into 2 subgroups based on the Km values as follows:

6.3.1.1. Low Magnetic Susceptibility (Km) Group.

Seven samples H4, H7, H19, H23, U2, U4 and U7 (appendix) collected from the study area comprise this group. This group contains both the metachert and the silica rich bands and the magnetic susceptibility (k_m) ranges between 5 and 920 X 10^{-6} SI (Fig 6.2a). These bands are composed mainly of quartz, chlorite, altered plagioclase, muscovite and secondary goethite.
The shape factors of the AMS ellipsoid shows often strong oblate character (disk shape) and very weak prolate shape (cigar shape) between – 0,1 and 0,9. The anisotropy factor (P`) ranges between 1.01 and1.3 for most of the samples (Fig 6.2b).

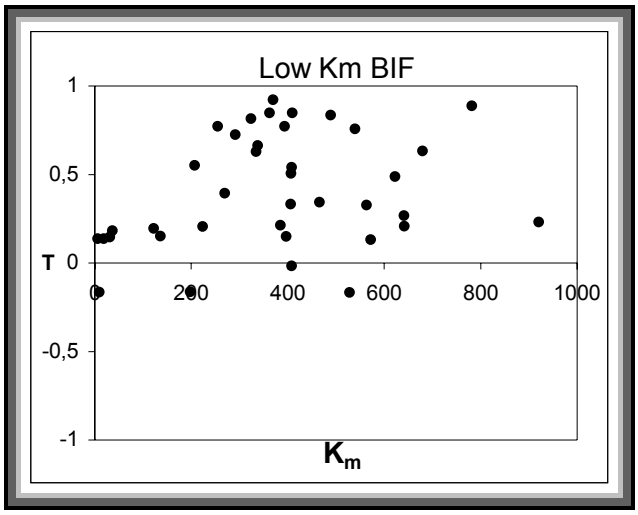

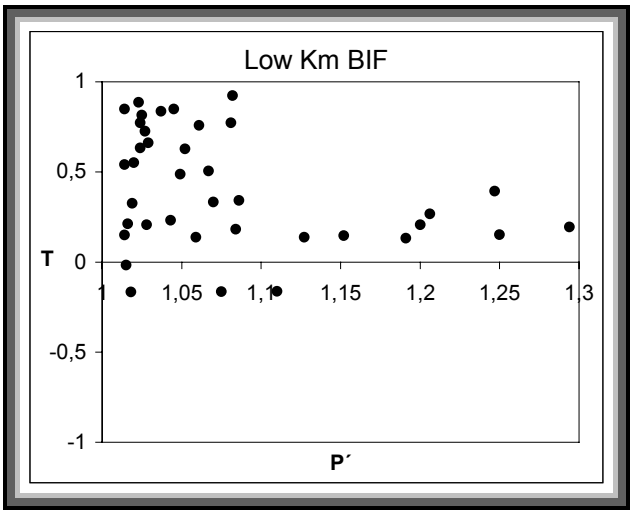

6.2a 6.2b

Fig 6.2a. Mean susceptibility (K_m) versus shape factor (T) diagram showing that the low susceptibility BIF are mostly oblate in shape.

Fig 6.2b. A diagram showing the relationship between anisotropy factor (P`) and shape factor (T) in the diamagnetic and paramagnetic minerals. The minerals are mostly oblate ellipsoid shapes. Strongly oblate shapes are related to low anisotropies (P`).

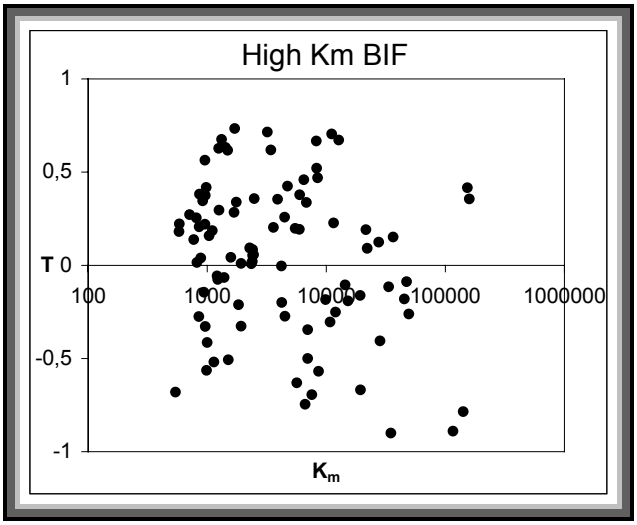

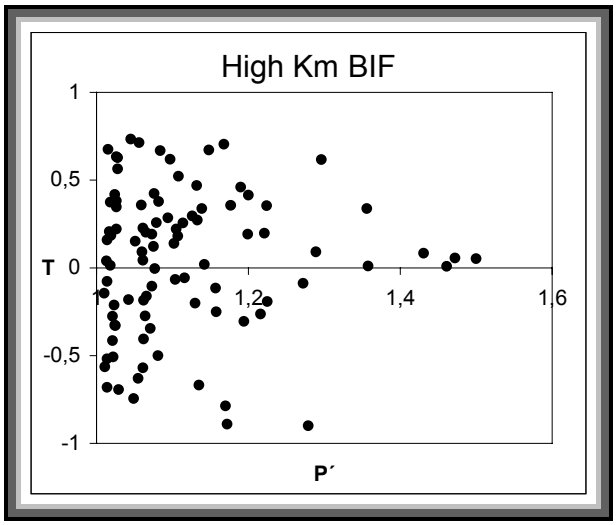

6.3a 6.3b

Fig 6.3a. A diagram of the mean magnetic susceptibility (Km) versus the shape factor (T), showing strong variations from oblate to prolate ellipsoids.

Fig 6.3b. A corrected magnetic anisotropy factor (P`) versus the shape factor (T) diagram showing variations from strongly oblate to strongly prolate ellipsoids.

6.3.1.2. High Magnetic Susceptibility (Km) Group

This group represents the well-defined hematite-magnetite bands and the pelite-volcanosedimentary-BIF bands. The mean susceptibly (k_m) values range between 800 to

> 150,000 x 10^{-6} SI (Fig 6.3a). The AMS ellipsoid shape (T) shows strong variation between (+0,7 and –0,9) oblate and prolate. The anisotropy factor (P`) shows also a strong variation between 1.5 and 1,1 (Fig 6.3b).

This group can be further subdivided into three subgroups based on the (k_m) values obtained from 15 samples as follows

a - Very high Km values ranging between 7000 and 159,000 x 10^{-6} SI, except three cores in different samples ranged between 4200 and 6800 x 10^{-6} SI, which are rich in silica.

b - Intermediate Km values that range between 1500 and 8306 x 10^{-6} SI showing minor overlap with subgroup (a).

c - Low Km values, ranging between 800 and 2000 x 10^{-6} SI, except for three cores in different samples, that ranged between 579 and 582 x 10^{-6} SI due to silica enrichment. This subgroup also shows overlap with the subgroup (b).

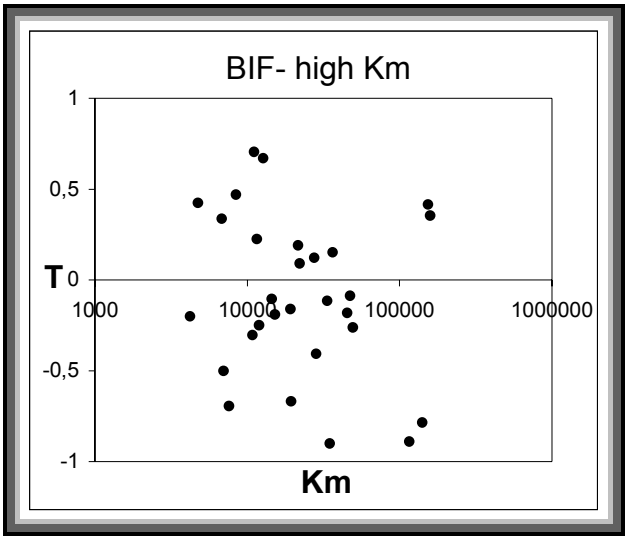

Fig 4a

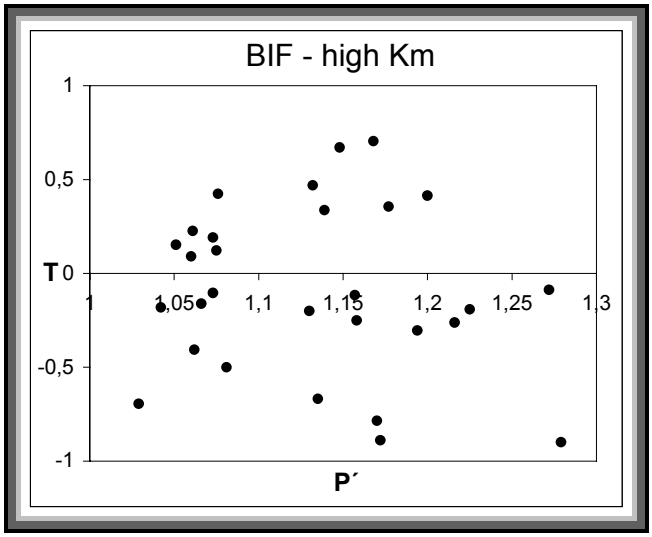

Fig 4b

Fig 6.4a. Mean magnetic susceptibility (km) versus the shape factor (T) diagram, showing strong variation from oblate to prolate ellipsoids shapes.

Fig 6.4b A diagram showing the relationship between anisotropy factor (P`) versus the shape factor (T). Shapes vary from oblate to prolate ellipsoids.

6.3.1.2.a- The Very High Values Between 7 and 159 x 10^{-3} SI.

This subgroup represents 5 samples labeled H3, H10, H13, U5, U6 (see appendix and Fig 6.15 for location) collected from the whole area. The samples consist of magnetite–hematite bands alternating with metapelite-volcanosedimentary and quartz bands. These bands contain high amounts of magnetite and subordinate amounts of garnet, amphibole and pyroxene minerals and are often strongly alterered and deformed. The microscopic texture of

these rocks shows mostly a very fine-grained groundmass of quartz and iron oxides (remnants of the earlier shear zones of D1), coarse-grained deformed quartz and large magnetite-hematite-grains, which overgrown from the fine-grained groundmass. These fine bands were subsequently deformed.

The measurements for these samples show strong variation in the magnetic ellipsoid shape, with T values ranging between + 0.7, which is strongly oblate to – 0.9, which is strongly prolate (Fig 6.4a). The anisotropy factor P` ranges between 1.05 and 1.29 for these samples (Fig 6.4b)

6.3.1.2.b- The Intermediate Km Values Between 1500 and 8306 x 10-6 SI

This sub-group represented by 5 samples from the center of the northern area labeled H14, H15, H16, U1, U3 (see appendix and Fig 6.15 for location). These rocks are composed mainly of iron oxide-rich bands alternating with silica bands. The corrected anisotropy factor P` shows gradation from 1.1 to 1.5 (Fig 6.5a). This gradation probably reflects an increase in deformation as in samples H15 and H16, which laying close to a minor reverse fault surface parallel to the major faults. The AMS ellipsoids shape (T) shows strong variation between oblate and prolate from -0,8 to +0,8 in the cores with high susceptibility to weak to medium oblate in the cores with lower susceptibility (Fig 6.5b).

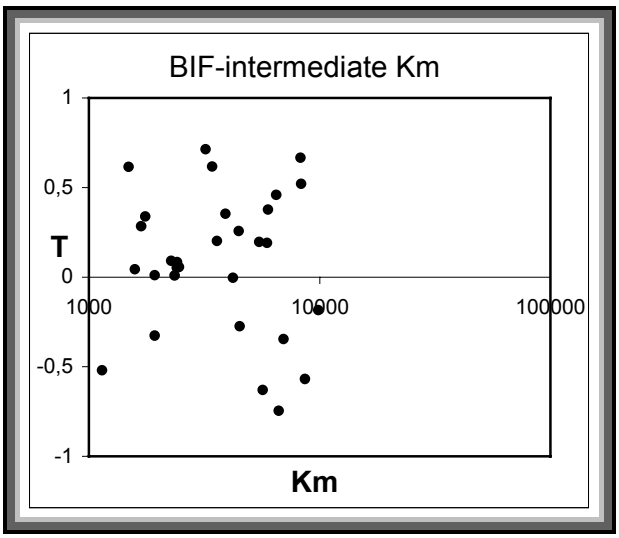

Fig 6.5a

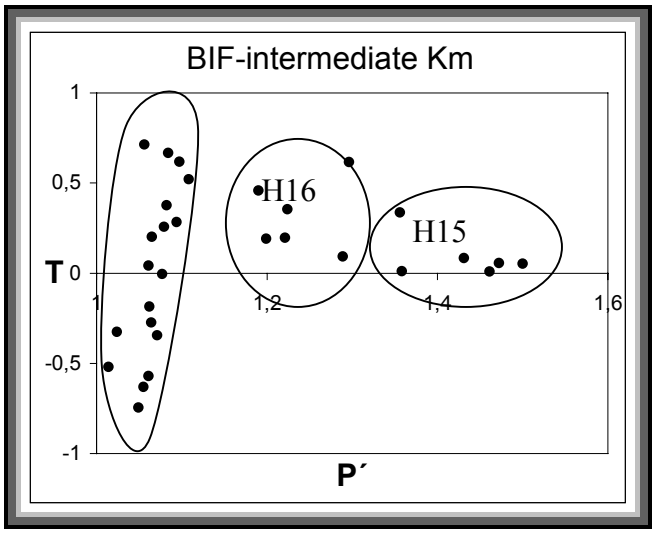

Fig 6.5b

Fig 6.5a. A diagram of the mean magnetic susceptibility (K_m) versus the shape factor (T), showing mostly moderate to strong oblate and a few prolate shapes.

Fig 6.5b. A corrected magnetic anisotropy factor (P`) versus the shape factor (T) diagram showing P` from 1,1 to 1,45 and vary shapes from oblate to prolate ellipsoids

6.3.1.2.c- The Low Km Values Range Between 800 and 2000 x 10^{-6} SI

This sub-group represented by 5 samples from the whole area labeled H11, H17, H20, U11, U13 (Fig 6.6a). (see also appendix). These rocks consist of thin magnetite-hematite bands alternating with thin silica bands (a few centimeter thick of both types). The P´ values, are concentrated in 2 separate groups, the first one from 1,01 to 1,05 and the second between 1,1 and 1,15 represented by sample U11, which placed close to the footwall of the major reverse fault in the southern part of the sub-area A (Figs 6.6b and 6.16). The higher values are attributed to the high deformation. The AMS ellipsoid shape shows strong variation between oblate and prolate with T values ranging from – 0,8 to + 0,9.

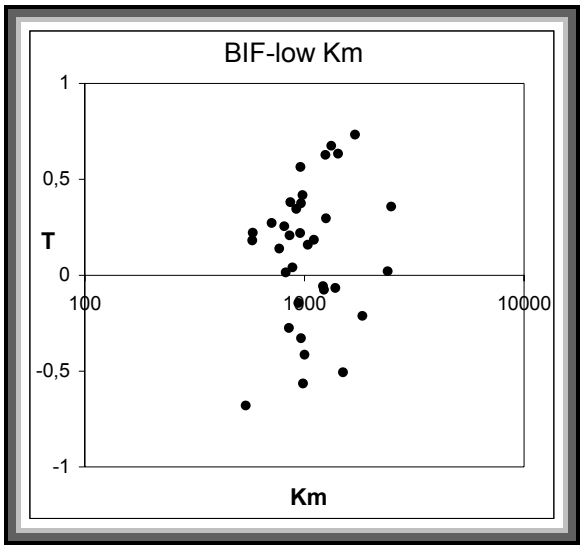

Fig 6.6a

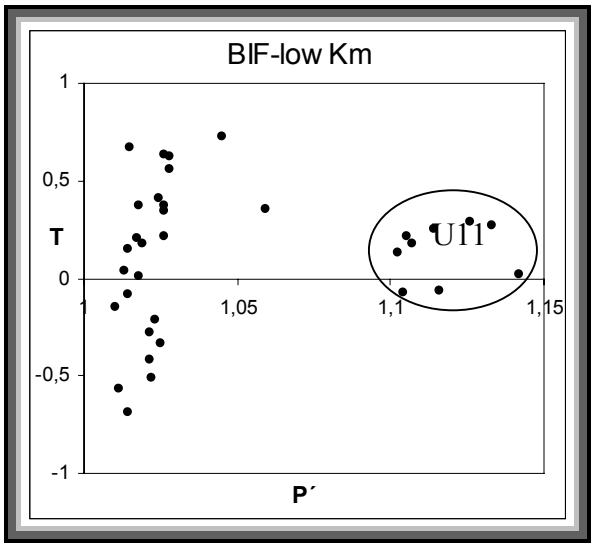

Fig 6.6b

Fig 6.6a. Mean magnetic susceptibility (Km) versus shape factor (T) diagram of the low ferrimagnetic bands showing both oblate to prolate shapes.

(Fig 6.6b) A diagram showing the relationships between T versus P`. The samples plot in two distinct groups. The first group contains most of the samples with values between 1,01 and1,04, while the second group has higher values between 1,1 and 1,14. The shape is more variable in he first group, between – 0,75 and + 0,8 than the values in the second group that vary between 0,07 and + 0,3.

6.3.2 The Magnetic Susceptibility of the Anatexite Sequence

The Anatexite sequence is represented by 9 samples collected from the whole area. Six samples H1, H2, H5, H9, H12 and U8 were collected from the light bands the other three H6, H21 and H22 represent dark bands (see appendix).

6.3.2.1 The light bands in the Anatexite Sequence

The light bands in the Anatexite Sequence are characterized by quartz, feldspar, chlorite, biotite, muscovite, amphiboles, pyroxene, garnet and magnetite. In general, the magnetic susceptibility (K_m) in the light bands varies from 25 x 10^{-6} to 15,240 x 10^{-6} SI. The shape factor (T) is strongly prolate to very strongly oblate and ranges in from - 0,56 to + 0,92 (Fig 6.7a). The corrected anisotropy factor (P`) ranges from 1,028 to 1,545 and mostly reflects strong progressive deformation, which placed the samples H5 and H12 close to the hanging wall of fault surface in the southern sub-areas, while the other samples laying about 3 kilometre far from the fault surfaces (Figs 6.7b, 6.15 and 6.16).

The samples (H1,H2 ,H5 and H12) collected from the southern part of the investigated area and the samples H9 and U8 collected from the northern area.

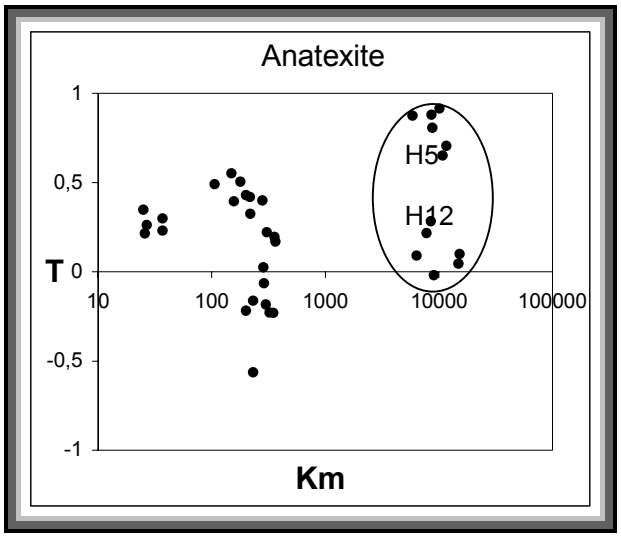

Fig 6.7a

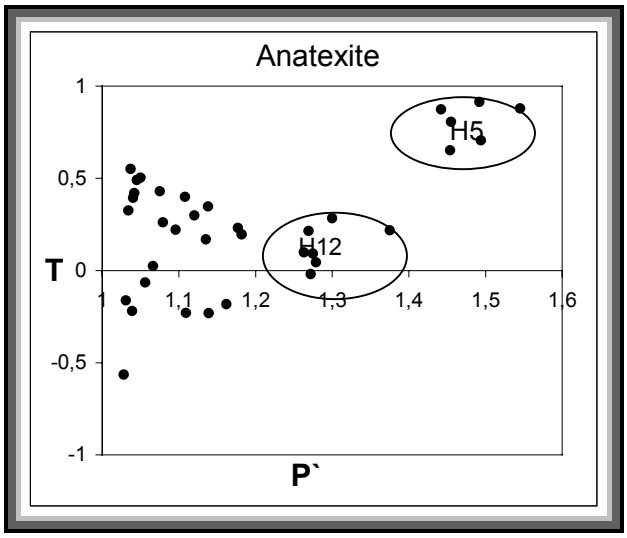

Fig 6.7b

Fig 6.7a. Diagram of the mean magnetic susceptibility (K_m) versus the shape factor (T), showing K_m between 25 and 15,240 x 10^{-6} SI, and strongly oblate to weakly prolate shapes between 0,56 and 0,92.

Fig 6.7b. Corrected magnetic anisotropy factor (P`) versus the shape factor (T) diagram showing the relationship between T versus P`, which shows P` values between 1 and 1,55.

6.3.2.2 The Dark Bands in the Anatexite Sequence

This group has three samples H6, H21 and H22, they composed mainly of amphibole, chlorite, plagioclase and pyroxene. The K_m versus T diagram shows mostly K_m values between 550 and 873 x 10^{-6} SI and the ellipsoid shape (T) ranging between strongly prolate (-0,62) and moderately oblate (+ 0,41) as shown in Fig 6.8a. The P` versus T relationship shows P` values between 1,015 and 1,046 Figure 6.8b.

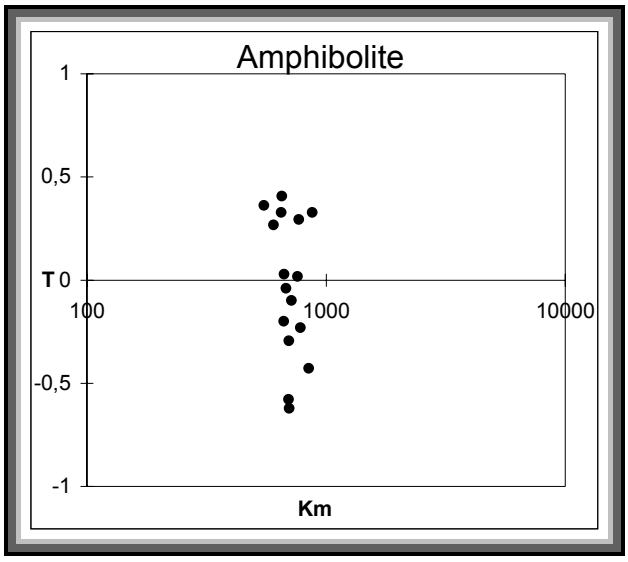

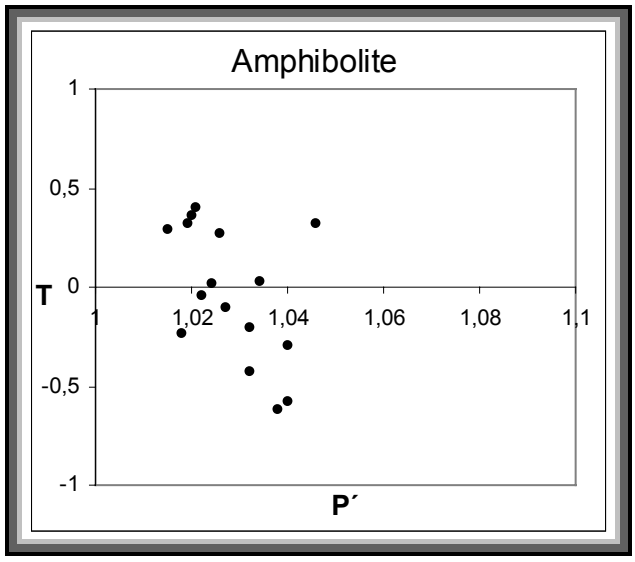

Fig 6.8a Fig 6.8b

Fig 6.8a. The relation between Km versus T in the amphibolite bands showing K_m between 550 and 873 x 10^{-6} SI, and prolate to oblate shape – 0,62 and 0,41.

Fig 6.8b. Diagram showing the relationship between T versus P`, with P` values between 1,015 and 1,046.

6.4. The Relationship Between the AMS and Field Measurements

Two profiles across the northern (Fig 6.9) and southern (Fig 6.10) parts of the study area illustrate the relationship between the magnetic foliations and the field foliations.

These profiles are accompanied by stereoplots of the magnetic foliation for a clearer view.

In the northern profile the field foliations represented by solid line great circle and the poles of magnetic foliation by a dense black circles. The magnetic foliation is mostly in conformity with the main structure

At the western side of the profile sample U6 shows shallow foliation dipping to the east. This sample was collected from a fold hinge where the foliation and the bands are nearly horizontal, direct to the east breakdown the fold and formed a reverse fault, while the eastern limb was depressed.

In the southern profile (Fig 6.10), the magnetic foliation shows varying directions and dips amounts and mostly dip to the west with steep to moderate angles. This is in agreement with the major structure. At the eastern side, gentle dips toward NE represents a crest of a major fold. The eastern side shows magnetic foliations dipping to the east with shallow angles while the field foliation is nearly parallel with the dominant foliation in this part which was observed in the field dipping steeply to the east.

6.4.1. The Relationship Between Magnetic Measurements with Major Structures in the Whole Area

In the AMS measurements K1 axes indicate magnetic lineations and k3 axes represent the poles of the magnetic foliation. These data of the BIF and Anatexite Sequence are shown in the stereograms as follows:

6.4.1.1. Magnetic Foliations in the BIF

The magnetic foliations in the BIF are illustrated in the stereographic plot Fig 6.11. The diagram indicates an east vergent fold plunging nearly to the north with 20° angle, which is related to the F3 fold phase.

In the stereographic plot there are several points of the poles of magnetic foliation placed with random distribution especially between the two fold limbs represented by two great circles. These poles define the earlier deformations, which dominate in the BIF and interpreted as micro and macro folds accompanied with shear zones parallel with the fold axial surfaces. These poles take the same place in the density contours and represent the earlier F2 fold (in D2), which rotated during the D3 deformation around an horizontal axis with about 90° anticlockwise and occur in the fold limbs of the F3 folds in the BIF with steep fold axes and at a different scales (Fig 6.11).

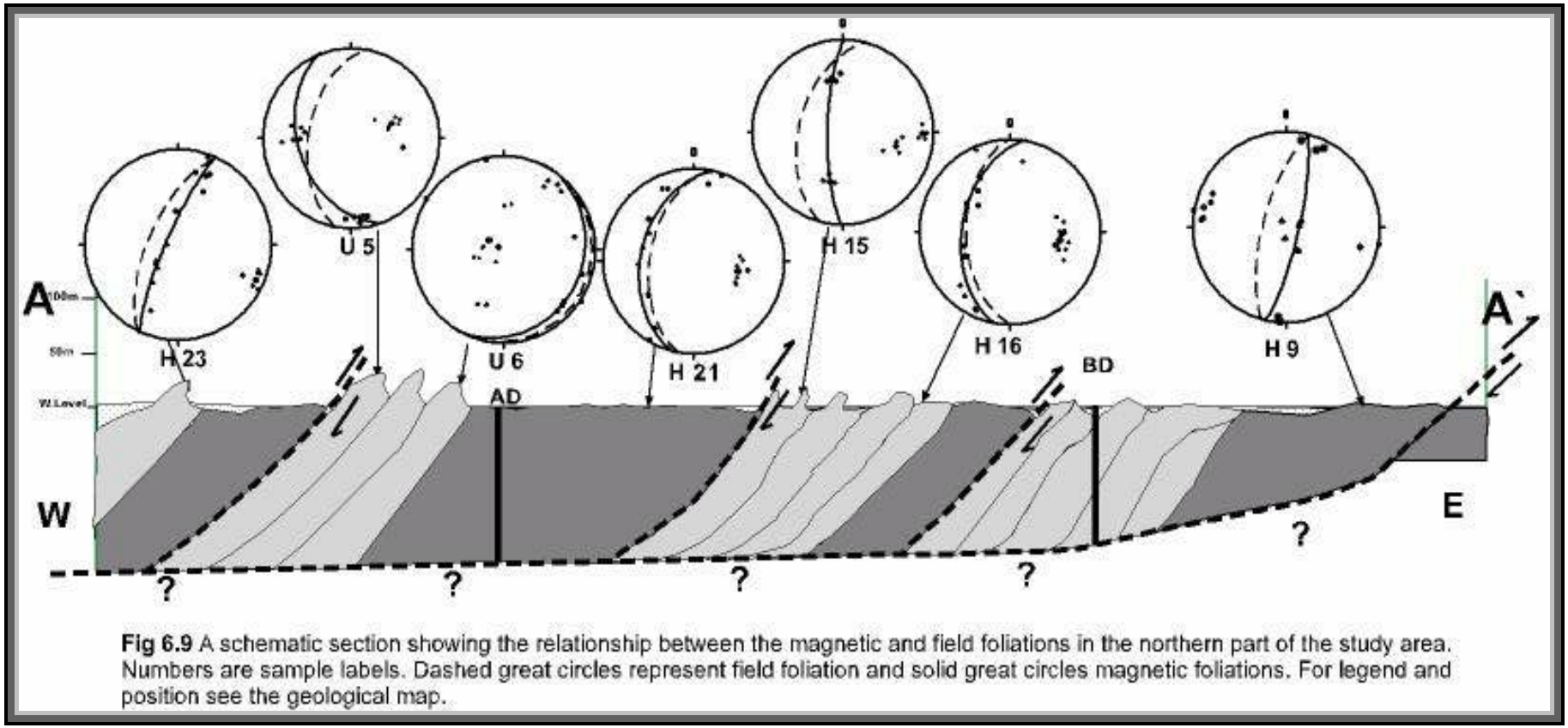

Fig 6.9 A schematic section showing the relationship between the magnetic and field foliations in the northern part of the study area. Numbers are sample labels. Dashed great circles represent field foliation and solid great circles magnetic foliations. For legend and position see the geological map.

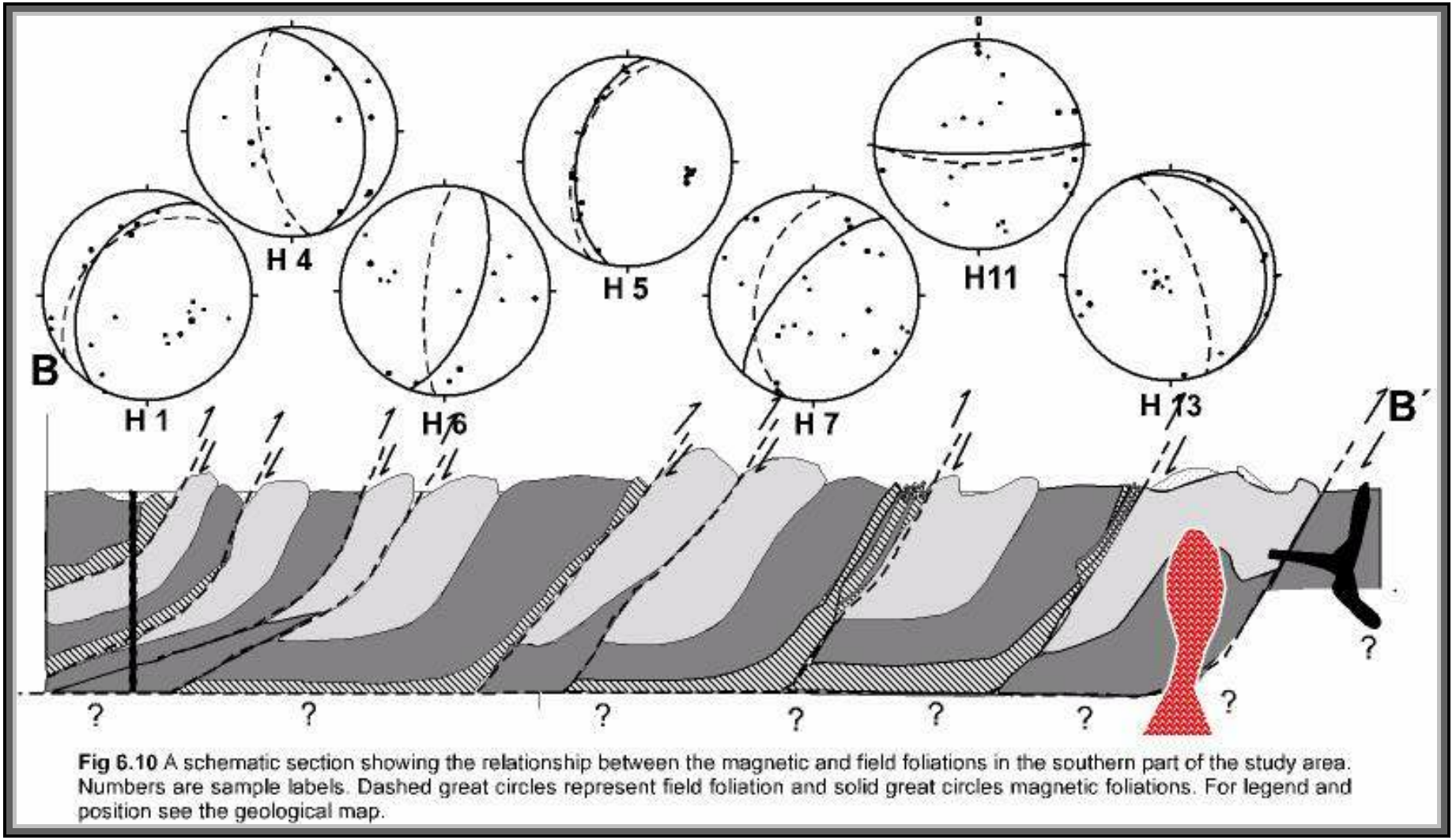

Fig 6.10 A schematic section showing the relationship between the magnetic and field foliations in the southern part of the study area. Numbers are sample labels. Dashed great circles represent field foliation and solid great circles magnetic foliations. For legend and position see the geological map.

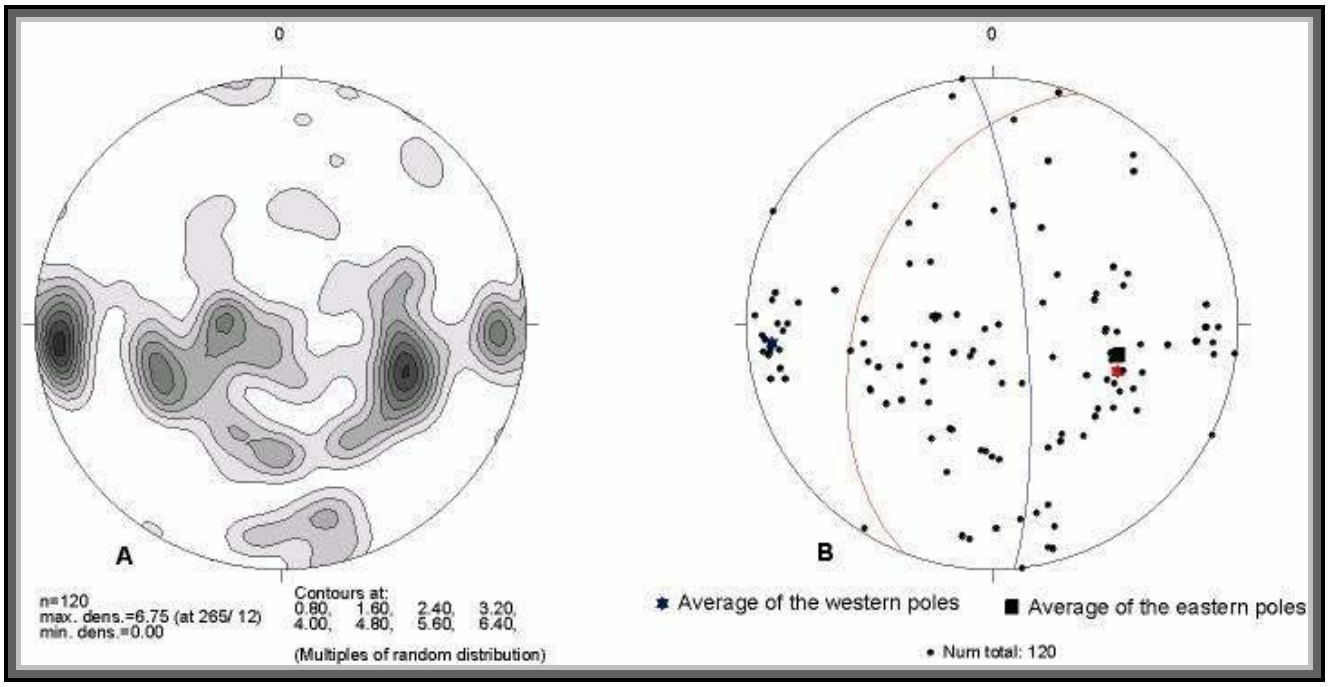

Fig 6.11 (A) Lower hemisphere equal area projections, for the density diagram and (B) pole to the magnetic foliation in the BIF.

6.4.1.2. Magnetic Foliations in the Anatexite Sequences

The magnetic foliations in the Anatexite Sequences are illustrated in the stereographic plot Fig 6.12. The diagram indicates also an east vergent fold plunging 5° with an azimuth of 7°. The main fold in the Anatexite observed in the field, is also depicted in the stereographic plot. The two maximum of the poles of the magnetic foliation represent two fold limbs of a north plunging, east vergent fold. The poles to the magnetic foliation are well concentrated in the eastern and western sides of the stereogram dominated by the poles of the western limb while the eastern limb is represented by a subordinate number of the poles. This fold represents the F3 fold phase as in the BIF. The correlation between the stereoprojections in the BIF and Anatexite Sequences indicate that the earlier deformations in the BIF are flattened in the Anatexite sequences. That is due to the migmatization processes during the S-N maximum stress. The poles of the western limbs dominate in both rock units, while the poles of the eastern limb have a subordinate number. This is because in the field only the western limbs and sometimes the fold hinges were observed. The eastern limbs were broken down as a result of the overthrusting and reverse faults.

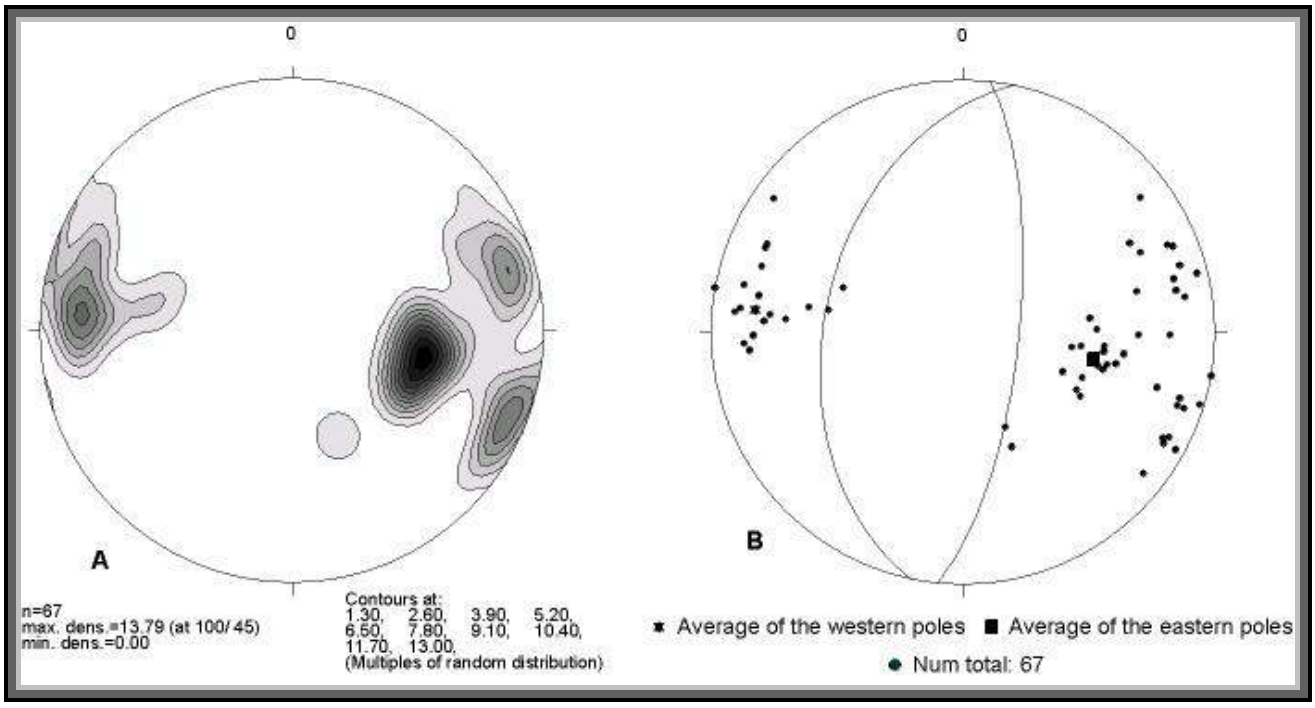

Fig 6.12. (A) Lower hemisphere equal area projections, for the density diagram and (B) pole to the magnetic foliation in the Anatexite Sequences.

6.4.1.3 The Magnetic Lineations in the BIF

The magnetic lineations in the BIF are shown in a stereographic plot (Fig 6.13). There are two maxima of the magnetic lineation, one dominant and the other subordinate. The first group has shallow to moderate plunges to the north or to the south and is due to the main deformation phase, which affected the BIF and Anatexite Sequences during D3 deformation. The second group is represented by a moderate to steep plunging lineation, related with the D2, early earlier folding (F2) in the BIF. The first type of the magnetic lineation trends between 340° and 20° with plunge angles ranging between 1° and 25°.

The second type of magnetic lineation plunges nearly vertical, locally more than 45° with trends of 300° N.

The first and second types of the magnetic lineations are parallel with the fold axes of F3 and F2, respectively. The randomly distributed magnetic lineation probably represent refolded F2 folds at different positions (Fig 6.13).

6.4.1.4 The Magnetic Lineations in the Anatexite Sequences

The magnetic lineations in the Anatexite Sequences are shown in the stereographic plot (Fig 6.14). They indicate nearly the same characters as the BIF (Fig 6.13) except for the steep magnetic lineation, which represent the steep fold axes in the BIF (F2). This indicates that the (F2) were less developed in the Anatexite sequences. The (D3) is dominated with magnetic

lineation trends between 340° and 20° with plunge angle ranging between 1° and 35°.or with plunging angle less than 10° to the south (Fig 6.14).

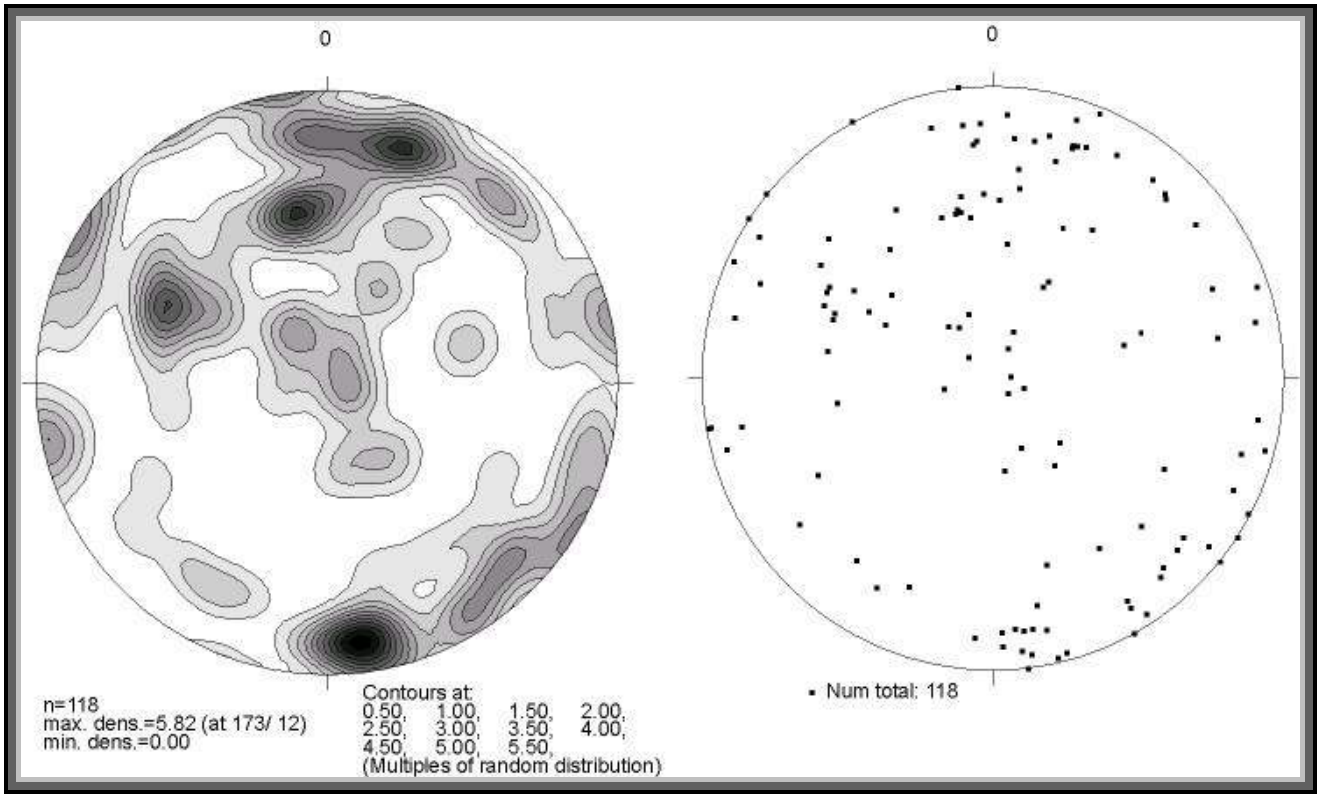

Fig 6.13. Lower hemisphere equal area projections, of the magnetic lineation in the BIF.

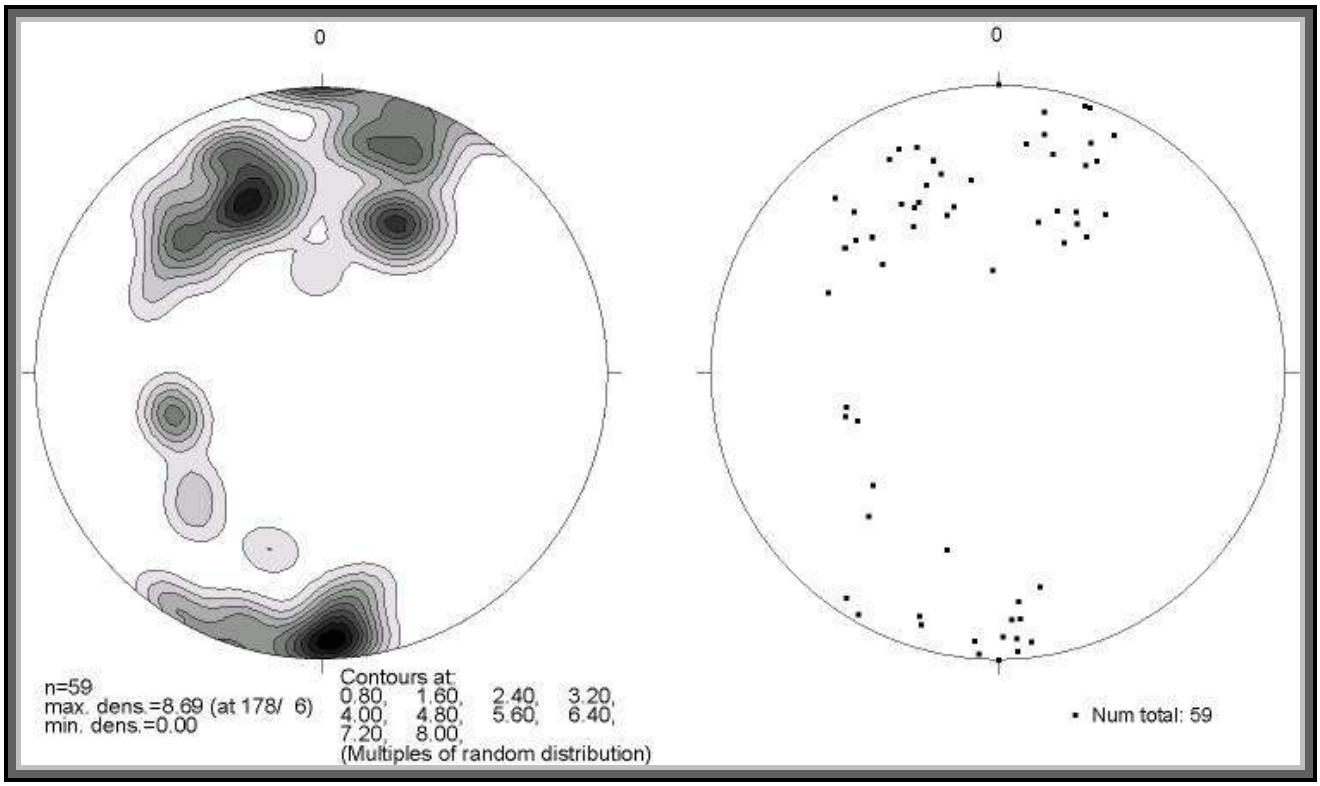

Fig 6.14. Lower hemisphere equal area projections, of the magnetic lineation in the Anatexite

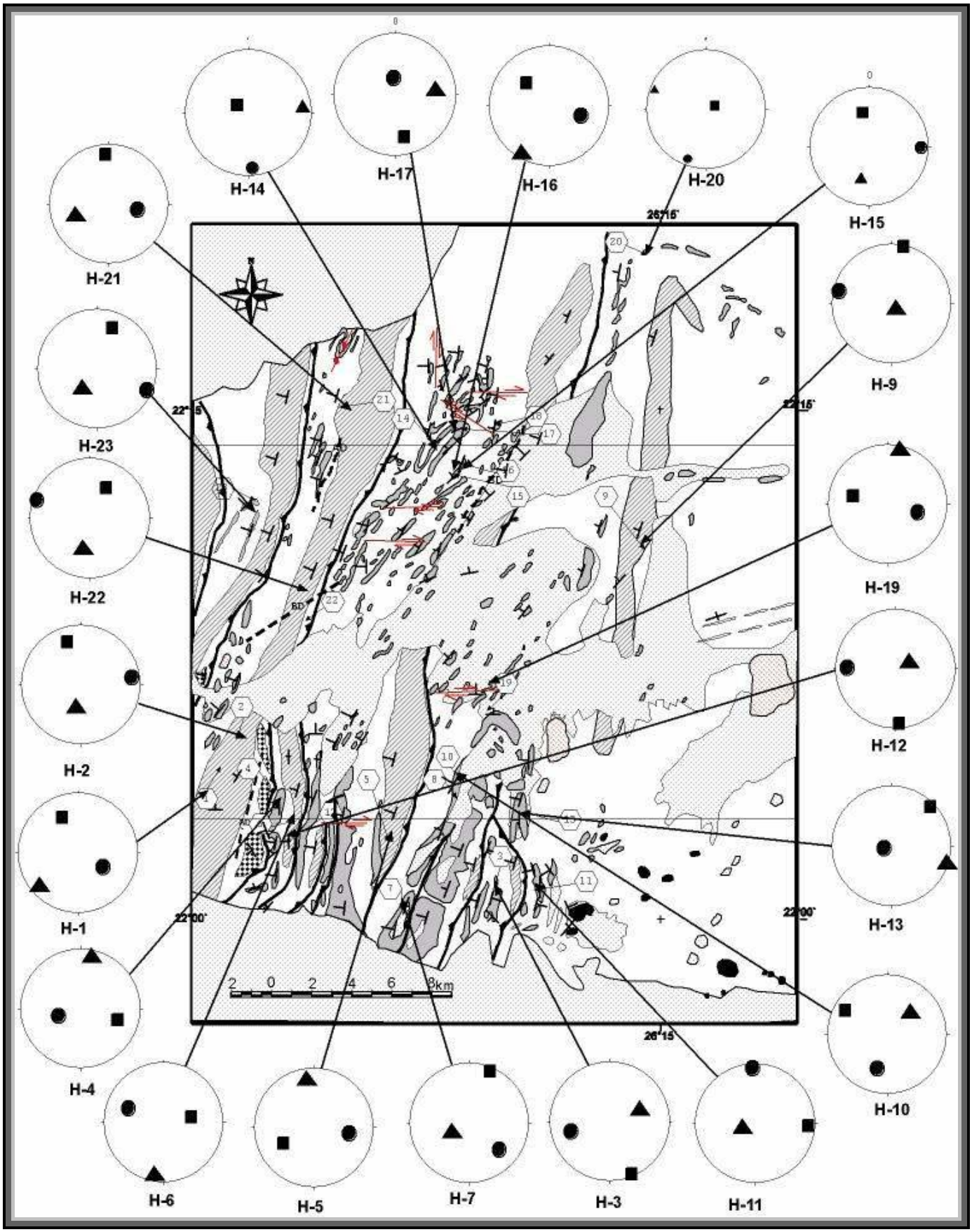

Fig 6.15 Map showing sample location and the position (for H serial) of the averaged AMS ellipsoid axes k1 (square), k2 (triangles) and k3 (circle). Major structural elements are also shown.

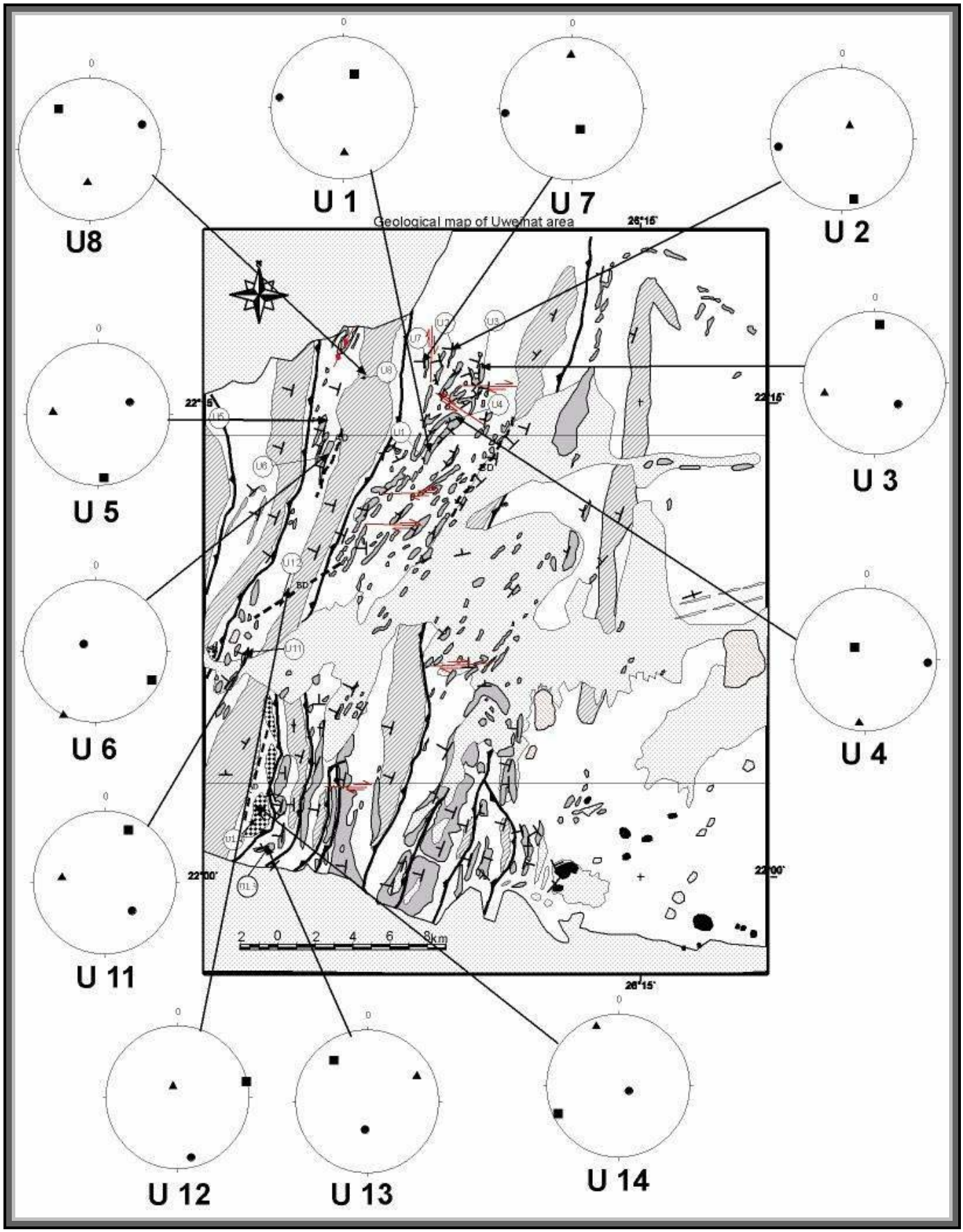

Fig 6.16 Map showing sample location and the position (for U serial) of the averaged AMS ellipsoid axes k1 (square) ,k2 (triangles) and k3 (circle). Major structural elements are also shown.

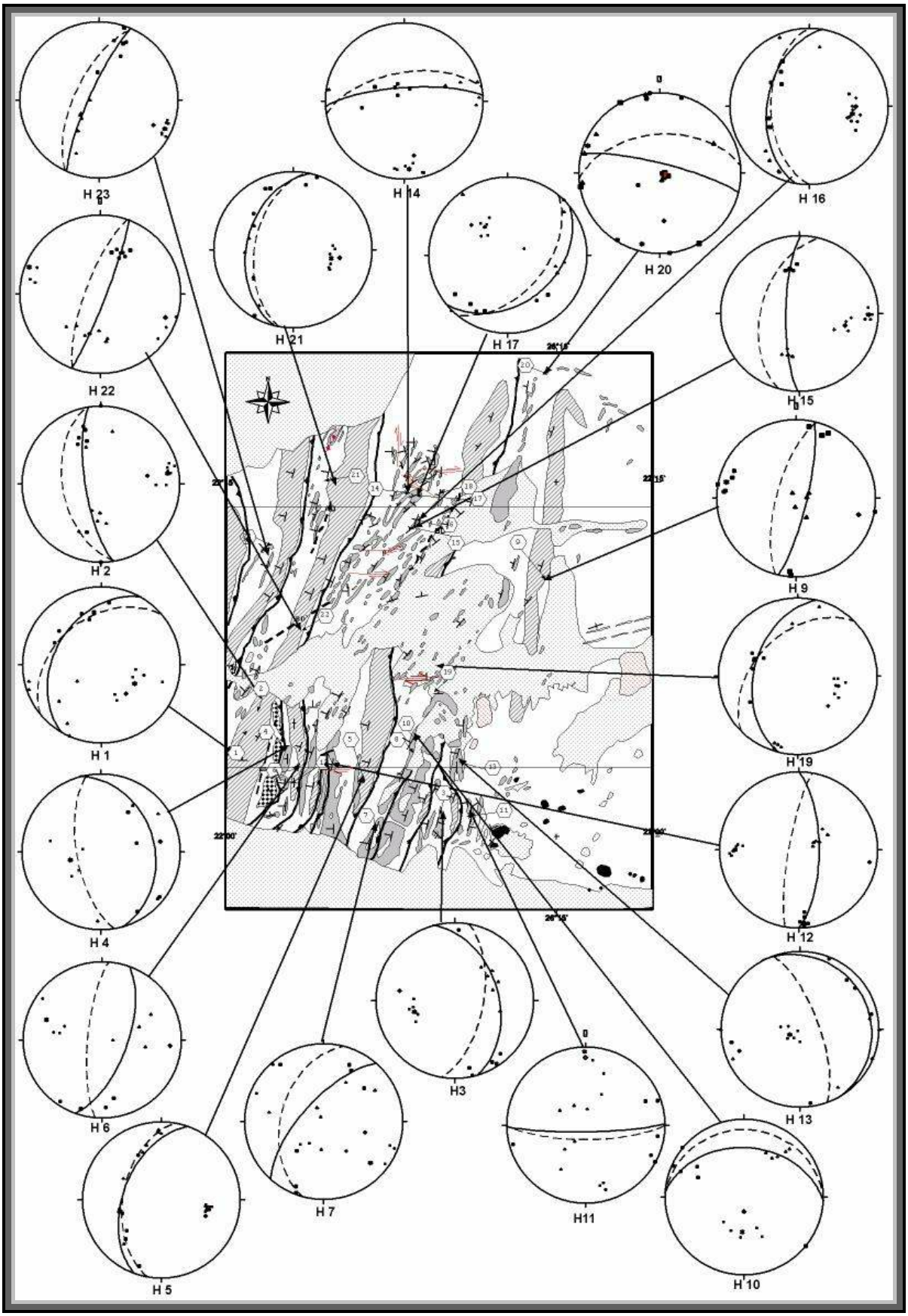

Fig 6.17 Map showing the sample location (for H serial) and the relationship between the magnetic and field foliations. Dashed great circles represent the measured field foliation around the sample location and the solid great circles are the magnetic foliation of the samples

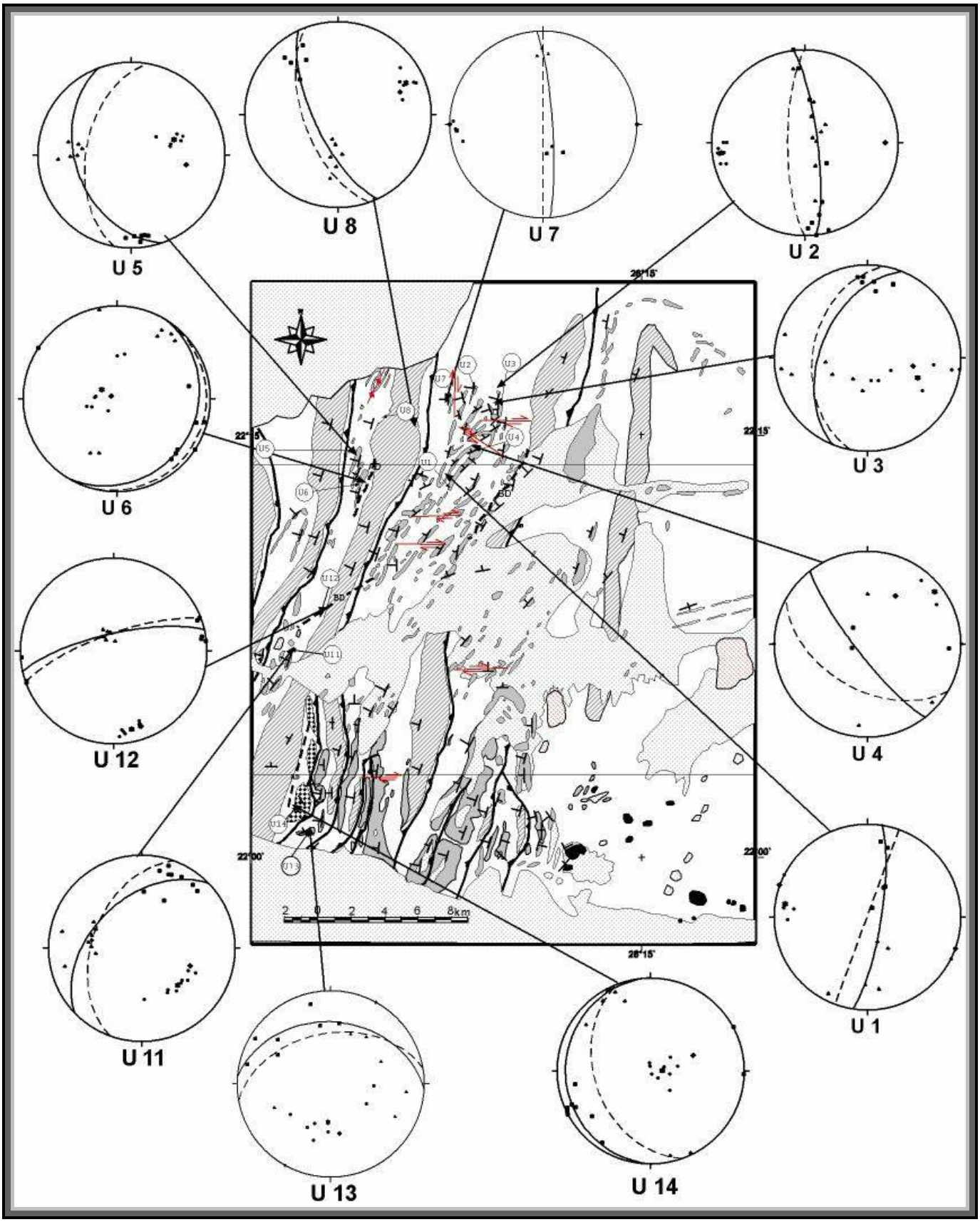

Fig 6.18 Map showing the sample location (for U serial) and the relationship between the magnetic and field foliations. Dashed great circles represent the measured field foliation around the sample location and the solid great circles are the magnetic foliation of the samples.

Sample No	k1	k2	k3	MS	F	L	P`	T	K1 dir	K2 dir	K3 dir
H4.1	1,007	1,006	0,987	781,7	1,019	1,001	1,023	0,887	128 7	34 29	230 60
H4.2	1,008	1,002	0,99	563,3	1,012	1,006	1,019	0,327	76 52	183 13	282 35
H4.3	1,009	1,005	0,986	679,3	1,019	1,004	1,024	0,633	149 12	56 14	278 71
H4.4	1,01	0,999	0,992	528,2	1,008	1,01	1,018	-0,166	34 39	130 8	230 50
H7.1	1,008	1,004	0,989	207,1	1,015	1,004	1,02	0,552	28 27	185 61	293 9
H7.2	1,013	1,002	0,985	223,9	1,017	1,011	1,028	0,207	24 22	280 31	143 51
H7.3	1,026	1,01	0,964	406,8	1,048	1,015	1,067	0,506	222 48	29 42	125 6
H7.4	1,012	1,009	0,979	489	1,031	1,003	1,037	0,836	50 34	319 3	225 56
H7.5	1,009	1,006	0,985	291,4	1,022	1,003	1,027	0,726	201 3	327 84	111 5
H7.6	1,01	1,006	0,984	337,9	1,023	1,004	1,029	0,663	203 11	335 74	110 12
H7.7	1,008	1,006	0,987	254,8	1,019	1,002	1,024	0,772	323 10	58 25	213 63
H19.1	1,038	1,005	0,958	36,57	1,049	1,033	1,084	0,183	241 32	354 33	118 41
H19.2	1,067	1,007	0,926	31,31	1,087	1,059	1,152	0,147	279 42	17 8	116 47
H19.3	1,056	1,006	0,938	18,27	1,072	1,051	1,127	0,138	298 50	196 10	098 39
H19.4	1,118	1,016	0,866	122,2	1,173	1,1	1,294	0,195	292 41	198 4	104 49
H19.5	1,104	1,011	0,885	136,2	1,143	1,092	1,25	0,152	297 36	199 11	094 52
H19.6	1,091	1,028	0,881	269,4	1,167	1,062	1,247	0,394	290 41	193 8	094 48
H23.1	1,004	1,004	0,992	362	1,012	1,001	1,014	0,849	357 61	203 27	107 11
H23.2	1,007	1,001	0,992	384,8	1,009	1,006	1,016	0,213	25 20	234 67	119 10
H23.3	1,005	1,002	0,992	408,1	1,01	1,003	1,014	0,541	23 23	231 65	118 11
H23.4	1,006	1,001	0,993	396,8	1,008	1,006	1,014	0,15	19 3	270 81	109 08
H23.5	1,007	1	0,993	408,3	1,007	1,007	1,015	-0,016	14 23	223 64	109 11
H23.6	1,008	1,006	0,986	323,6	1,02	1,002	1,025	0,816	26 38	214 51	119 04
U.2.1	1,02	1,014	0,966	539,2	1,006	1,049	1,061	0,758	006 52	170 37	266 08
U.2.2	1,026	1,018	0,956	393,8	1,008	1,065	1,081	0,773	165 03	055 82	256 08
U.2.3	1,036	1,009	0,955	465,7	1,026	1,056	1,086	0,343	178 09	056 73	270 14
U.2.4	1,019	1,003	0,977	920,1	1,016	1,027	1,043	0,232	169 22	014 66	262 09
U.2.5	1,029	1,007	0,963	405,9	1,022	1,046	1,07	0,333	175 15	048 66	270 18
U.2.6	1,019	1,008	0,973	622,6	1,012	1,035	1,049	0,488	164 34	012 53	263 14
U.2.7	1,024	1,021	0,955	369,5	1,003	1,069	1,082	0,923	355 21	155 68	263 07
U.2.8	1,014	1,011	0,975	409,4	1,003	1,038	1,045	0,849	134 64	351 21	255 14
U.2.9	1,019	1,01	0,971	334,3	1,009	1,04	1,052	0,629	173 00	081 80	263 10
U.4.1	1,038	1,005	0,957	8,98	1,033	1,045	1,075	-0,165	257 76	132 08	040 12
U.4.5	1,033	1,003	0,963	5,69	1,051	1,035	1,059	0,137	259 60	115 09	020 32
U.7.3	1,084	1,013	0,904	642	1,121	1,07	1,2	0,208	155 70	358 18	266 07
U.7.4	1,083	1,016	0,901	641	1,129	1,066	1,206	0,268	158 69	359 19	267 07
U.7.5	1,055	0,994	0,951	197,7	1,046	1,061	1,11	-0,163	173 64	004 25	272 04
U.7.6	1,087	1,008	0,91	572,3	1,108	1,075	1,191	0,132	145 60	355 27	258 13

Table 10 BIF with para-diamagnetic carrier.

Sample No.	k1	k2	k3	MS	F	L	P`	T	K1 dir	K2 dir	K3 dir
H3.2	1,028	1,002	0,97	22030	1,033	1,026	1,06	0,091	167 2	74 49	259 41
H3.3	1,033	1,004	0,963	21510	1,043	1,028	1,073	0,191	140 12	38 45	241 43
H3.4	1,034	0,997	0,97	19220	1,028	1,037	1,066	-0,161	147 4	53 47	241 43
H3.5	1,036	0,998	0,966	14450	1,032	1,039	1,073	-0,104	149 9	51 39	249 49
H3.6	1,035	1,003	0,963	27560	1,042	1,032	1,075	0,123	3 11	103 41	261 46
H10.1	1,016	0,994	0,99	7572	1,004	1,022	1,029	-0,694	293 37	42 23	156 44
H10.2	1,027	1,004	0,969	11560	1,037	1,022	1,061	0,226	294 3	26 37	201 52
H10.3	1,034	0,992	0,975	28350	1,018	1,042	1,062	-0,406	292 15	35 39	185 47
H10.4	1,022	0,998	0,981	45200	1,017	1,024	1,042	-0,181	129 0	39 34	219 56
H10.5	1,024	1,003	0,974	36400	1,029	1,021	1,051	0,152	303 30	158 55	43 17
H13.1	1,106	0,983	0,911	49450	1,079	1,125	1,216	-0,262	22 3	112 2	233 87
H13.2	1,069	0,019	0,912	159100	1,117	1,05	1,177	0,355	172 5	81 12	284 78
H13.3	1,076	0,994	0,93	33460	1,069	1,082	1,157	-0,115	53 14	147 13	277 70
H13.4	1,094	0,957	0,949	116100	1,008	1,143	1,172	-0,89	259 13	90 0	181 77
H13.5	1,092	0,962	0,946	141100	1,016	1,135	1,17	-0,786	78 9	246 8	215 79
H13.6	1,075	1,024	0,901	153300	1,137	1,05	1,2	0,415	43 15	134 3	233 74
U.5.1	1,127	0,993	0,881	34850	1,135	1,127	1,279	-0,9	168 13	270 42	065 45
U.5.2	1,097	0,982	0,921	10790	1,117	1,067	1,194	-0,304	171 14	267 23	053 63
U.5.3	1,074	0,999	0,927	11970	1,075	1,077	1,158	-0,25	174 07	269 35	074 54
U.5.4	1,124	0,993	0,883	47210	1,132	1,124	1,272	-0,087	173 14	278 46	070 41
U.5.5	1,108	0,987	0,905	15190	1,122	1,091	1,225	-0,191	178 14	282 42	074 44
U.5.6	1,065	0,992	0,943	4218	1,074	1,052	1,13	-0,2	184 12	282 32	077 55
U.6.1	1,074	0,973	0,953	19410	1,103	1,021	1,135	-0,668	107 12	206 36	001 52
U.6.2	1,056	1,014	0,93	6796	1,041	1,091	1,139	0,337	080 23	349 03	251 67
U.6.3	1,049	1,028	0,923	12750	1,02	1,114	1,148	0,671	138 14	045 13	274 71
U.6.4	1,054	1,033	0,913	11090	1,02	1,131	1,168	0,705	133 15	040 10	277 72
U.6.5	1,044	0,987	0,969	7001	1,057	1,02	1,081	-0,5	105 04	198 39	010 50
U.6.6	1,05	1,018	0,932	8437	1,031	1,093	1,132	0,469	130 16	033 21	255 63
U.6.7	1,03	1,01	0,96	4735	1,02	1,052	1,076	0,424	123 00	033 13	214 77

Table 11 BIF with High Ferrimagnetic carrier.

Sample No.	k1	k2	k3	MS	F	L	P`	T	K1 dir	K2 dir	K3 dir
H14.1	1,029	1,017	0,954	8269	1,065	1,012	1,084	0,667	310 81	75 5	166 7
H14.2	1,034	1,018	0,948	3421	1,074	1,016	1,097	0,618	296 56	71 26	172 21
H14.3	1,04	1,017	0,943	8306	1,078	1,023	1,108	0,521	24 76	279 4	188 14
H14.4	1,019	1,012	0,969	3202	1,044	1,007	1,056	0,714	261 45	69 44	165 6
H14.5	1,033	1,01	0,957	5985	1,055	1,024	1,082	0,378	326 73	93 10	186 13
H14.6	1,034	1,006	0,96	4459	1,049	1,027	1,079	0,258	339 71	87 6	179 18
H15.1	1,186	1,001	0,813	2355	1,232	1,185	1,461	0,009	347 42	196 44	91 15
H15.2	1,186	1,007	0,807	2459	1,248	1,178	1,472	0,056	349 42	195 45	91 14
H15.3	1,171	1,01	0,819	2415	1,232	1,159	1,431	0,084	348 41	203 43	95 18
H15.4	1,116	1,008	0,871	2276	1,157	1,113	1,289	0,092	357 37	199 51	95 11
H15.5	1,195	1,007	0,798	2409	1,262	1,187	1,5	0,053	342 42	189 44	85 14
H15.6	1,151	1,001	0,848	1933	1,181	1,15	1,358	0,011	352 44	190 44	91 9
H16.1	1,091	1,013	0,896	5477	1,131	1,078	1,221	0,197	302 43	204 9	105 46
H16.2	1,129	1,033	0,839	1756	1,231	1,093	1,356	0,338	73 46	337 5	242 43
H16.3	1,086	1,023	0,891	3908	1,148	1,061	1,224	0,354	309 53	205 10	108 36
H16.4	1,07	1,025	0,905	6487	1,133	1,043	1,19	0,459	330 34	224 22	107 48
H16.5	1,083	1,011	0,905	5928	1,117	1,071	1,199	0,192	321 43	216 16	110 43
H16.6	1,094	1,048	0,858	1487	1,222	1,043	1,296	0,616	118 34	10 24	253 46
U.3.1	1,028	0,989	0,983	6653	1,039	1,006	1,049	-0,745	019 17	265 53	121 32
U.3.2	1,037	1	0,963	4210	1,037	1,038	1,077	-0,004	019 18	286 09	171 70
U.3.3	1,034	0,994	0,972	4502	1,04	1,023	1,064	-0,273	356 20	263 08	154 68
U.3.4	1,038	0,992	0,97	6965	1,046	1,023	1,071	-0,345	005 19	215 68	098 10
U.3.5	1,034	0,989	0,977	8636	1,045	1,013	1,061	-0,569	353 14	258 18	119 67
U.3.6	1,031	0,989	0,98	5665	1,042	1,01	1,055	-0,63	007 29	189 61	097 01
U.3.7	1,032	0,996	0,972	9854	1,035	1,025	1,062	-0,184	357 14	096 30	245 56
U.1.1	1,029	1,001	0,97	1581	1,028	1,032	1,061	0,043	016 24	147 57	276 22
U.1.2	1,029	1,004	0,967	3594	1,025	1,039	1,065	0,202	029 61	171 23	268 16
U.1.3	1,023	0,996	0,982	1931	1,027	1,014	1,024	-0,326	030 59	182 28	278 12
U.1.4	1,04	1,008	0,952	1685	1,031	1,059	1,094	0,284	010 19	158 67	276 11
U.1.5	1,008	0,998	0,994	1140	1,01	1,003	1,014	-0,519	027 81	207 09	117 00

Table 12 BIF with Intermediate ferromagnetic carrier.

Sample No.	k1	k2	k3	MS	F	L	P`	T	K1 dir	K2 dir	K3 dir
H11.1	1,011	0,998	0,991	850,1	1,007	1,013	1,021	-0,275	118 1	209 36	27 54
H11.2	1,009	1,001	0,99	1106	1,011	1,008	1,019	0,185	255 6	5 73	163 15
H11.3	1,012	0,998	0,989	1837	1,009	1,014	1,023	-0,212	71 5	330 66	163 24
H11.4	1,011	1,003	0,986	863	1,018	1,008	1,026	0,381	99 9	214 70	6 18
H11.5	1,01	1,005	0,984	1247	1,021	1,005	1,028	0,627	68 20	300 59	167 22
H11.6	1,007	1	0,993	882,2	1,007	1,006	1,013	0,04	115 10	221 57	19 31
H17.1	1,012	0,997	0,991	1500	1,005	1,016	1,022	-0,507	233 18	324 4	68 72
H17.2	1,011	1,005	0,984	958,6	1,021	1,006	1,028	0,564	148 32	52 11	306 56
H17.3	1,012	1,002	0,987	582,5	1,015	1,01	1,026	0,221	202 24	326 51	97 29
H17.4	1,011	1,003	0,986	918,4	1,017	1,008	1,026	0,346	135 29	45 0	315 61
H17.5	1,007	1,001	0,993	1036	1,008	1,006	1,014	0,158	217 23	110 34	334 46
H17.6	1,006	0,998	0,996	986,2	1,002	1,008	1,011	-0,564	209 19	103 38	320 46
H20.1	1,005	1	1,005	939,5	1,004	1,006	1,01	-0,145	260 1	163 83	350 7
H20.2	1,008	1,002	0,99	966,3	1,012	1,006	1,018	0,374	85 85	263 5	353 0
H20.3	1,008	1,001	0,991	855,6	1,01	1,007	1,017	0,207	108 81	302 9	212 2
H20.4	1,005	1,003	0,992	1325	1,012	1,002	1,015	0,675	136 84	285 5	16 3
H20.5	1,011	0,997	0,991	1003	1,006	1,014	1,021	-0,414	151 0	61 25	241 65
H20.6	1,007	1	0,003	1226	1,006	1,007	1,014	-0,076	260 2	350 1	101 88
U.11.1	1,05	0,998	0,952	1384	1,053	1,048	1,104	-0,066	020 17	272 45	125 40
U.11.2	1,046	1,007	0,947	955	1,038	1,063	1,105	0,22	013 16	264 49	115 37
U.11.3	1,046	1,004	0,95	768,7	1,041	1,058	1,102	0,138	029 14	285 44	132 43
U.11.4	1,056	0,998	0,946	1215	1,058	1,055	1,116	-0,057	044 16	299 41	150 44
U.11.5	1,052	1,011	0,936	1256	1,04	1,08	1,126	0,296	002 39	257 17	148 46
U.11.6	1,066	1,001	0,933	2393	1,065	1,073	1,142	0,02	025 43	282 14	177 44
U.11.7	1,055	1,011	0,934	710,3	1,044	1,083	1,133	0,272	018 08	280 45	116 44
U.11.8	1,048	1,009	0,943	809,6	1,039	1,07	1,114	0,255	022 16	277 42	129 44
U.11.9	1,047	1,006	0,947	579	1,041	1,063	1,107	0,181	039 14	293 46	141 41
U.13.1	1,052	1,01	0,975	1701	1,005	1,036	1,045	0,734	283 10	022 42	183 47
U.13.2	1,013	0,997	0,989	965	1,016	1,008	1,025	-0,329	299 36	209 00	119 54
U.13.3	1,01	1,003	0,987	979,5	1,007	1,016	1,024	0,418	346 13	247 35	093 52
U.13.4	1,008	0,997	0,995	541,3	1,011	1,002	1,014	-0,68	008 35	117 24	233 45
U.13.5	1,025	1,007	0,969	2484	1,018	1,039	1,059	0,358	310 27	066 41	197 37
U.13.6	1,009	1	0,991	821,1	1,009	1,009	1,018	0,015	350 37	096 20	208 46
U.13.7	1,009	1,005	0,986	1422	1,004	1,02	1,026	0,633	301 07	037 37	202 52

Table 13 with BIF Low Ferrimagnetic carrier.

Sample No.	k1	k2	k3	MS	F	L	P`	T	K1 dir	K2 dir	K3 dir
H1.1	1,016	0,998	0,986	231,8	1,013	1,018	1,031	-0,163	7 21	236 60	106 21
H1.2	1,02	0,997	0,982	200,6	1,015	1,023	1,039	-0,219	309 32	210 15	098 54
H1.3	1,03	1,01	0,96	200,5	1,052	1,02	1,075	0,429	352 33	257 7	156 56
H1.4	1,043	1,013	0,944	280,7	1,073	1,029	1,108	0,4	295 35	204 1	112 55
H1.5	0,973	1,028	0,999	289,6	1,029	1,026	1,056	-0,065	339 31	229 30	104 44
H1.6	0,989	1,016	0,995	231,6	1,021	1,006	1,028	-0,564	345 40	251 4	157 49
H2.1	1,056	0,992	0,952	323	1,042	1,064	1,109	-0,229	337 27	182 60	073 11
H2.2	1,08	0,991	0,93	299,8	1,066	1,09	1,162	-0,183	196 36	338 48	091 19
H2.3	1,07	0,99	0,94	348,7	1,053	1,08	1,139	-0,231	344 29	192 58	081 12
H2.4	1,032	1,001	0,968	286,1	1,034	1,031	1,066	0,024	342 42	172 48	076 05
H2.5	1,042	1,007	0,952	305,1	1,058	1,035	1,096	0,222	330 41	205 34	091 31
H2.6	1,059	1,007	0,934	365,4	1,079	1,052	1,135	0,169	343 24	198 61	079 15
H2.7	1,077	1,011	0,913	356,8	1,108	1,065	1,182	0,196	335 35	185 51	076 15
H5.1	1,13	1,072	0,798	10820	1,343	1,054	1,454	0,651	333 36	220 28	103 41
H5.2	1,134	1,082	0,784	11650	1,38	1,048	1,494	0,705	228 41	345 28	098 36
H5.3	1,109	1,09	0,801	5883	1,361	1,018	1,442	0,874	198 12	300 44	096 43
H5.4	1,117	1,086	0,797	8795	1,363	1,029	1,455	0,806	222 33	339 35	102 38
H5.5	1,128	1,106	0,767	8592	1,443	1,02	1,545	0,879	254 44	0 16	105 42
H5.6	1,115	1,101	0,784	10130	1,405	1,013	1,492	0,915	257 45	358 11	098 43
H9.1	1,074	1,012	0,914	37,02	1,107	1,061	1,177	0,231	185 7	66 76	276 12
H9.2	1,055	1,014	0,93	25,02	1,09	1,04	1,138	0,347	26 9	146 97	294 16
H9.3	1,108	1,017	0,876	25,78	1,161	1,09	1,269	0,214	184 2	82 79	275 10
H9.4	1,034	1,007	0,959	26,8	1,049	1,028	1,079	0,262	22 15	152 68	288 17
H9.5	1,05	1,011	0,939	37,07	1,076	1,038	1,12	0,298	10 9	187 81	280 00
H12.1	1,112	1,008	0,881	15240	1,144	1,103	1,263	0,099	179 9	68 67	273 22
H12.2	1,121	0,998	0,881	9031	1,133	1,122	1,272	-0,02	175 15	62 56	274 30
H12.3	1,115	1,024	0,862	8485	1,188	1,089	1,3	0,283	173 6	63 73	265 16
H12.4	1,12	1,004	0,876	14870	1,145	1,116	1,279	0,045	175 21	48 57	275 24
H12.5	1,143	1,022	0,835	7801	1,225	1,118	1,375	0,217	176 3	75 75	267 14
H12.6	1,116	1,007	0,877	6378	1,149	1,108	1,275	0,091	176 8	62 70	269 18
U.8.1	1,017	1,006	0,977	217,3	1,012	1,029	1,042	0,419	317 18	185 64	053 18
U.8.2	1,017	1,005	0,978	157,1	1,012	1,027	1,04	0,395	330 33	174 55	068 11
U.8.3	1,015	1,004	0,982	219,6	1,011	1,022	1,034	0,325	317 36	182 44	066 24
U.8.4	1,018	1,007	0,975	106,1	1,011	1,032	1,045	0,491	333 18	193 68	067 13
U.8.5	1,014	1,006	0,979	149,5	1,008	1,028	1,037	0,551	313 44	187 32	077 30
U.8.6	1,019	1,008	0,973	178,8	1,011	1,036	1,05	0,504	318 26	190 52	062 26

Table 14 for the Anatexite light bands

Sample No.	k1	k2	k3	MS	F	L	P`	T	K1 dir	K2 dir	K3 dir
H6.1	1,012	1	0,988	758,5	1,012	1,012	1,024	0,018	169 25	62 31	290 48
H6.2	1,02	1,005	0,976	873,4	1,03	1,015	1,046	0,328	214 6	90 79	305 9
H6.3	1,007	1,001	0,992	768,9	1,009	1,005	1,015	0,294	177 15	70 49	279 38
H6.4	1,01	0,999	0,992	780	1,007	1,011	1,018	-0,23	197 9	99 44	279 45
H21.1	1,008	1,002	0,99	648,1	1,012	1,006	1,019	0,328	336 16	233 38	84 48
H21.2	1,017	0,996	0,987	846,2	1,009	1,022	1,032	-0,428	313 33	211 18	97 51
H21.3	1,011	1	0,989	679,7	1,01	1,011	1,022	-0,039	340 18	235 39	89 46
H21.4	1,009	1,003	0,989	652,2	1,014	1,006	1,021	0,408	11 17	267 39	119 46
H21.5	1,012	1,002	0,986	603,3	1,017	1,009	1,026	0,268	210 3	302 42	117 48
H21.6	1,009	1,002	0,989	549,9	1,014	1,006	1,02	0,362	18 3	285 42	111 48
H22.1	1,014	0,999	0,987	716	1,012	1,015	1,027	-0,098	15 45	200 44	107 2
H22.2	1,021	0,993	0,986	700,8	1,007	1,029	1,038	-0,621	33 43	173 40	282 12
H22.3	1,017	0,998	0,985	663,9	1,013	1,019	1,032	-0,2	34 34	182 52	293 16
H22.4	1,023	0,993	0,985	695,8	1,008	1,03	1,04	-0,578	28 41	171 43	280 19
H22.5	1,017	1	0,983	666,2	1,017	1,016	1,034	0,029	20 40	217 49	117 9
H22.6	1,021	0,996	0,982	698,1	1,014	1,025	1,04	-0,294	27 48	226 41	128 10

Table 15 for the Anatexite Dark bands

CHAPTER 7
SUMMARY AND CONCLUSIONS

The study area is a part of the Nile Craton or the Sahara Craton, to the west of the Arabo-Nubian shield. It covers about 400 km^2 in the south-west corner of the Western Desert of Egypt, which lies between lat 22° 00‘00“and 22° 15‘00“, long 26° 00‘00“ and 26° 12’00.

The objective of this study was mapping the area, assess the structures, establish the tectonic evolution in Archaean – Early Proterozoic times, and discuss the effect of the Pan-African orogeny on the study area.

Detailed field mapping of the investigated area revealed the presence of three tectonostratigraphic rock units arranged from the bottom to top as follows:

3 - Banded Iron Formation (BIF).

2 - Anatexite Sequence

1 - Ultramafic-mafic and calc-silicate rocks (UM).

Harris et al. (1984) give an age of 3.200-3.000 Ma by Rb/Sr age dating method for the crustal building around the Uweinat area. Cahen et al. (1984) give an age of 2.900 Ma by the same method for the prograde metamorphism of granulite facies in the area. Klerkx (1980), Cahen et al. (1984) and Harris et al. (1984) give the age of 2.640 Ma for the retrograde metamorphism of amphibolite facies. Klerkx (1980) and Cahen et al. (1984) give the migmatization or anatexis processes an age of 1.800 Ma. The BIF in the study area did not have any age dating. Recently the age of 1974 $^{+}/_{-}$ 4 Ma by U/Pb for the time of granulite-facies metamorphism and orogenic reworking in Uweinat area was given by Schenk et al.(2002)

7. 1 Lithologic Sequences

7.1.1 Ultramafic-Mafic and Calc-Silicate Rocks (UM).

The mafic and mafic-ultramafic rocks are poorly exposed (5%) but well delineated in the southern part of the investigated area at the contact with the Anatexite Sequences, consisting of several hundred metres thick interlayered wherlite (olivine + clinopyroxene ± chromite cumulates), clinopyroxenite (cpx cumulates), and gabbro (cpx + plagioclase cumulates). Olivine compositions are quite forsteritic. The rocks are variably transformed into foliated metamorphic equivalents (talc-tremolite serpentinite, talc-serpentine tremolitite, hornblendite,

amphibolite) characterized by pervasive metamorphic recrystallization under amphibolite facies metamorphism.

7.1. 2 Anatexite Sequence

The Anatexite Sequence occupies about 30% of the rock units in the study area. Microscopic studies indicate a replacement of primary prograde mineralogy (granulite facies) by a later retrograde facies (amphibolite facies). The Anatexite Sequence consists of leucosome and melanosome bands. The leucosome bands with felsic components are buff grey to white, of medium to coarse grain size, and composed mainly of quartz, alkali-feldspar, subordinate amounts of biotite, chlorite and orthopyroxene.

The melanosome bands of mafic components are greyish green to dark, fine to medium-grained, and are composed mainly of amphibole, plagioclase ad subordinate amounts of biotite, chlorite and orthopyroxene. Both of these bands are arranged in layers or schlieren and as patches. Generally the bands are parallel with the main foliation trends with mainly azimuth of 010°/55° to the west. Minor ptygmatic folds with nearly vertical fold axes represent F2 folding phase and some minor tight and isoclinal folds with nearly horizontal fold axes can be distinguished as an F3 fold phase

7.1. 3.The Banded Iron Formation (BIF)

The BIF in the investigated area represents about another 30 % of the rock units. It crops out in a repetition of elongate low to moderate hills with an average of 50-70 metre elevation from the ground, trending in NNE direction.

In general the Banded Iron Formations are composed of alternating thin layers of silica (chert) and iron minerals. The BIF is built up of four units, with gradational contact between them. The stratigraphy of the units is shown below:

4- Meta-chert and jaspilite bands.

3- Well-banded iron-silica succession.

2- Fuchsite-bearing quartz bands.

1- Metapelite volcanosedimentary bands alternating with iron-silica bands.

The upper three units represent the upper BIF (4, 3, 2), they have a Superior-type BIF character, which has about 500 metres thickness. The lower unit (1) is the base of the BIF. It has Algoma-type character and forms relatively small bodies consisting of lenticular masses of about 200 metres thickness. The iron minerals consist mostly of iron oxides, e.g. hematite and magnetite.

7.1. 4.Younger Intrusion and Sedimentary Cover

Around 35% of the area is covered by small, young intrusions represented by granites, trachyte, Tertiary basalts in addition to Phanerozoic sandstone and Quaternary sand dunes.

7.2 The Anisotropy of Magnetic Susceptibility (AMS) Analysis

The AMS analysis was done for 31 samples from the BIF and the Anatexite sequences, 22 of them are BIF and 9 of the Anatexite. For every sample about six cylinders, totally 200 cylinders, were measured.

7. 2. 1 AMS of the BIF

The bulk susceptibility allows to distinguish the different BIF bands with different magnetic susceptibility amounts, as follows:

The Metachert bands have main susceptibility from 316 – 632 x 10^{-6} SI, the well-banded iron-silica bands have 6,607 – 25,816 x 10^{-6} SI, the Fuchsite bearing quartz bands 4 – 1,273 x 10^{-6} SI and the pelite-volcanosediments alternating with BIF bands contain 1,119 – 108,752 x 10^{-6} SI. The well-banded iron-silica bands and the pelitic bands show very high values in mean susceptibility pointing to ferrimagnetic carriers, while the metachert and quartz bands exhibit lower magnetic susceptibility values. They are dominated by diamagnetic and paramagnetic minerals.

The interpretation of the AMS magnetic foliation and magnetic lineation shows that are parallel these features with the field measurements of the major structures in the whole area. The magnetic foliations and magnetic lineations are shown in a stereographic plot and show F2 fold phase with nearly vertical fold axes, while F3 fold phase has a north plunged fold with amount of 20°.

7. 2. 2 AMS of the Anatexite Sequences

The bulk susceptibility allows to distinguish the different bands. The light bands have main susceptibility from 25 - 15,240 x 10^{-6} SI partly reflecting high feldspar and quartz contents (dia-paramagnetic) partly a high iron oxide amount (ferrimagnetic carriers). The dark bands indicate main susceptibility between 550 and 873 x 10^{-6} SI, due to the hornblende, biotite and orthopyroxene content (paramagnetic carriers).

The interpretation of the AMS magnetic foliation and magnetic lineation in the Anatexite shows that these features are parallel with the field measurements of the major structures in the whole area. The magnetic foliations and magnetic lineations are shown in a stereographic plot and show less F2 fold phase with nearly vertical fold axes, while F3 fold phase shows an east vergent fold plunging 5° with an azimuth of 7°.

7. 3 Geochemistry of BIF and Related Rocks

Twenty-five selected samples representing the three main units: BIF, Anatexite Sequences and the ultramafic-mafic rocks were analyzed for their major, minor and trace element contents. Chemical analyses were carried out in the Laboratories of the Geological Survey of Egypt, by XRF technique for major, and spectral analysis for trace elements. In this study area neither rare earth elements analysis nor quantitative complete trace element analyses have been done for any of the collected sample.

Due to the intense deformation and metamorphism observed in the study area the geochemical analyses did not show any significant conclusion except the following:

7. 3. 1 BIF

It is possible to distinguish the different bands of the Banded Iron Formation and Superior or Algoma type due to the alumina content. The Superior type has Alumina content from 0,66% to 0.15%, while the Algoma type has Alumina content from 0,75% to 1,5%. These support the field observations and the petrographic studies.

7. 3. 2 Anatexite Sequences

It is possible to distinguish the leucosome and melanosome in the Anatexite Sequences pointing to the silica and mafic minerals content. The major oxides such as SiO_2, Al_2O_3, Na_2O, K_2O and P_2O_5 have a higher content in the leucosome bands, while TiO_2, MnO_2, MgO, CaO and the total FeO are higher in the melanosome bands.

7. 4 The Deformation Phases

Three deformation phases overprint the study area (D1, D2, and D3).

The three phases D1, D2 and D3 affected only the basement rocks, while late, brittle deformations of Phanerozoic ages affected all the units in the investigated area.

The earliest D1 deformation is partly erased and observed only in the thin sections.

Table 11 summarizes the structural events. Figures (7.1) and (7.2) try to show the development of the study area during the D2 and D3 deformation phases

7. 4. 1 D1

During this early phase developed the leucosome and melanosome bands in the Anatexite sequences. The earlier trend of these bands is not clear due to the overprinting with the later deformations. During the deformation D1 all the older structures in the crust (Anatexite and Ultramafic-mafic rocks) were erased or flattened and formed the leucosome and

melanosome. The primary bands in the BIF survived this phase. At the same time, in the BIF bands mylonitic foliation developed. This mylonitic foliation indicates simple shear.
There are not enough indicators preserved from this deformation phase to distinguish, whether it developed during crustal thickening or crustal thinning, due to the erased structures during the later deformations.

7. 4. 2 D2 (East-West Folding)

D2 folded the bands in the BIF and the Anatexite sequences, into disharmonic and tight isoclinal folds (F2). The folds dominate in the higher unit (BIF), while in the Anatexite sequences and UM rocks the F2 appears as less extensive. The F2 folds are separated by some shear zones parallel with the fold axial surfaces (S2). The F2 folds have generally steep fold axes due to the rotation by subsequent horizontal east-west fold axes (D3).

7. 4. 3. D3 (North-South Folding)

The D3 is characterized by development of a regional anticline-syncline belt with NNE-SSW oriented fold axes (F3). The folding developed east vergent folds and overturned folds and thrusts (reverse faults). The axial surfaces of these folds trend 15°, dipping to the NW with angles between 55° and 70°. This is parallel to thrust surfaces. F3 affected F2 by refolding, thereby rotating the F2 folds around a horizontal axis. The resulting foliation, S3, is parallel to the thrust surfaces. The dip angle ranges between 20° and 70° to the WNN (285°).

7. 4.4. Late Brittle Deformation

7. 4. 4. 1 East-West Wrench Faulting

Minor strike slip faults, trending E-W, are often accompanied with fault breccia cemented with goethite or hematite. The faults affected the basement and the cover sedimentary rocks, but with minor displacement. These faults have Phanerozoic ages, since they cut through the Mesozoic sedimentary rocks.

7. 4. 4. 2 Normal Faults

Normal faults with E-W direction overprinted the area and produced a graben in the middle of the area and two horsts in the southern and northern parts of the area. The sedimentary rocks cover the middle part except for some erosional windows of the basement.

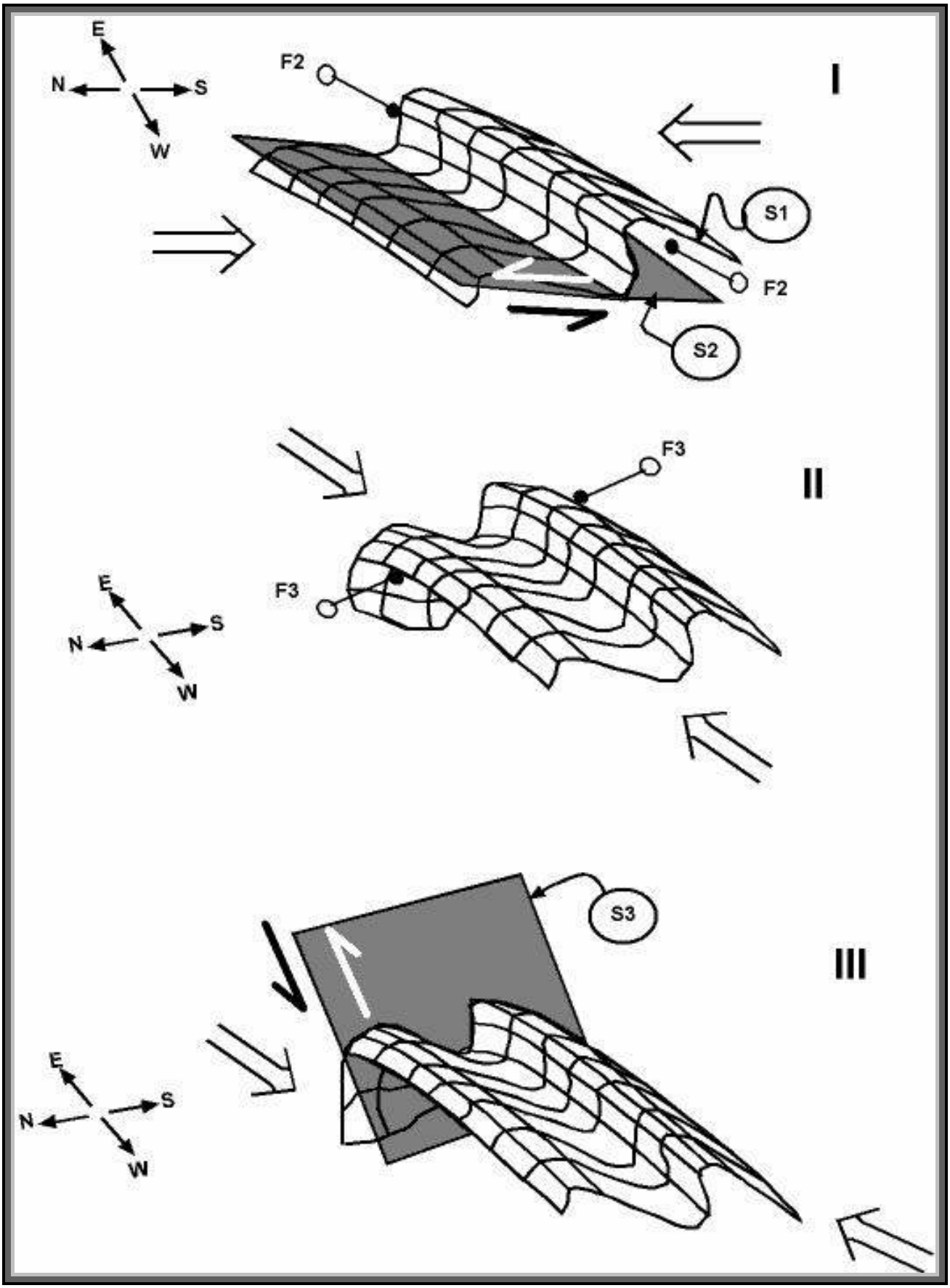

Fig 7.1 Sketch showing the development of F2 and F3 folds by two phases of folding in the investigated area.

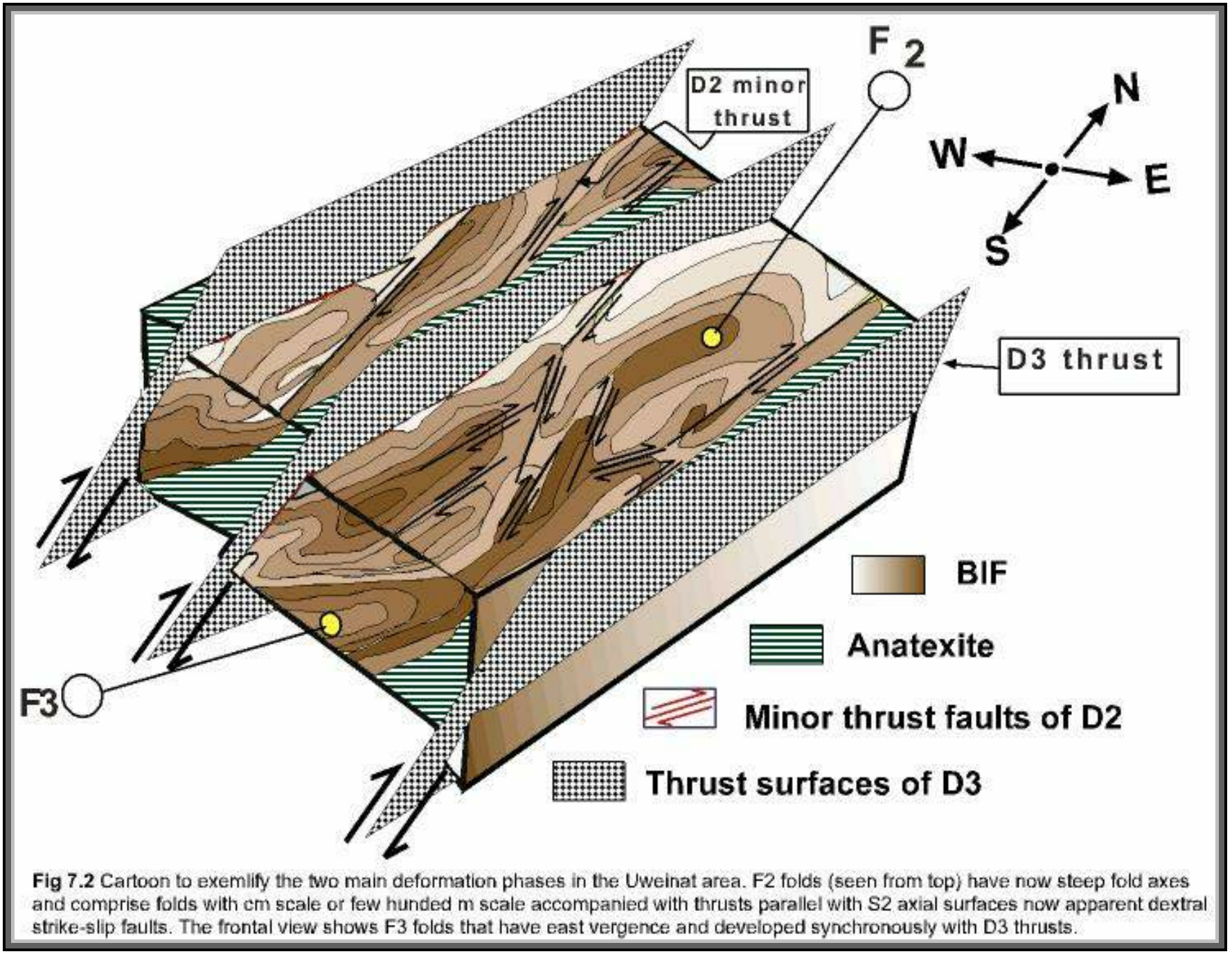

Fig 7.2 Cartoon to exemlify the two main deformation phases in the Uweinat area. F2 folds (seen from top) have now steep fold axes and comprise folds with cm scale or few hunded m scale accompanied with thrusts parallel with S2 axial surfaces now apparent dextral strike-slip faults. The frontal view shows F3 folds that have east vergence and developed synchronously with D3 thrusts.

Deformation	Age	Major Structures (map scale)	Minor Features (outcrop and microscopic scale)	Metamorphic Events and Indicative Minerals	Igneous events	Tectonic events
	3200-3000				Ultramafic	Crust formation,
	2900 Ma		? ? ⇈ ? BIF sedimentation (primary bedding) ? ⇊ ?	prograde metamorphism of the granulite facies	(orthogneiss)	??
	2640 Ma			retrograde metamorphism of the amphibolite facies		
	1974 Ma			prograde metamorphism of granulite facies	Volcanics	Orogenic reworking
D1	Around 1800 Ma	**??**	Leuco- and melanosome as metamorphic banding in the Anatexite, shear bands dominate in the BIF.	Anatexis processes caused partial melting, retrograde metamorphism	No evidence	(D1) Crustal thickening or thinning?? Remnant of mylonitic bands
D2		Upright, tight, disharmonic and isoclinal folds with steep fold axes, with scale up to 500 m, accompanied by apparent minor dextral strike-slip faults parallel with the fold axial surfaces.	Minor tight-isoclinal and disharmonic folds with steep fold axes, with scale between a few mm and few metres in BIF. Anatexite shows Ptygmatic steeply plunging fold axes.	Retrograde metamorphism, to amphibolite-greenschist grade	No evidence	(D2) S-N crustal shortening Pure shear dominant
D3		Regional anticlinal-synclinal fold pairs, developed into east vergent folds and thrusts. Generally the eastern limb was suppressed. The fold axes trend 015°/15°, thrusts 285°/65°, while S3 foliation strike to 15°/60° west.	Minor tight and isoclinal folds, east vergent, the fold axial surfaces are parallel with the major thrusts in the area. Folds range from a few mm (microscopic) to metres.	---	No evidence	W-E crustal shortening
--	Pan-African age		--		Small granitic intrusion	Uplift
Late, brittle deformation	Phanerozoic	E-W right lateral faults with a few hundred m displacement. E-W normal faults formed a graben and horst.	E-W right lateral faults with a few cm displacement cut through the BIF and the young sediments. Fault breccia cemented with goethite and hematite -----	**----**		Intra-cratonic faulting

Table 16 Compilation of deformational phases, isotopic ages, major and minor deformation, metamorphism, magmatic activity and tectonic events.

7. 5 Tectonic Evolution of the Study Area

On the base of this summary a tectonic evolution can be concluded as follows:

1- The formation of continental crust occurred up to the west of the study area 3200 to 3000 Ma ago (Harris et al. 1984).

2- Deposition of Banded Iron Formation in continental marginal basins. The time of this deposition may be between 2900 and 1800 Ma in accordance with the world-wide deposition of the BIF (Windley 1979).

3- In the time-span from 1974 Ma to 1800 Ma crustal thickening followed by crustal thinning (D1), led to the pro-grade and subsequent retrograde metamorphism in this period. In this period developed the anatexite bands in the deeper units and the above-mentioned shear zones in the BIF.

4- Somewhat later, further crustal shortening (D2) occurred in north-south direction by regional folds with E-W fold axes, associated with pure shear. In this period the area was still subjected to retrograde metamorphism.

5-Continued crustal shortening due to forces from west-east direction (D3) caused folding with NNE-SSW fold axes plunging to the north or south directions with shallow angles. Continued folding processes caused a series of reverse faults. This group of faults extends in the NNE-SSW direction with dip angles between 25° and 65° to the NW. These types of faults are prevailing in the area.

6- During the Pan-African times a series of granitic intrusions intruded into the Anatexite Sequences and the BIF, followed by regional uplift and erosion.

7-In Phanerozoic times the area was subjected to a series of E-W wrench faults with a few hundred metres displacement, followed by E-W striking normal faults producing regional horst and graben structures.

7.6 Conclusion

The detailed work presented here includes a detailed geological map at the scale of 1:60,000. The detailed field work and structural analysis established for the first time the following:

- BIF rock type is preserved with primary layering, represented by chert, jaspilite, metapelite-volcanosedimentary and magnetite bands as the highest Precambrian unit. It is overlies Anatexite and Ultramafic-mafic rocks. (see Fig 2.18& 2.19).

- Complex, polyphase folding is recorded within the Ultramafic-mafic rocks, Anatexite and BIF, during peak of metamorphism of granulite facies at ca. 1970 Ma age and subsequent retrograde metamorphism of amphibolite and greenschist facies.
- Three phases of deformation are imprinted on the rock units. Relics of the first phase (D1) deformation are hardly recognizable in the field, but visible as shear zone in thin sections. The second phase (D2) is represented by east–west folds (F2) accompanied with shear zones. The third deformation phase (D3) is a regional anticline-syncline belt with NNE-SSW oriented fold axes (F3). The folding developed east vergent folds and overturned folds and thrusts (reverse faults). The (D3) affected (D2) by refolding, thereby rotating the F2 folds around a horizontal axis to show now steep fold axis.
- Pan-African-age events are, apparently, restricted to isolated granite intrusions with no related deformation.

References

Abdel-Monem, A.A.& P.M. Hurley (1979): U-Pb dating of zircons from psammitic gneisses, Wadi Abu Rosheid-Wadi Sikait area, Egypt, Bull. Inst. Applied Geol., King Abdul Aziz Univ., Jeddah 3(2): 165-170.

Abdelsalam, M.G., Dawoud A.S. (1991): The Kabus ophiolitic melange, Sudan, and its bearing on the W boundary of the Nubian Shield. Journal Geological Society, London 148:83-92.

Bennet, J. D. and Mosley, P. N. (1987): Tiered tectonics and evolution, E. Desert and Sinai, Egypt. In: Matheis and Schandelmeier (eds.), Current Res. Africa. Earth Sci.,Balkema, 79-82.

Bernau, R., D.P.F. Darbyshire, G. Franz, U. Harms, A. Huth, N. Mansozr, P. Pasteels & H. Schandeleier (1987): Petrology, geochemistry and structural development of the Bir Safsaf-Aswan uplift, southern Egypt. Journal Africa Earth Sci.6: 79-90.

Burollet,P.F. (1962): Reconnaissance geolgique dans la sud-est du bassin de Kufra.-Rev.Inst.Franc. Petrole, 18, 11, 1537-1545, Paris.

Cahen, L., and Selling N.J. (1984): The Geochronology and Evolution of Africa (Clarendon Press, Oxford)

Condie, K.C. (1982): Plate tectonics and Crustal Evolution (Pergamon Press, New York).

Conoco-Corporation LTD (1987): Geological Map of south Western Desert Egypt. Scale 1:500.000, sheet No NF 53 NV, Gilf Kabeir Plateau.

Dahl, N., and McNaughton, N.J. (1987): Evidence for an epigenetic origin for BIF-hosted gold deposits in the greenstone belts of the Yilgran Block, Western Australia. In Recent advances in understanding Precambrian gold deposits. Edited by S.E. Ho and D.I.Groves. Geology Department and University Extension, University of Western Australia Nedlands, WA, Publication II,pp. 167-179.

Desio, A. (1933): Relazione preliminare sulle ricerche compuite della“Missione Desio“nel deserto Libico.-R. Accad Italia, Viaggio di Studio ed Explorazioni,1,1-67.

De Wall, H. (1991): Die Gefüge der Paragneise in der KTB-Vorbohrung und ihr Einfluss auf gesteinsphykalische Eigenschaften. Diss., Geol.-Paläont. Inst., Univ. Göttingen,129 p.

Dixon, T. H.., and Golombek, M. P. (1988): Precambrian crustal accretion rates in northeast Africa and Arabia: Geology, v. 16, p. 991-994, and cover

El-Gaby, S., O.M. El Nady, & A.M. Khudeir, (1984): Tectonic evolution of the basement complex in the central Eastern desert of Egypt. Geol. Rundschau 73:1019-1036.

El-Gaby, S., F.K. List, & R. Tehrani., (1988): Geology, evolution and metallogenesis of the Pan-African belt in Egypt. In: El-Gaby S. & R.O.Greiling (eds). The Pan-African belt of northeast Africa and adjacent areas. Braun-Schweig (Vieweg):17-68.

Floyd, P. A. and Winchester, J. A. (1975): Magma type and tectonic setting discrimination using immobile elements. Earth Planet. Sci. Lett., 27,211-218.

Fripp, R.E.P. (1976): Stratabound gold deposits in Archean banded iron formation, Rhodesia. Economic Geology, 71:58-75.

Garcia, M. O. (1978): Criteria for the identification of ancient volcanic rocks. Earth Sci. Rev., 14, 147-165.

Gass, I.G. (1981): Pan-African (upper Proterozoic) plate tectonics of the Arabian Nubian shield. In: A. Kröner, Precambrian plate tectonics. Elsevier:387-405.

Greiling, R.O., El Ramly, M.F., El Akhal, H. and Stern, R.J. (1988): Tectonicevolution of the Red Sea margin as related to basement structure. Tectonophysics, 153:179-191.

Greiling, R.O., Abdeen, M. M., Dardir, A. A., El Akhal, H., El Ramly, M. F., Kamal El Din, G. M., Osman, A. F., Rashwan, A.A., Rice, A. and Sadek, M. F. (1994): A structural synthesis of the Proterozoic Arabian-Nubian Shield in Egypt. Geol. Rundsch., v. 83, p. 484-501.

Greiling, O. R.; Kontny, A.; Khalid, A.M., and El Kady, M.F. (2000): Geology of the Banded Iron Formation West Gabal Kamel. Western Desert. Egypt. [Geology of Arab world (GAW)] Conf. Cairo Uni. Cairo 2000 (Abstract).

Goodwin, A.M., (1996): Principles of Precambrian Geology (Academic Press Limited, Great Britain 1996)

Groves, D.I., Phillips. G.N., Flaconer. L.J., Houston, S.M., Ho.S.E., Browning, P., Hassanein Bay, A. M. (1924): Through Kufra to Darfur- Geography Journal, 64,273-291,London.

Harris, N.B.W., Hawkesworth, C.J. & Ries, A.C. (1984): Crustal evolution in north-east and east Africa from model Nd ages.- Nature, 309, 773-776, London.

Hrouda, F. (1982): Magnetic anisotropy of rocks and its application in Geology and Geophysics. Geophys. Surv., 5, 37-82.

Hunting Geology & Geophysics LTD. (1974): Geology of the Jabal al Uwaynat area, Libyan Arabic Republic.-Unveröff.Bericht, Indust.Res. Cent.,Dep.Geol.Res.and Mineral.,Tripolis.

Issawi, B. & Jux, U. (1982): Contribution to the stratigraphy of the paleozoic in Egypt. Geol.Surv.paper No.64, 28 pp.

Jakes, P., and White, A. J. (1972) Major and trace element abundance in volcanic rocks of orogenic areas. Geol. Soc. Am. Bull., 83, 29-35.

Jelinek, V. (1977): The statistical theory of measuring anisotropy of magnetic susceptibility of rocks and its application. Geofyzika, Brno, 1-88.

Jelinek, V. (1980): Kappabridge KLY-2. A precision Laboratory Bridge for Measuring Magnetic Susceptibility of Rocks (Including Anisotropy). Leaflet, Geofyzika, Brno.

Jelinek, V. (1981): Characterization of the magnetic fabric of rocks. Tectonophysics, 79, 63-67.

Kennedy, W.O. (1964): The structural differentiation of Africa in the Pan-African tectonic episode. 8th Annual Report, Res.Inst.Afr.Geol.,Leeds Univ.:48-49.

Khalid, A.M., Said, M.M., Shaaban, G.M., Khattab, M.M., El Banna, R.E. (2000):
Al Uwaynat Banded Iron Formation. Distribution and probable origin of both
Iron and Gold. Geol. and Develop. Symp. no. 3. Al Monufia Uni.

Klerkx, J. (1969): Le Jebel Uweinat: temoin de l´histoire geologique de Sud de la Libya.-Africa-Tervuren, 15,4, 108-110, Tervuren.

Klerkx, J. (1971): Cerateres metamorphiques et stracturaux du socle precambrian de la region d`Uweinat (Libye).-C.R. Acad. Sci. Paris, 272,3246-3248, Paris

Klerkx, J. & C. Rundle (1976): Preliminary K/Ar ages of the different igneous rock formations from Gebel Uweinat region (SE Libya). Rapp.Ann. (1975), Mus. Roy. Afr. Centrale,Dep.Geol.Min., Tervuren:105-111.

Klerkx, J.& Deutsch, S. (1977): Resultats preliminares obtenus par la methode Rb/Sr sur l´age des formations precambriennes de la region d´Uweinat (Libye).-Mus.Roy. Afr. Centr., Dep. Geol.Min., Rapp. Ann. 1976, 83-94, Tervuren.

Klerkx, J. (1980): Age and metamorphic evolution of the basement complex around Jabel Awaynat.-In:Salem & BUSREWIL (Eds.),The Geology of Libya, 3, 901-906, London (Academic Press)

Klitzsch, E. (1983): Geological research in and around Nubia. Episodes 3:15-19.

Kröner, A.(1979): Pan-African plate tectonics and ist repercussions on the crust of northeast Africa. Geol.Rundscahu 68:565-583.

Kröner, A. (1984): Late Precambrian plate tectonics and orogeny: A need to redefine the term Pan-African. In: J. Klerkx & J. Michot (eds) Geologie africane, Tervuren: 23-28.

Macdonald, A.J. (1983). The iron formation – gold association evidence from the Geraldton area. In the geology of gold in Ontario. Edited by A.C. Colvine. Ontario Geological Survey, Miscellaneous Paper 110, pp. 75-83.

Marholz, W.W. (1968): Geological exploration of the Kufra-region.- Geol.Sect.Bull., 8, Ministry of Indust. Of the Kingdom of Libya,Tripolis.

Menchikoff, N. (1927): Etude petrographique des roches cristallines volcaniques de la region d´Ouenat (Desert de Libye).- Bull.Soc. Geol. France, 27, 4, 337-354, Paris

Naim, G. M.; Oweiss, Kh. A.; Khalid A.M., Shaaban, G. M., Sweissi, KH. S., and Diaf, A. A. (1996): Regional Geological and Geochemical Exploration at Al Uwaynat area. Abstract, Centennial of Geological Survey, Cairo.

Naim, G. M., Khalid, A. M., Said, M. M., Shaaban, G.M., Hussein, A. M. and El Kady, M. F. (1998): Banded Iron Formation Discovery at west of Gabal Kamel and its gold potential. Western Desert. Egypt. Annal. Geol. Surv. V. XXI. PP. 303-330.

Pearce, J. A., and Cann, J. R (1971) Ophiolite origin investigated by discriminant analysis using Ti, Zr and Y. Earth Planet. Sci. Lett., 12, 339-349.

Pearce, J. A., and Cann, J. R (1973) Tectonic setting of basic volcanicrocks determined using trace element analyses. Earth Planet. Sci. Lett., 19, 290-300.

Phillips, G.N., Groves, D.I., and Martyn, J.E. (1984): An epigenetic origin for Archean banden-iron-formation-hosted gold deposit. Economic Geology, 79: 162-171.

Pohl, W. (1984): Large scale metallogenic features of the Pan-African in east Africa, Nubia and Arabia. Bull. Fac. Earth Sci., King Abdull Aziz Univ., Geddah 6:592-601.

Owens, W. H. (1974A): Mathematical model studies on factor affecting the magnetic anisotropy of deformed rocks. Tectonophysics, 24, 115-131.

Owens, W. H. (1974B): Representation of finite strain state by three-axis planar diagrams. Bull. Geol. Soc. Am., 85, 307-310.

Richter, A. (1986): Geologie der metamorphen und magmatischen Gesteine im Gebiet zwischen Gebel Uweinat und Gebel Kamil, SW-Ägypten/ NW-Sudan. Berl.Geowiss.Abb. 73 (A) pp. 1-201.

Ries, A. C., Shackleton, R. M., Graham, R. H. and Fitches, W. R. (1983): Pan-African structures, ophiolite and melange in theEastern Desert of Egypt: a traverse at 26° N. J. Geol. Soc. Lond., 140,75-95.

Rocci, G. (1965): Essai d´interpertation de mesures geochronologiques. La structure de l´Ouest africain. Sciences Terre Nancy 10, 461

Said, M.M., Attia, M. N., Habib,A.H., Ibrahim,S.M., Turky, S., & Al Shareif, Kh. (1996): Correlation between Paleozoic and Mesozoic formations in Egypt and Libya. Cent. Ann. Geol. Surv. Egyp ,(19-22 Nov.), pp. 711- 725.

Said, M.M.; Khalid, A.M.; El Kady, M.F.; Abu Salem, A.O.; and Ibrahim, S.M. (1998): On the structural evolution of the Banded Iron Formation of Gabal Kamel and its role in the gold mineralization. Annal, Geol. Surv. V. XXI. pp.345-352.

Said,M.M., Habib,A.H., El Mahdi, B., & Turky, S. (2000): Contribution to the geology of Jabal Al Uwaynat Area ,Libya,. Ann. Geol. Surv. Egypt, V. XXIII, pp. 539- 554.

Sandford, K.S (1935): Geological observations on the south western frontiers of the Anglo-Egyptian Sudan and the adjoining part of the southern Libyan Desert. Quart. J. Geol. Soc. London 80: 323-381.

Schandelmeier, H., A. Richter & G. Franz (1983): Outline of the geology of magmatic and metamorphic units fron gabal Uweinat to Bir Safsaf (SW-Egypt / NW-Sudan) J.Afr. Earth Sci. 1: 275-283.

Schanelmeier, H. & F. Darbyshire (1984): Metamorphic and magmatic events in the Uweinat-Safsaf uplift (Western Desert, Egypt). Geol.Rundscahu 73: 819-831.

Schandelmeier, H., A. Richter & U. Harms (1987): Proterozoic deformation of the east Saharan craton in SE-Libya, S-Egypt and N-Sudan. Tectonophysics, 140:233-246.

Schandelmeier, H., Huth, A., Harms, U., Franz, G. and Bernau, R. (1987): The East Saharan Craton in Southern Egypt and Northern Sudan: lithology, metamorphism, magmatism, geochronology and structural development. *Berliner geowissenschaftliche Abhandlungen,* (A) 75.1: 25-48.

Schandelmeier, H., Wipfler, E., Küster, D., Sultan, M., Becker, R.,Stern, R.J., Abdelsalam, M.G. (1994): Atmur-Deglo sutur: Aneoproterozoic oceanic basin extending into the interior of northeast Africa. Geology 22:563-566.

Schenk, V., Wulff, K.Khalid, A. M., Shabaan, M., Abu Salem, A., Bredemeyer, S.,John, T., Kontny, A. (2002) Granulite-facies metamorphism at Gebel Uweinat (SW-Egypt) : Eburnian orogenic reworking of the Archean “Ghost-Craton”. 19th Colloquium of African geology-ElJadida, Morocco, 19-22 March 2002, P 166-167.

Shackleton, R. M., Ries, A. C., Greham, R. H. andFitces, W. R. (1980): Late Precambrian ophiolite melange in the Eastern Desert of Egypt. Nature,285, 472-474.

Smith, G.M., & Banerjee, S. K. (1987): The dependance of weak field susceptility on applied magnetic field. Phys.earth. Planet.,46: 71:76.

Sultan, M., Tucker, R.D., Gharbawi, R.I., Ragab, A.I., Alfy, Z. (1993): On the location of the boundary between the Nubian Shield and the old African continent: inferences from U-Pb (zircon) and common Pb data. In: Thor weihe, U., Scandelmeier, H. (eds), Geoscientific Research in NE Africa. Balkema, Amsterdam, pp.75-77.

Sultan, M., El Alfy, Z., and Tueker, R. (1996): U-Pb (Zircon) ages from the Uweinate area. Geol. Surv. Egypt. Centennial. Cairo. (Abstract).

Tarney. J. (1976) Geochemistry of Archean high grade gneisses, with implications as to the origin and evolution of the Precambrian crust. In: The Early History of the Earth, B.F. Winley (ED.), John Wiley, London, 405-417.

Tarling, D. H. & Hrouda, F. (1993): The magnetic anisotropy of rocks. 212 p., Chapman & Hall, London.

Vail, J. R., (1983): Pan-African crustal accretion in NE Africa. Journal African Earth Sciences 1, 285-294.

Vincent, P.M. (1970): The evolution of the Tibesti Volcanic Province, eastern Sahara. In African Magmatism and Tectonics (eds. Clifford, T.N., and Gass, I.G.) (Hafner Publishing Co., Darien,Conn.,) pp. 301-319.

Wicander,R .,and Monroe,J.S. (1989): Historical Geology: Evolution of Earth and Life Through Time. West Publishing Company, Los Angeles.

Windley, B.F. (1979): The evolving continents.- 385 S., 5. Aufl., Chichester (Wiley & Sons).